IN-37

NASA Technical Memorandum 110318

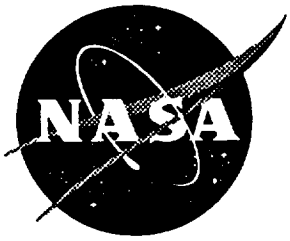

DAC-3 Pointing Stability Analysis Results for SAGE III and Other Users of the International Space Station (ISS) Payload Attachment Sites (PAS)

Jessica A. Woods-Vedeler
Langley Research Center, Hampton, Virginia

Gabriel Rombado
Grumman Aerospace Corporation, Houston, Texas

January 1997

National Aeronautics and
Space Administration
Langley Research Center
Hampton, Virginia 23681-0001

DAC-3 Pointing Stability Analysis Results for SAGE III and Other Users of the International Space Station (ISS) Payload Attachment Sites (PAS)

Jessica A. Woods-Vedeler
NASA Langley Research Center

Gabriel Rombado
Grumman Aerospace Corp.

Abstract

The purpose of this paper is to provide final results of a pointing stability analysis for external payload attachment sites (PAS) on the International Space Station (ISS). As a specific example, the pointing stability requirement of the SAGE III atmospheric science instrument was examined in this paper. The instrument requires 10 arcsec stability over 2 second periods. SAGE III will be mounted on the ISS starboard side at the lower, outboard PAS. In this engineering analysis, an open-loop DAC-3 finite element model of ISS was used by the Microgravity Group at Johnson Space Flight center to generate transient responses at PAS to a limited number of disturbances. The model included dynamics up to 50 Hz. Disturbance models considered included operation of the solar array rotary joints, thermal radiator rotary joints, and control moment gyros. Responses were filtered to model the anticipated vibration attenuation effects of active control systems on the solar and thermal radiator rotary joints. A pointing stability analysis was conducted by double integrating acceleration transient responses and evaluating the displacements which occurred over a 2 second period. Results of the analysis are tabulated for ISS X, Y and Z Axis rotations. These results indicate that the largest excursions in rotation during pointing occurred due to rapid slewing of the thermal radiator. Even without attenuation at the rotary joints, the resulting pointing error was limited to less than 1.6 arcsec. With vibration control at the joints, the pointing error could be reduced by a factor of three to a maximum 0.5 arcsec over a 2 second period. Based on this current level of model definition, it was concluded that between 0 - 50 Hz, the pointing stability requirement for SAGE III will not be exceeded by the disturbances evaluated in this study.

Introduction

One of the major benefits of the International Space Station (ISS) will be its use as a platform for long term atmospheric science and astronomical observations. It is anticipated that numerous users will take advantage of this benefit to demonstrate advanced instrument technologies while obtaining valuable scientific data about the earth, solar system and universe. Unavoidably, however, the ISS will be a dynamic platform. Disturbances introduced by its many operational elements will be propagated through the flexible structure and create an undesirable microgravity environment for some science users. The platform may actually interfere with the science observations it was designed to enable.

In order to accommodate this motion, it is useful for designers of the science instruments and their ISS interconnection devices to have access to specific information about motion which is likely to occur during observations. For remote sensing instruments, this information is typically the pointing stability at the instrument mount location. Pointing stability, or jitter, is the maximum amount of rotational displacement which will occur over a specified period of time. Until now, no information about the pointing stability has been available to users of the ISS external payload attachment sites (PAS). Thus, the purpose of this paper is to summarize results of a joint effort between NASA Langley Research Center's Research and Technology Group (LaRC/ RTG) and the Microgravity Group at Johnson Spaceflight Center (JSC) to evaluate the pointing stability of instruments located at the ISS payload attachment sites (PAS).

Of specific interest is the pointing requirement of the Stratospheric Aerosol and Gas Experiment III (SAGE III) instrument which is scheduled to be used at one of the PAS. The SAGE III project has reached a point where it has become essential to obtain pointing stability information in order to proceed with instrument design. Since this information has not been obtainable in the past, one objective of this analysis is to provide the SAGE III project team with such data using the most current ISS model information available.

This paper will begin with a brief description of the ISS and the SAGE III atmospheric science instrument. A description of the finite element model used for this engineering analysis will be then presented as well as a description of the disturbances and control system effects. The pointing stability analysis procedure used will be discussed and results summarized.

SAGE III and ISS

The science objective of the Stratospheric Aerosol and Gas Experiment III (SAGE III) will be to measure vertical profiles of O_3, NO_2, H_2O, NO_3, OClO, temperature, neutral air density and aerosols. [1] The measurements range will be from the cloud tops in the troposphere through the mesosphere using solar and lunar occultation methods. The spectrometer has a continuous wavelength range between 280 nm and 1030 nm with a resolution of 0.94 nm. This allows for measurement of multiple absorption features of each gaseous species and multi-wavelength measurements of broadband extinction by aerosols. SAGE III is the fifth generation of occultation instruments developed by NASA Langley Research Center for monitoring aerosols and gaseous constituents in the stratosphere and troposphere.

Solar and lunar occultation methods involve viewing the sun and moon, respectively, through the earth's atmosphere during solar and lunar rise. Because the sun and the moon emit known spectra of light, chemical constituents of the atmosphere can be determined by evaluating the spectra of light absorption which occurs when viewing the bodies through our atmosphere. The experimental procedure involves multiple vertical scans of the sun or moon during its rise over the horizon. The science instrument "finds" the top edge of the body and begins a set of 2 second vertical scans of the body lasting 2-6 minutes in duration. The location being observed on the body is calculated based on the known location of the top edge of the body and the velocity of scan. Thus, if vibration of the instrument occurs during the scan, the calculated observation location on the body will differ from where the instrument is actually pointing. The implication of this is that the atmospheric science data will be correlated with incorrect Earth altitudes. Fortunately, due to a finite resolution of the SAGE III spectrometer, some low level disturbances can be tolerated without creating errors. However, any excursion in rotation which occurs over 10 arcsec during the 2 second scan can cause errors. This, then, is the pointing stability requirement for SAGE III.

The platform for SAGE III will be the International Space Station (ISS). ISS is a multinational venture to provide a permanent, gravity free, orbital research platform for long duration microgravity research [2], Fig. 1. The initial launch is currently planned for November, 1997 and is due to be completely assembled by 2002.

Three years after the initial launch of ISS, flight 13A will take place. During this flight, truss segment S3 will be attached on the starboard side of the orbiting platform. S3 is the site of the four external Payload Attachment Sites (PAS). Figure 2 illustrates the S3 truss and locations of the PAS relative to the ISS Basic coordinate system with additional detail in Figure 3. The four sites are labeled according to their location: Starboard Inboard Upper (SIU), Starboard Outboard Upper (SOU), Starboard Inboard Lower (SIL), Starboard Outboard Lower (SOL). Also shown in the figure are the Solar Array Rotary Joint (SARJ) and Thermal Radiator Rotary Joint (TRRJ) locations. SAGE III will be located at SOL.

Model Descriptions

Finite Element Model

The ISS finite element model used was the model that served as the basis for the Incremental Design Review No.2, Design Analysis Cycle No. 3 (DAC-3) microgravity structural dynamics assessment. [3] The FEM is based on the Stage 44 configuration description specified in the baseline ISS Assembly Sequence Rev A .[4]

As described in reference [5], a NASTRAN FEM was provided to the JSC Microgravity Group by McDonnell Douglas (MDA). Several modifications were made to this model. Since this model was developed for the purpose of transient loads analysis below 7.5 Hz, the modal content of the internal and external superelements was limited to about 30 Hz. The structural dynamics assessment required modal content much higher in order to obtain results in the 0.1-50 Hz range. Thus, superelements were regenerated to increase the modal content to 100 Hz. In addition, photovoltaic array models with modal content up to 5.7 Hz were replaced with higher fidelity models having modal content of 25 Hz. Other modifications were made to increase the fidelity and detail of the model at the MDA US Laboratory and ESA-APM.

Disturbance Models

In order to perform a transient analysis, it was necessary to define a set of transient disturbances for input. [6,7] Since, it was possible to consider only a very small set of disturbers for this study, a set of four was selected which were most likely to impact the pointing stability of instruments at PAS. Figures 4-7 illustrate the disturbances used. Each disturbance contained 1000 points with 0.01 second time steps.

The first disturbance considered was input torque due to SARJ motor operation. The SARJ joint has a nominal rate of 4°/minute with an expected variation of +/- 10% due to changes in solar angle through each orbit. Figure 4 shows the torque disturbance due to motor operation at 0.6 Hz and includes joint unbalance, friction and resolver errors. The disturbance has a modal content of 0.6 to 10 Hz. This disturbance was applied at the ISS starboard side node connecting the S3 truss inboard of the SARJ to the S4 truss outboard of the SARJ. It was simultaneously applied on the ISS port side node. This torque was applied about the -Y axis of the ISS Basic Coordinate System.

Figure 5 illustrates the torque due to TRRJ Motor operation. Similar to the SARJ, this model also describes joint unbalance, friction and resolver errors. Due to its single axis control, joint rates for the TRRJ vary much more than those for the SARJ which has multiaxis control. For the TRRJ, the rates vary from 0.7 °/minute to 45°/minute in order to accommodate a much wider range of sun angles and orbital positions. Figure 5 illustrates the TRRJ disturbance with a nominal motor speed of 0.6 Hz; the modal content ranged from 0.6 to 10 Hz. This disturbance was applied at the ISS starboard node connecting the radiator beam to the TRRJ motor and about the +X direction of the ISS Basic Coordinate System. It was simultaneously applied to the ISS portside node.

A special case of TRRJ motion considered was TRRJ slew. Normally, the TRRJ rotates smoothly to maintain a radiator position perpendicular to the sun. However, in two cases, the radiators must rotate more quickly through large angles. In the first case, they periodically must rotate through 180° to avoid 360° rotations during normal tracking. In the second case, they must perform large slews of up to 90° to reorient themselves toward the Earth to prevent freezing while in the Earth's shadow. Both slews are performed by accelerating the radiator at a maximum acceleration rate of $0.01°/sec^2$ to the maximum velocity of 45°/minute. The radiator travels to near the desired position and then decelerates to rest at $0.01°/sec^2$. The TRRJ slew disturbance used is shown in Figure 6. As for the TRRJ motor operation, this disturbance was applied at the node connecting the radiator beam to the TRRJ motor and about the +X direction of the ISS Basic Coordinate System.

The fourth disturbance considered was a Control Moment Gyro (CMG) operational disturbance which occurs primarily due to rotor imbalance. [7] The torque input with the CMG operating at a nominal speed of 6600 rpm is illustrated in Figure 7. This disturbance was applied simultaneously to all four nodes connecting the CMGs to the Z1 truss. It was applied only in the +Y Moment direction of the ISS Basic Coordinate System. Closed loop control effects of the CMG were not available for this analysis.

Knowledge of the phasing and duration of disturbances is important. This information must be available to provide the most accurate pointing stability predictions. Correct phasing of disturbances is important because of the constructive and destructive interference which occurs when disturbances propagate through the structure as vibrations. Thus, predicted vibration levels at a particular point will vary according to the phasing of applied disturbances. As a result, the pointing stability predicted at a particular point will also be effected.

Disturbance phasing information was not available for ISS disturbances. Thus, it was necessary to obtain transient responses to uncombined disturbances. That is, a transient acceleration response was obtained and pointing stability analysis performed for each disturbance forcing function when applied alone. A combined root-sum-squared (RSS) measure of pointing stability from the set of disturbances could be computed, however, it should be viewed conservatively because phasing was not accounted for.

More detail on the disturbances can be obtained in ref [6, 7].

Control Models

In order to alleviate some of the vibration caused by the solar and thermal array rotary joint motion, active control systems are being developed by the ISS team. However, at the time of this study, it was not possible to perform the analysis of interest with closed loop SARJ and TRRJ control on the ISS assembly complete model. Instead, the acceleration responses to disturbances obtained during open-loop analysis were attenuated using filters approximating the attenuation affect of these controllers.

Figures 8 and 9 show comparisons between the approximation and anticipated attenuation effect of active control. The approximation for the SARJ controller is shown in Figure 8. The first order filter is described by

$$\frac{0.3s}{s+2\pi}$$

In the TRRJ case, the second order filter is described by

$$\frac{0.3s^2}{s^2+4\pi s+4\pi^2}$$

In both cases, the approximation is first order. The SARJ approximation is very conservative in the 0.1 to 2 Hz range and over attenuated in the 0.03-0.08 Hz range. For the TRRJ, the approximation is better. Although, the curve is conservative in the 0.2-0.7 Hz range and over attenuated in the 1-2 Hz range. These approximations were not ideal, however, they were adequate and commensurate with the level of detail currently available in other parts of the analysis.

In addition, the analytical model did not include any closed loop effects of an attitude control system (ACS). It was assumed that the effect of an ACS would be to remove drifting that might occur at very low frequencies. Therefore, the effect of using a 2 Hz high pass filter on pointing stability is evaluated on SARJ, TRRJ and CMG responses. The high pass filter is given by

$$\frac{s}{s+4\pi}$$

It is noted that the level of detail required for a definitive pointing stability analysis is not available in current ISS FEM, disturbance or control system models. Therefore, this analysis should be viewed conservatively as a "first estimate" of the pointing stability achievable.

Procedure

Using the analytical models, a study was conducted to evaluate pointing stability at the PAS. The procedure involved two parts: transient acceleration response analysis and pointing stability analysis.

Transient acceleration responses due to disturbances were computed by JSC's Microgravity Group using the NASTRAN FEM and the disturbances described above. The effort is documented in [5]. One hundred seconds of response were obtained at each PAS for each of the four disturbances. The time step was 0.01 second. Time responses due to SARJ and TRRJ motion were attenuated using the previously described first and second order filter approximations in a linear simulation.

For the pointing stability analysis, it was necessary to integrate acceleration responses twice to obtain displacements. Initial conditions on velocity and displacement were zero. Several options were available for integration including second to fourth order Runga Kutta methods. However, in this case, it was found that Simpson's Rule provided equivalent integration accuracy at a fraction of the computational time. Simpson's Rule is given as follows:

$$I = 0.5(x_1 + 2x_2 + 2x_3 + 2x_4 + \ldots 2x_{n-1} + x_n)$$

where x_i indicates the acceleration or velocity at time, t_i, n=1000 and I is the integral value.

The pointing stability analysis was conducted by computing the maximum rotational displacement which occurred over any 2 second interval of time in each of the displacement time responses. Two seconds was chosen because it represents the SAGE III pointing stability requirement. The unit arcsec is defined as 1/3600th of one degree of rotation.

Results

Figure 10 illustrates the integration results for a typical response. In this figure, the rotational acceleration response at SOL in the ISS X Axis is due to excitation by TRRJ slewing without the vibration control attenuation. The displacement shows up to 0.003 deg drifting in Fig. 10 (c). This is removed by using a 2 Hz high pass filter as shown in Fig. 10 (d). The drifting occurs in several sets of results obtained and may be due to the absence of ACS. It may also be due to the duration of disturbance inputs. For all disturbances except the TRRJ slew, the duration of the disturbance was unknown. As such, the disturbance was a continual energy input. With a finite disturbance duration, the drifting may have been less pronounced. The same effect is obtained by using the control attenuation model, which is basically a high pass filter. The controlled response for the same case is shown in Figure 11. It is seen by comparison with Figure 10 that the effect of controller attenuation is to reduce the magnitude of response by an order of magnitude.

Pointing stability was computed using each disturbance response and at each PAS. An example of the stability analysis results is shown in Figure 12. Index points in this figure represent initial time steps for the 2 second windows of analysis. At each index point, the value maximum displacement which occurred in rotation over a 2 second interval is shown. Plateaus in the plot represent periods of time in which the maximum

displacement was a constant value over several 2 second intervals. In this particular figure, it is seen that the pointing error at PAS SOL about the ISS X due to the TRRJ slewing disturbance is a maximum of about 0.47 arcsec without control or filtering. With control and low frequency filtering, the pointing stability is about 0.1 arcsec. This is a typical result for effect of active control of vibration due to SARJ and TRRJ motion.

Additional figures showing rotational displacements due to each disturbance at each PAS are included in Appendix A. For SARJ and TRRJ disturbances, results presented are uncontrolled and controlled responses with and without the 2 Hz high pass filtering. CMG responses are not controlled, however, results showing the effect of the 2 Hz high pass filter are shown.

A summary of pointing stability results is given in Tables 1-4. Due to the typical nature of instrument requirements, only pointing stability in rotational displacements was considered. There is a 0.02 arcsec numerical confidence in the numbers shown. In general, these results show that the largest contributor to pointing error occurs due to TRRJ slewing, primarily about the ISS Y Axis. In other axes, the pointing error does not exceed 0.6 arcsec and, in no case does it exceed 1.6 arcsec. For SARJ motion, pointing error does not exceed 0.13 arcsec, with values typically much less. TRRJ results are similar. The CMG disturbance about the Y Axis produced a maximum pointing error of 0.03 arcsec about the ISS Y axis and had less effect on pointing in other axes.

Since the quantities presented are the maximum pointing errors over responses, it is possible to extrapolate these results somewhat to other intervals of time besides 2 seconds. For instance, for 4 second periods of time, values can be doubled for an approximate upper bound on pointing stability. For periods of time shorter than 2 seconds, the value itself represents an upper bound on pointing stability.

The critical instrument scanning axis of interest for SAGE III is rotation about the ISS Y axis. These results show that none of the disturbances produce pointing errors at PAS SOL which exceed 1.6 arcsec, even without vibration control. With control, the limit is 0.4 arcsec. Even when disturbance phasing is disregarded and a RSS value of all pointing errors is considered, the value is still less than 1.6 arcseconds. Since the SAGE III pointing stability requirement is 10 arcsec over 2 second intervals, it can be concluded that the pointing stability requirement for SAGE III will not be exceeded by the disturbances investigated. This statement is based on the most current information available.

Conclusions

In conclusion, a pointing stability analysis was performed at the four ISS PAS. Responses to SARJ, TRRJ and CMG operational disturbances were considered. Results showed that over a 2 second period, pointing error did not exceed 1.6 arcsec in any axis of rotation for the uncontrolled cases. With vibration control at the rotary joints, the error could be reduced by a factor of three to 0.5 arcsec. For the SAGE III instrument, which has a pointing stability requirement of 10 arcsec for 2 second durations, this implied that the SAGE III pointing stability requirement will not be exceeded by the disturbances investigated over the range of 0.1 to 50 Hz.

References

1. SAGE III Homepage: http://arbs8.larc.nasa.gov/sage3/
2. ISS Homepage: http://issa-www.jsc.nasa.gov/ss/welcome/overview.html
3. Rombado, G., "DAC-3 S3 Truss Segment Payload Attach System Acceleration Response Environment," Memorandum SSP-MG96-033, May 21, 1996.
4. International Space Station On-Orbit Assembly, Modeling and Mass Properties Databook, Design Analysis Cycle #3, Rev A Assembly Sequence, Nov., 1995.

5. Rombado, G., "IDR-2A DAC-3 'Structural Dynamic' Finite Element Model and Post-Processing Documentation," Memorandum SSP-MG96-036, July 11, 1996.
6. Boucher, R., "Microgravity Disturbance Forcing Functions," Memorandum A3-J012-R-M-9402343 R1, Nov. 15, 1994.
7. Swindle, J., "CMG Force and Torque Noise Microgravity Forcing Functions," Memorandum A03-2012-JS-M-9501550 R2, Sept. 29, 1995.

Table 1
Pointing Errors at SIL PAS
over 2 second intervals

Disturbance Source	ISS Axis of Rotation	Pointing Error (arcsec) Uncontrolled Unfiltered	Controlled Unfiltered	Controlled Filtered
SARJ	X	0.05	0.01	0.01
	Y	0.52	0.13	0.01
	Z	0.09	0.02	0.02
TRRJ	X	0.08	0.02	0.02
	Y	0.14	0.04	0.04
	Z	0.05	0.01	0.01
TRRJ Slew	X	0.45	0.06	0.06
	Y	1.61	0.49	0.49
	Z	0.13	0.04	0.04
CMG Y	X	0.01		
	Y	0.05		
	Z	0.01		

Table 2
Pointing Errors at SIU PAS
over 2 second intervals

Disturbance Source	ISS Axis of Rotation	Pointing Error (arcsec) Uncontrolled Unfiltered	Controlled Unfiltered	Controlled Filtered
SARJ	X	0.06	0.01	0.01
	Y	0.51	0.12	0.09
	Z	0.06	0.02	0.01
TRRJ	X	0.06	0.02	0.02
	Y	0.16	0.05	0.04
	Z	0.03	0.01	0.01
TRRJ Slew	X	0.46	0.05	0.05
	Y	1.45	0.44	0.44
	Z	0.11	0.03	0.03
CMG Y	X	0.01		
	Y	0.03		
	Z	0.01		

Table 3
Pointing Errors at SOL PAS
over 2 second intervals

Disturbance Source	ISS Axis of Rotation	Pointing Error (arcsec) Uncontrolled Unfiltered	Controlled Unfiltered	Controlled Filtered
SARJ	X	0.08	0.02	0.02
	Y *	0.49	0.13	0.10
	Z	0.07	0.02	0.01
TRRJ	X	0.05	0.01	0.01
	Y *	0.13	0.04	0.04
	Z	0.03	0.01	0.01
TRRJ Slew	X	0.47	0.12	0.12
	Y *	1.41	0.35	0.35
	Z	0.27	0.08	0.08
CMG Y	X	0.01		
	Y *	0.03		
	Z	0.00		

* SAGE III Critical Axis

Table 4
Pointing Errors at SOU PAS
over 2 second intervals

Disturbance Source	ISS Axis of Rotation	Pointing Error (arcsec) Uncontrolled Unfiltered	Controlled Unfiltered	Controlled Filtered
SARJ	X	0.09	0.03	0.02
	Y	0.55	0.13	0.09
	Z	0.05	0.01	0.01
TRRJ	X	0.05	0.02	0.02
	Y	0.12	0.03	0.03
	Z	0.03	0.01	0.01
TRRJ Slew	X	0.47	0.13	0.13
	Y	1.41	0.43	0.43
	Z	0.27	0.08	0.08
CMG Y	X	0.01		
	Y	0.03		
	Z	0.01		

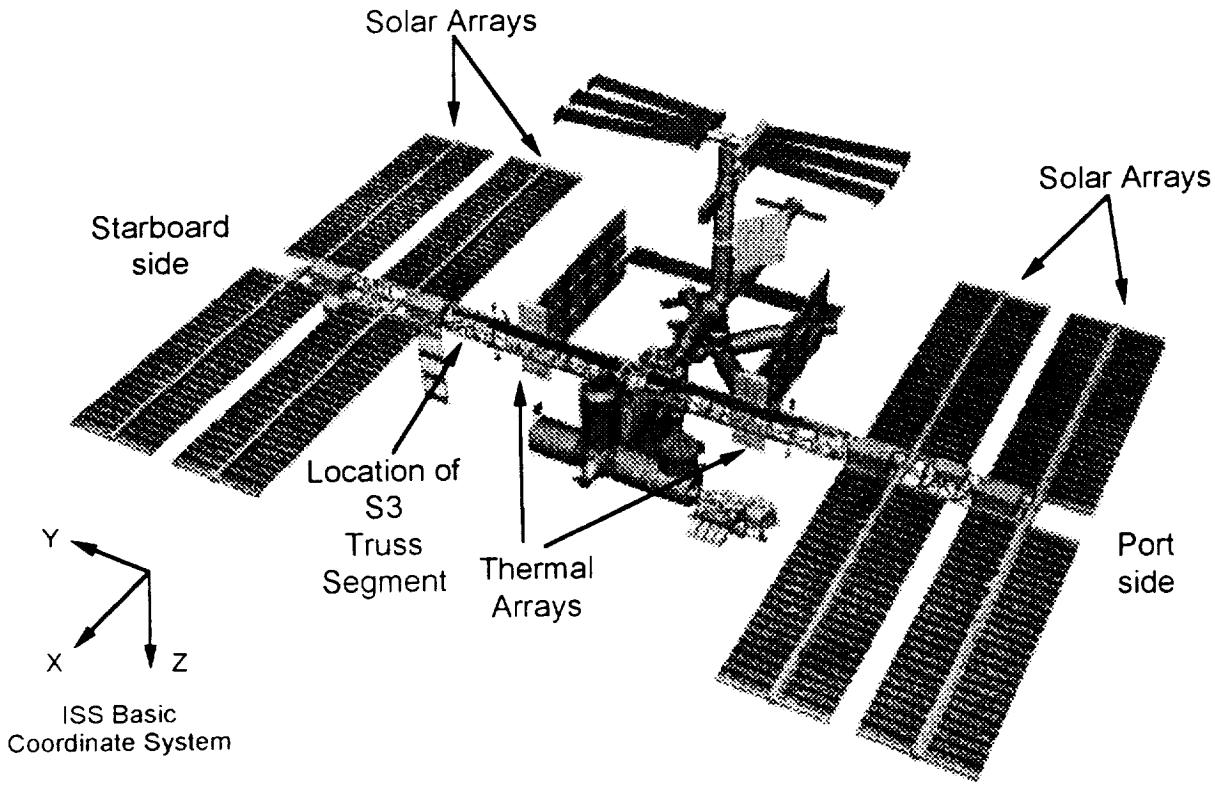

Figure 1. - Assembly Complete Configuration of the International Space Station (ISS)

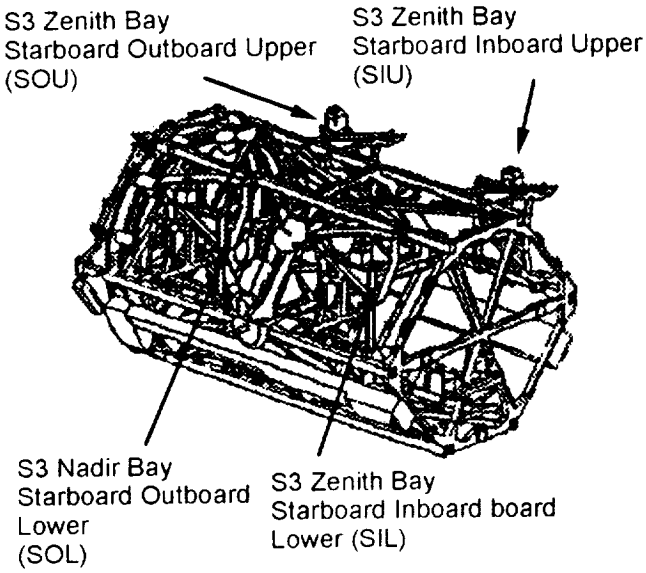

Figure 2.- S3 Truss Segment showing Payload Attachment Sites (PAS)

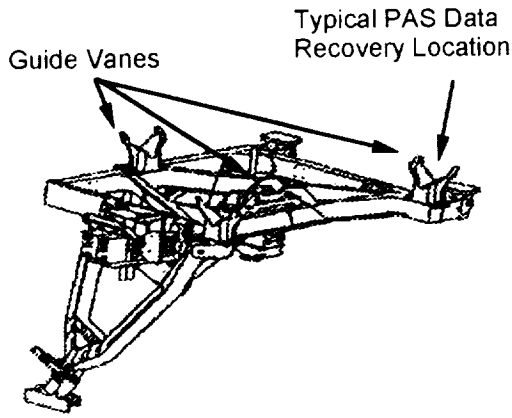

Figure 3.- Payload Attach System

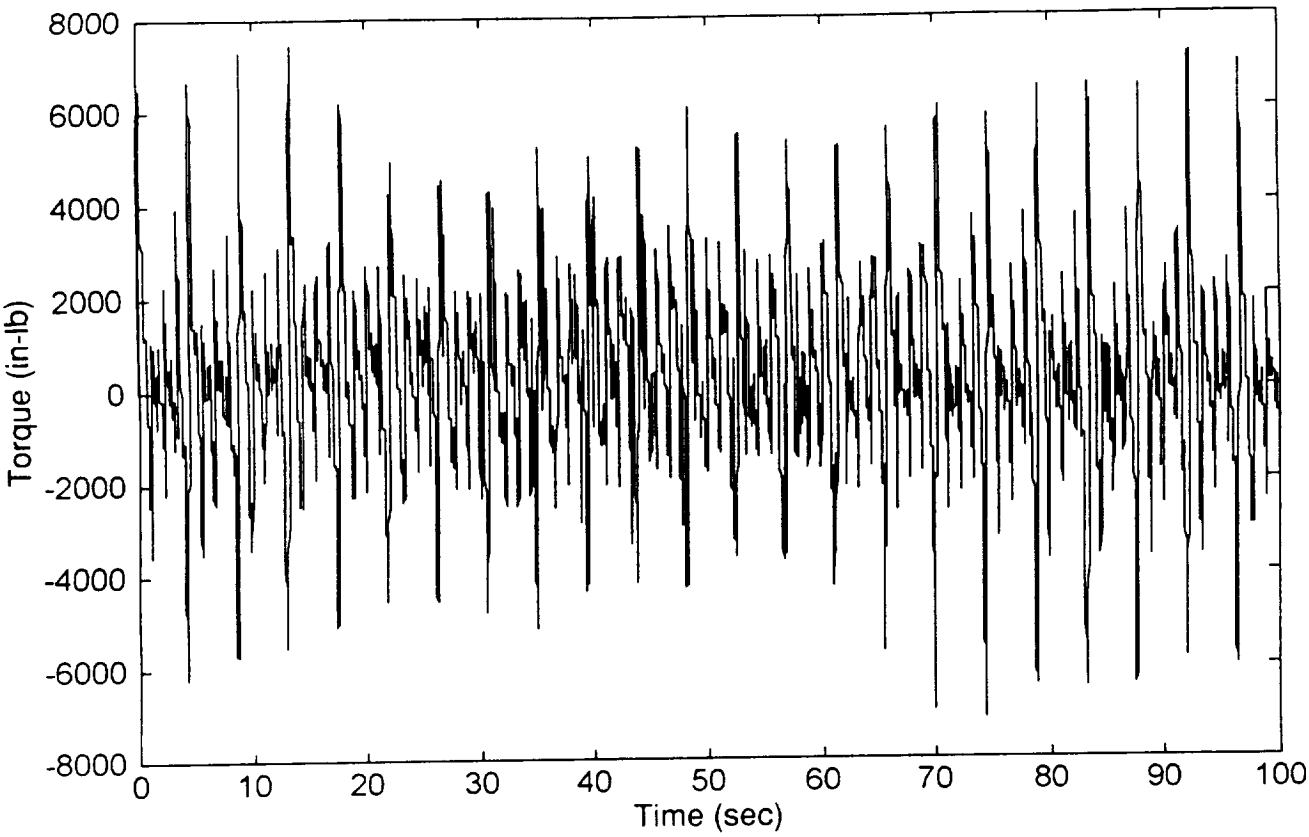

Figure 4.- Solar array disturbance. (SARJ)

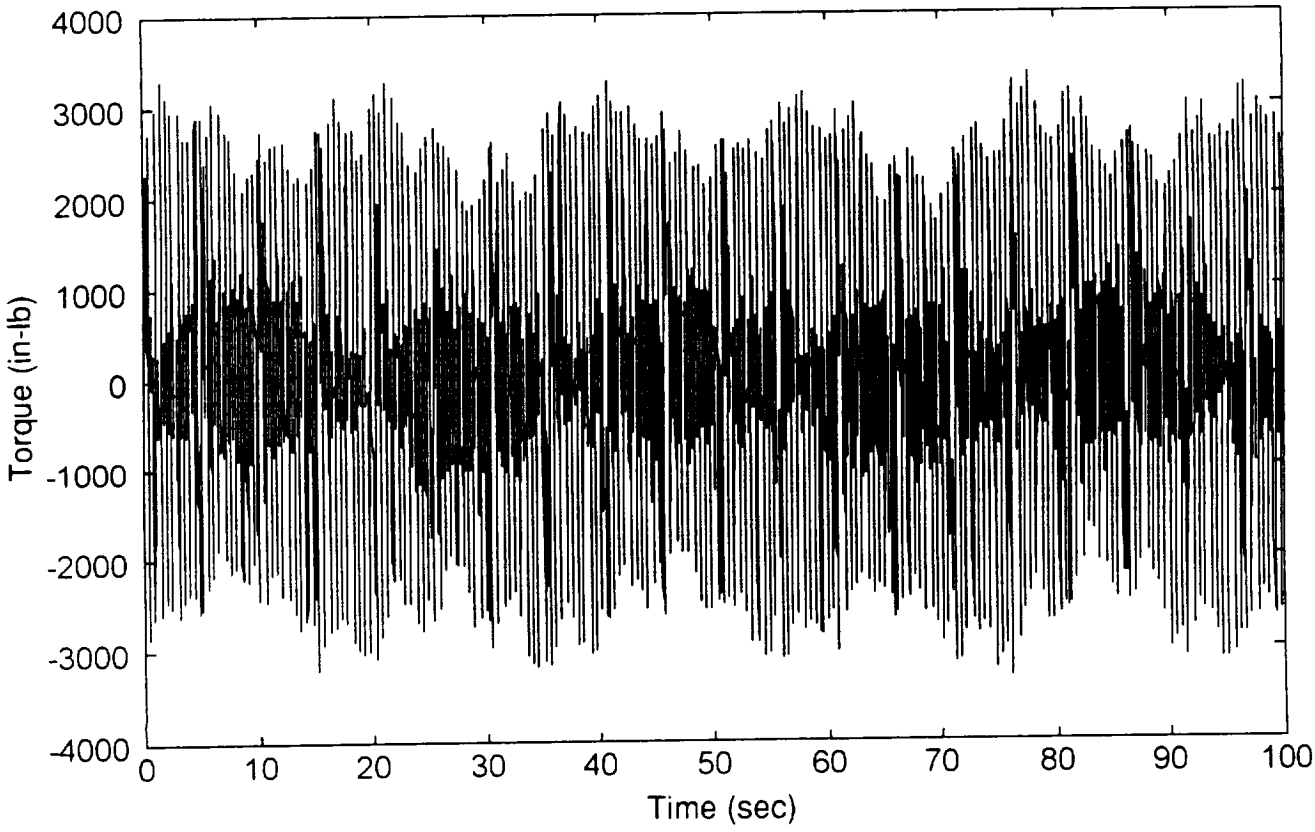

Figure 5.- Thermal array disturbance. (TRRJ)

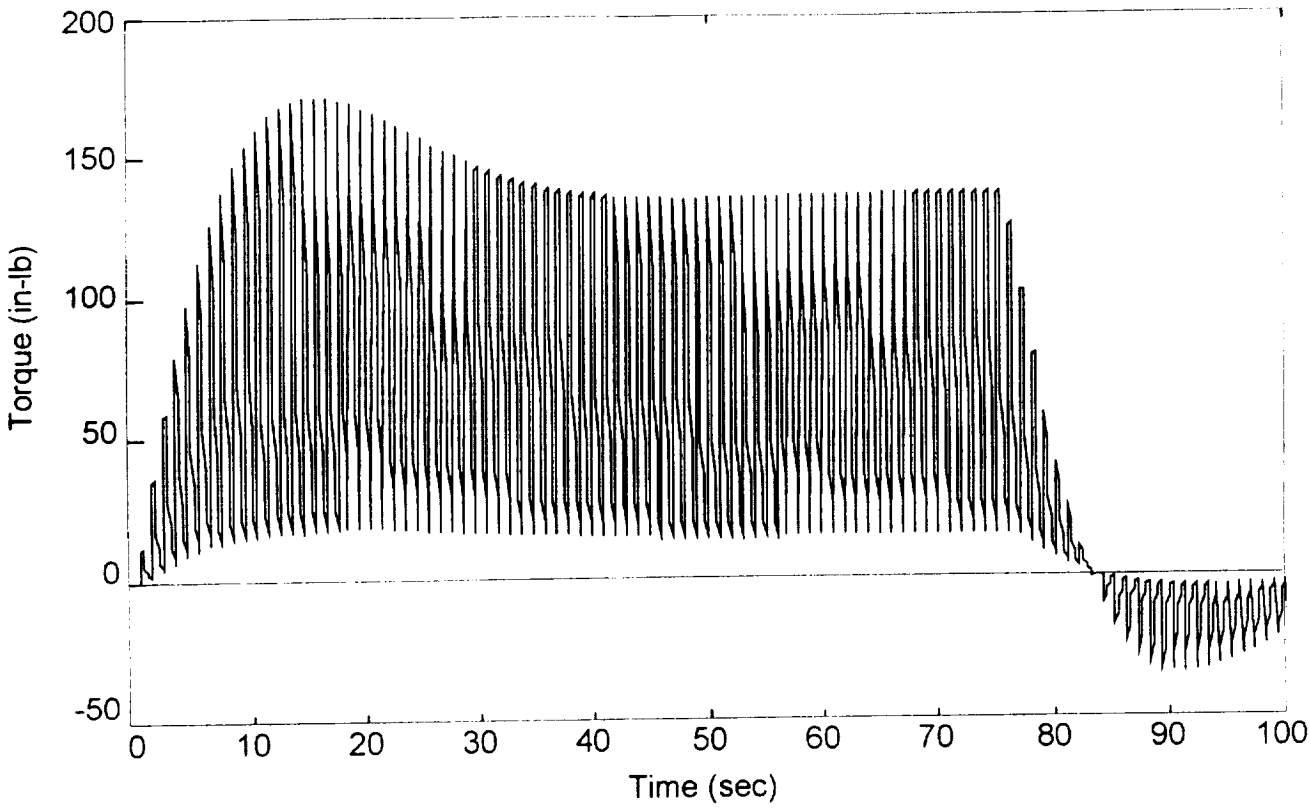

Figure 6.- Thermal array disturbance in ISS Y Axis due to slewing. (TRRJ Slew)

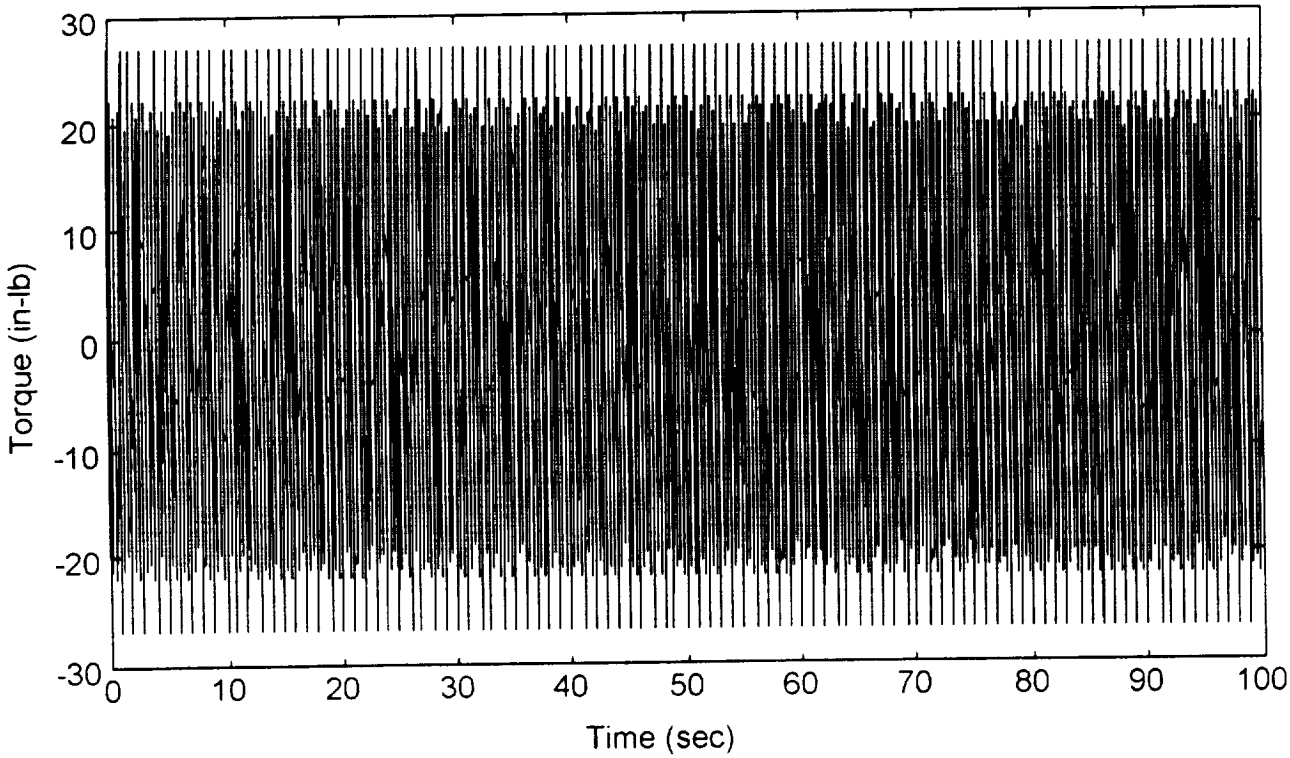

Figure 7.- Control moment gyro disturbance in ISS Y Axis. (CMGY)

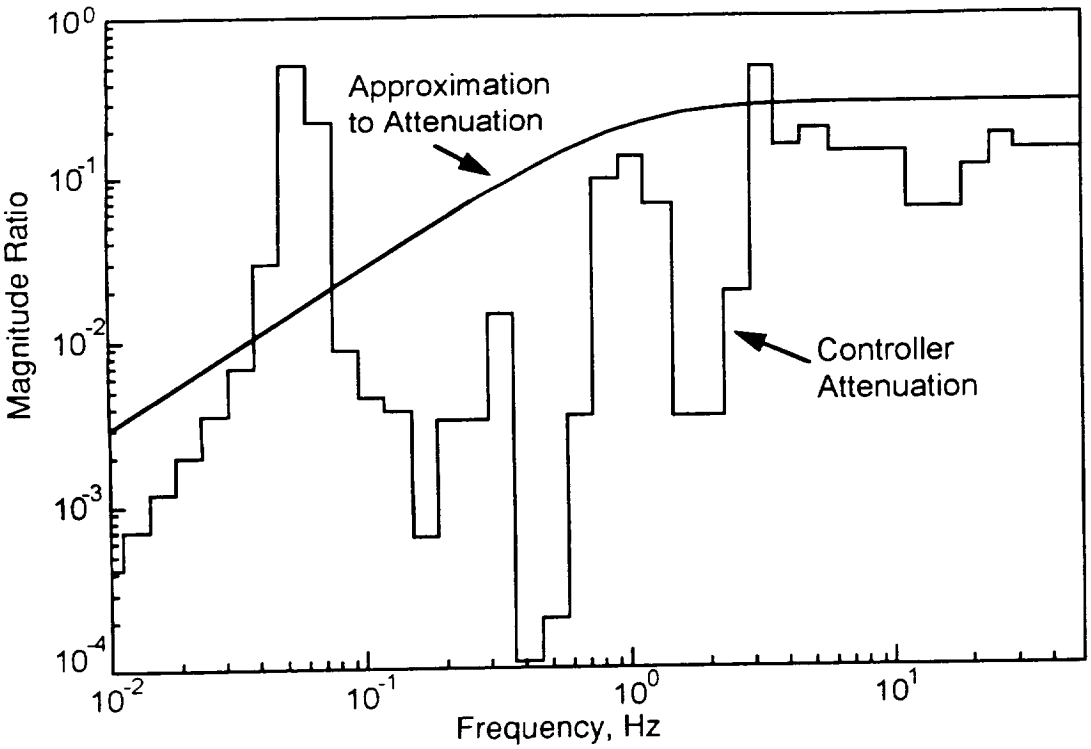

Figure 8.- SARJ attenuation approximation

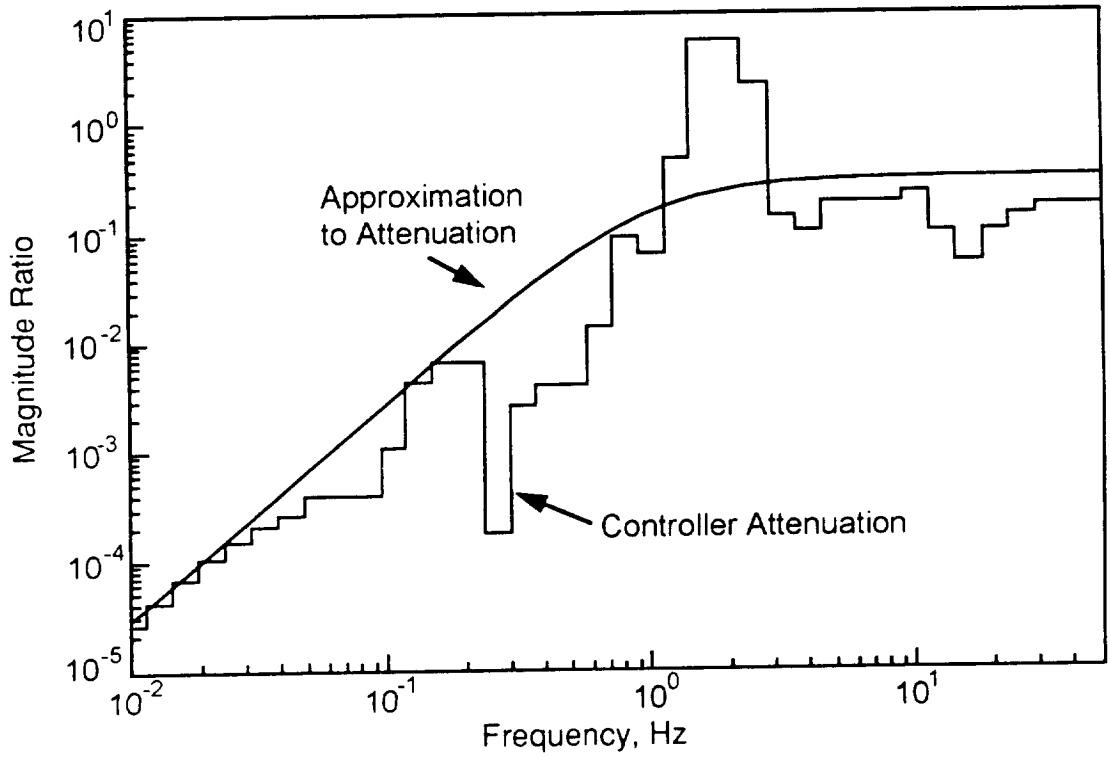

Figure 9.- TRRJ attenuation approximation

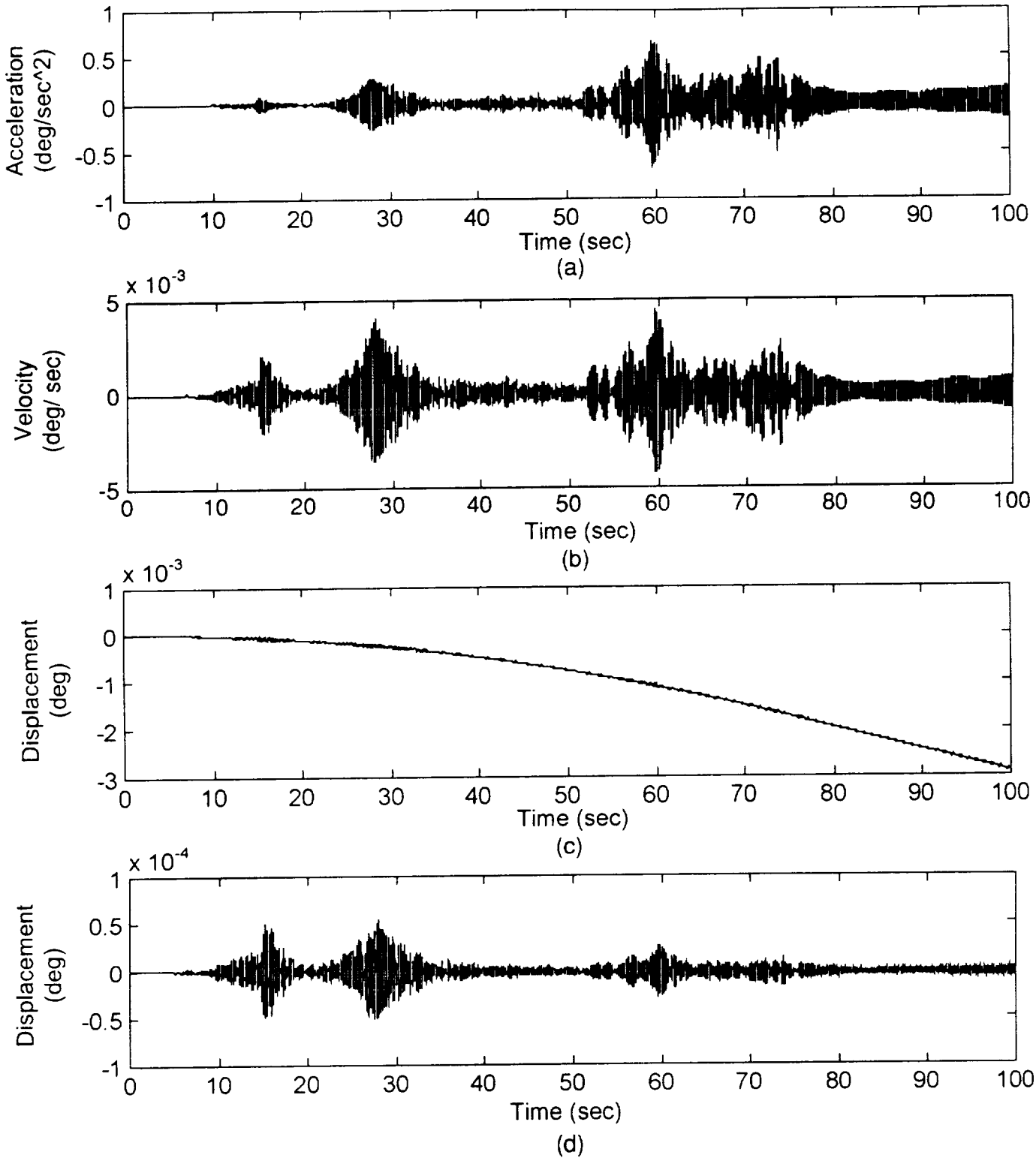

Figure 10. - Integration for the unattenuated response due to TRRJ Slew disturbance at the SOL PAS in the -X ISS Axis: a) acceleration, b) velocity, c) unfiltered displacement, and d) displacement filtered with 2 Hz filter.

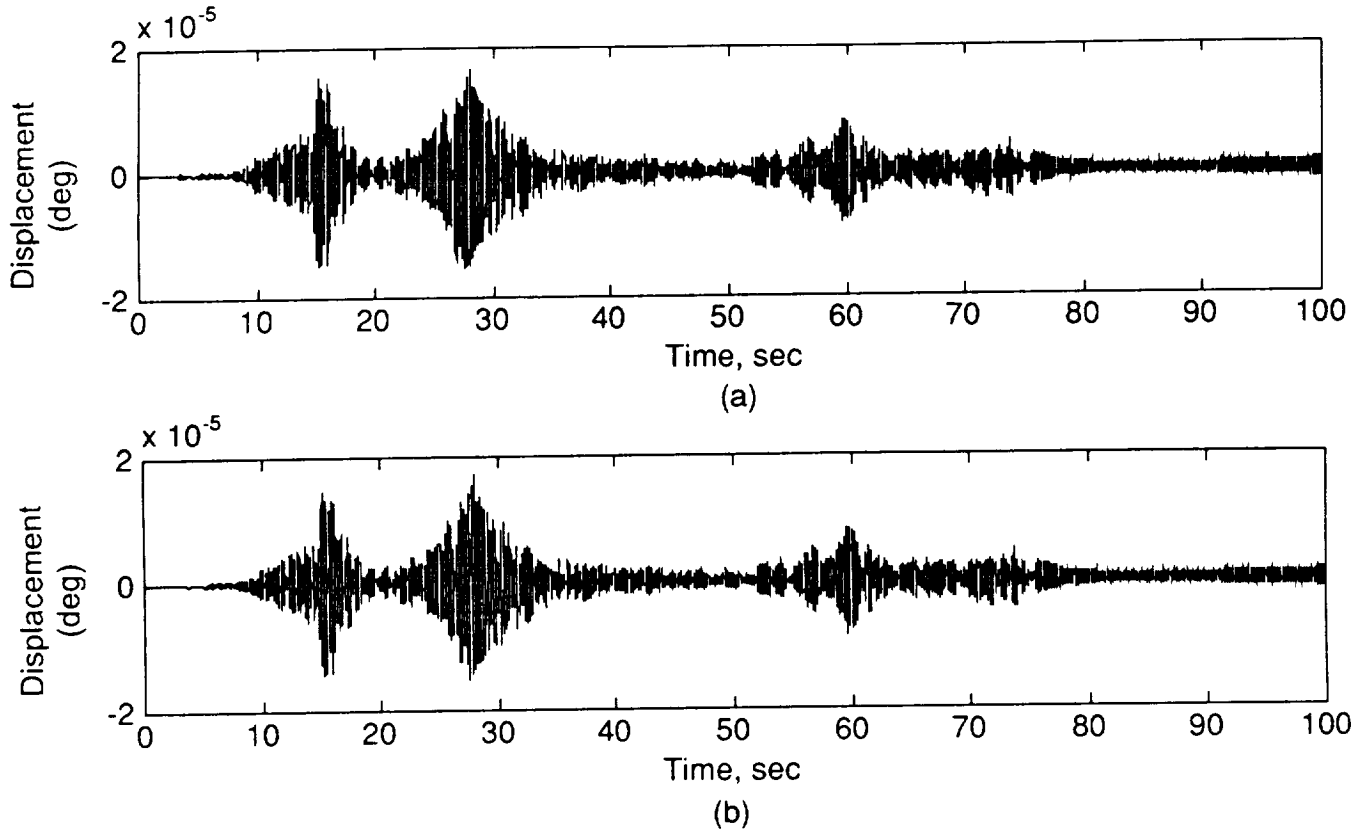

Figure 11.- Attenuated responses due to TRRJ Slew disturbance at the SOL PAS in the -X ISS Axis: a) unfiltered and b) filtered with 2 Hz high pass filter.

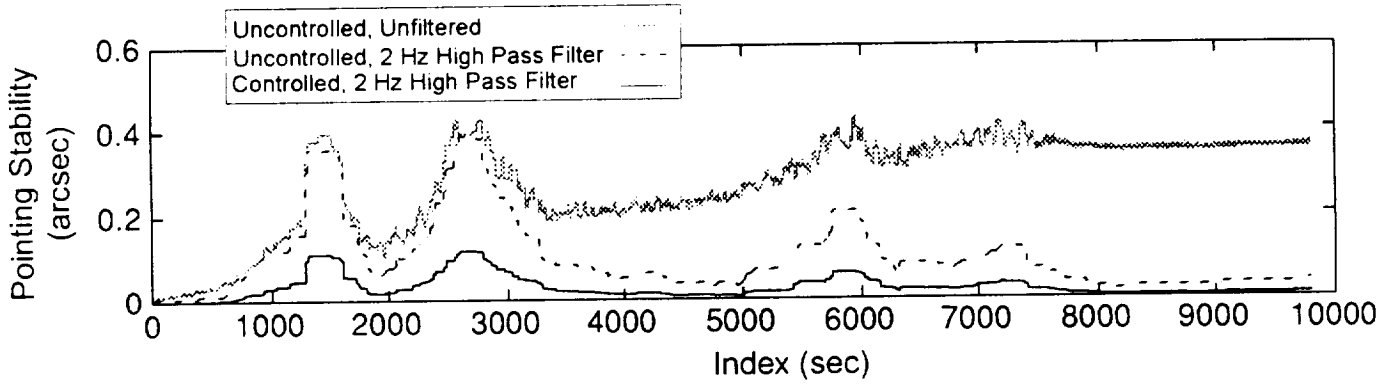

Figure 12.- Pointing results for the response due to TRRJ Slew disturbance at the SOL PAS in the -X ISS Axis.

APPENDIX A

EXPANDED ANALYSIS RESULTS

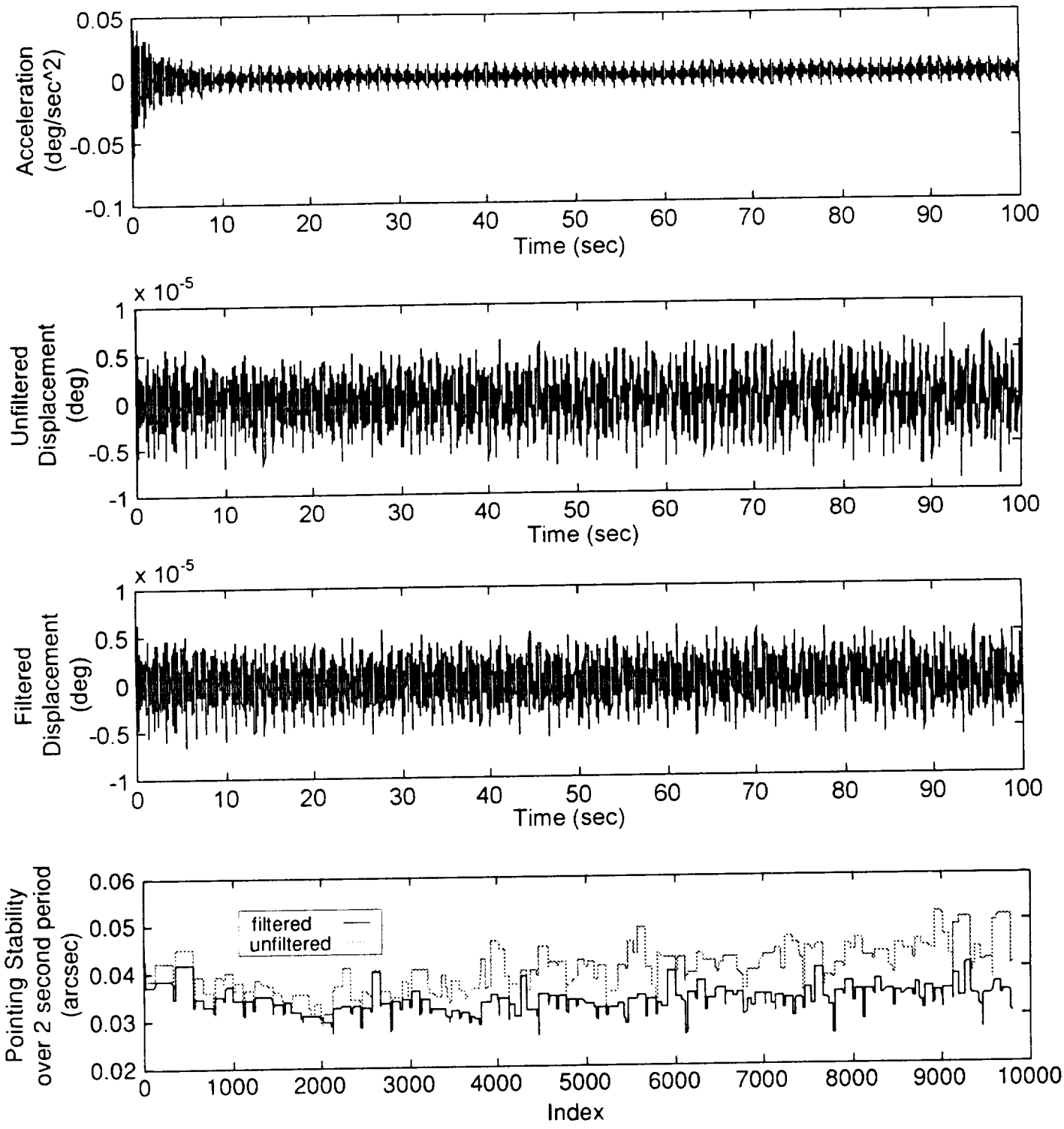

(a) Uncontrolled response

Figure 1. - Integration and pointing stability results for the response at the SIL PAS in the - X ISS Axis due to SARJ disturbance .

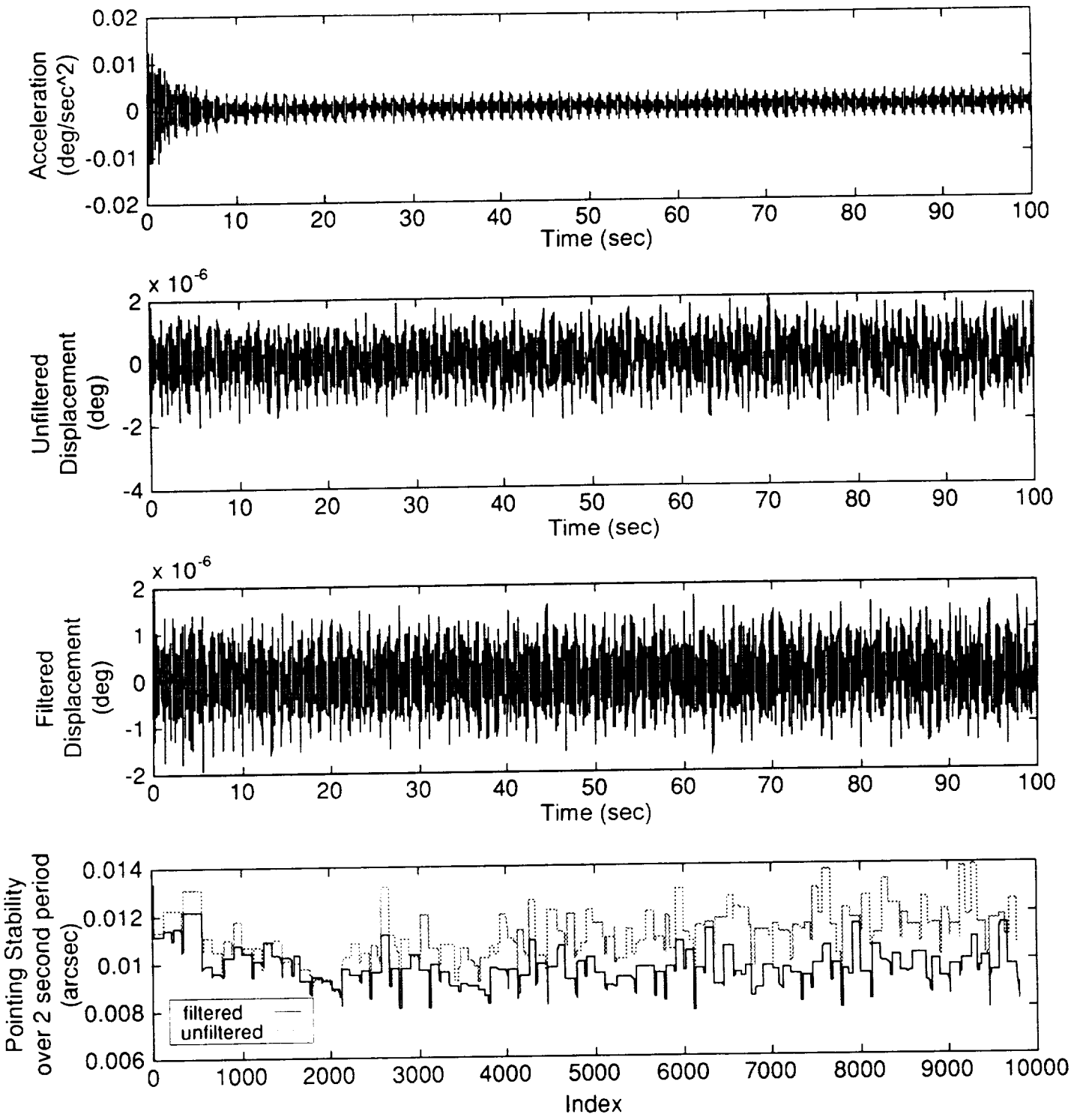

(b) Controlled response

Figure 1. - Concluded.

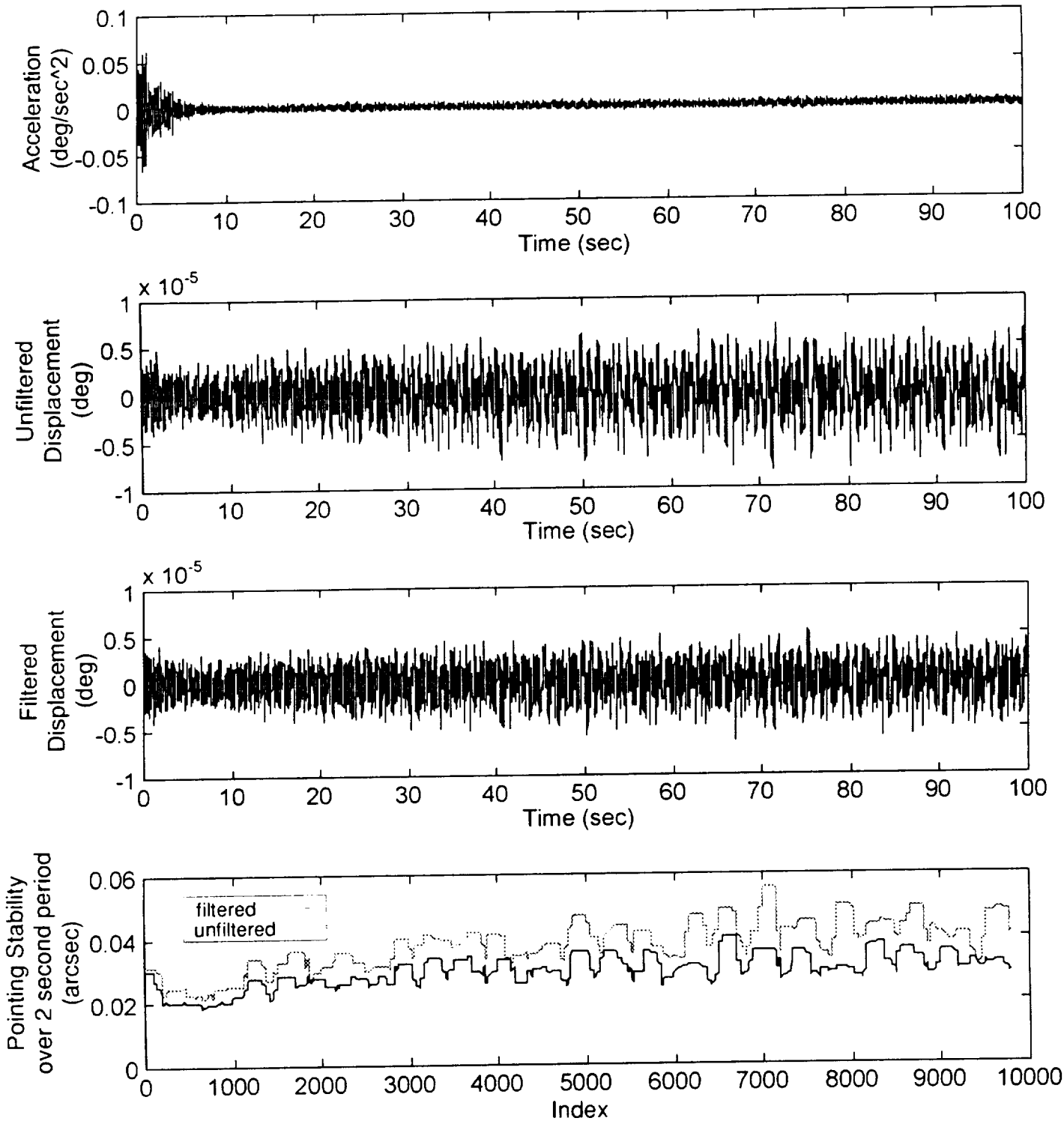

(a) Uncontrolled response

Figure 2.- Integration and pointing stability results for the response at the SIU PAS in the -X ISS Axis due to SARJ disturbance.

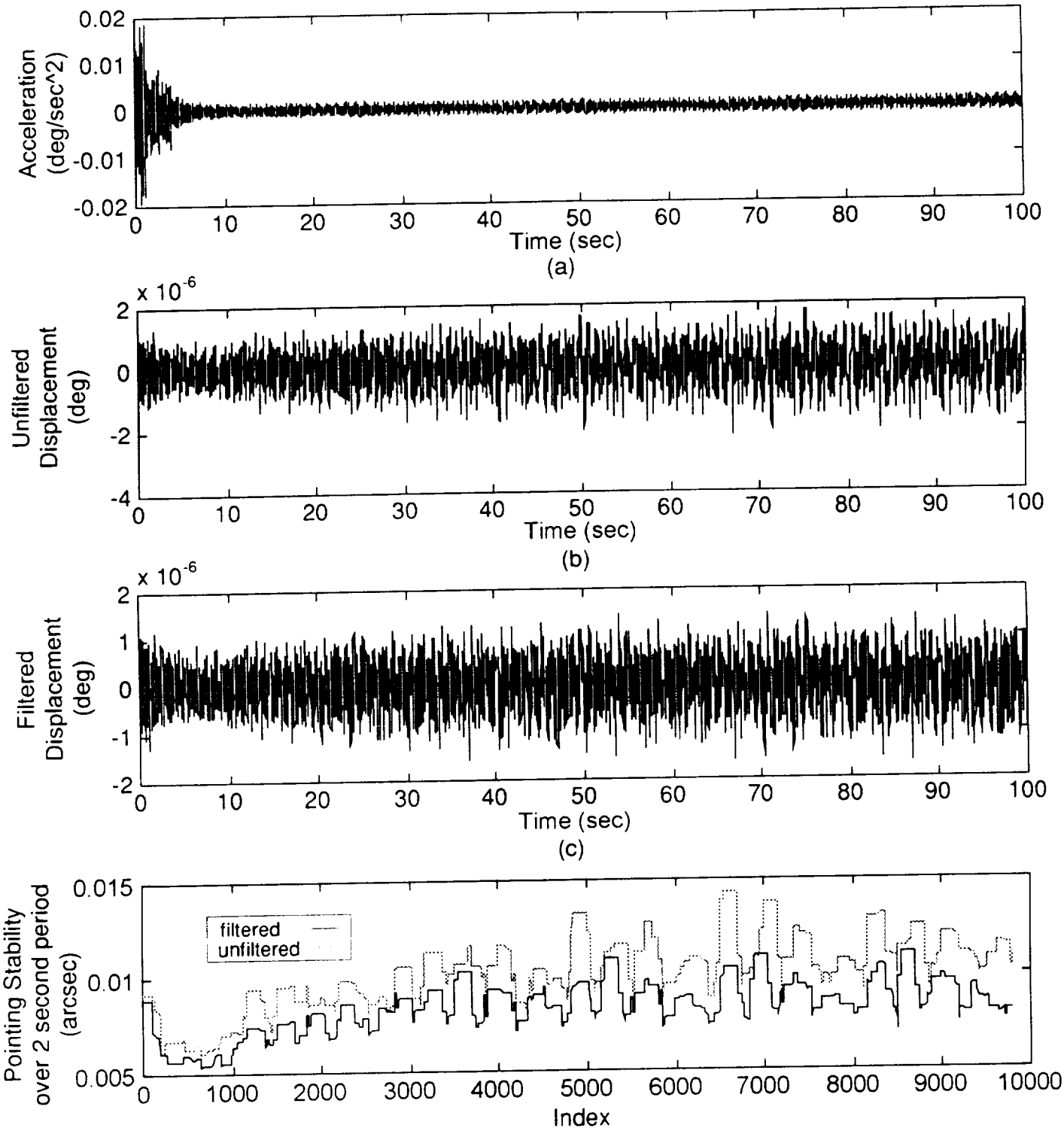

(b) Controlled response

Figure 2. Concluded.

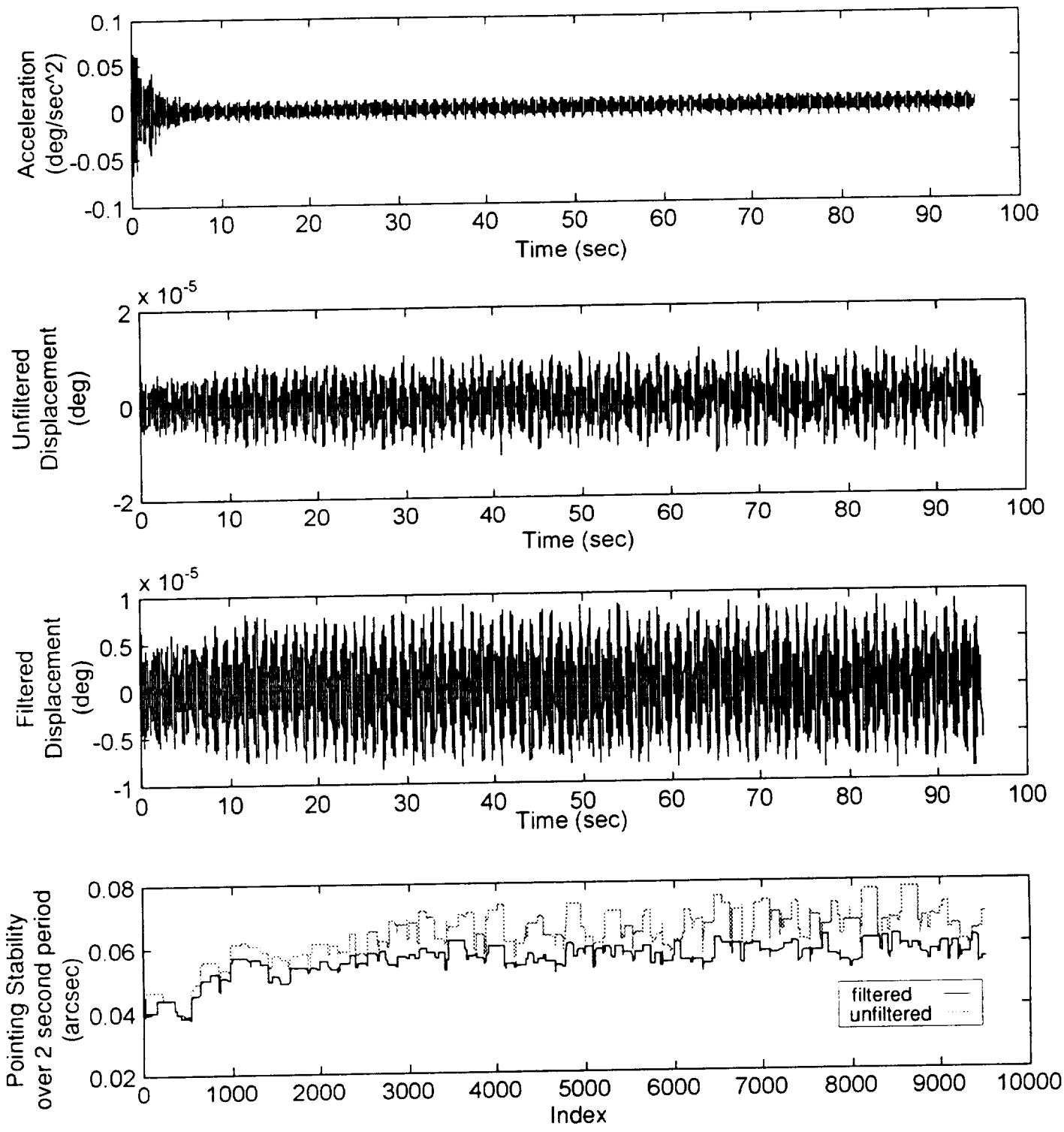

(a) Uncontrolled response

Figure 3. - Integration and pointing stability results at the SOL PAS in the -X ISS Axis for the response due to SARJ disturbance.

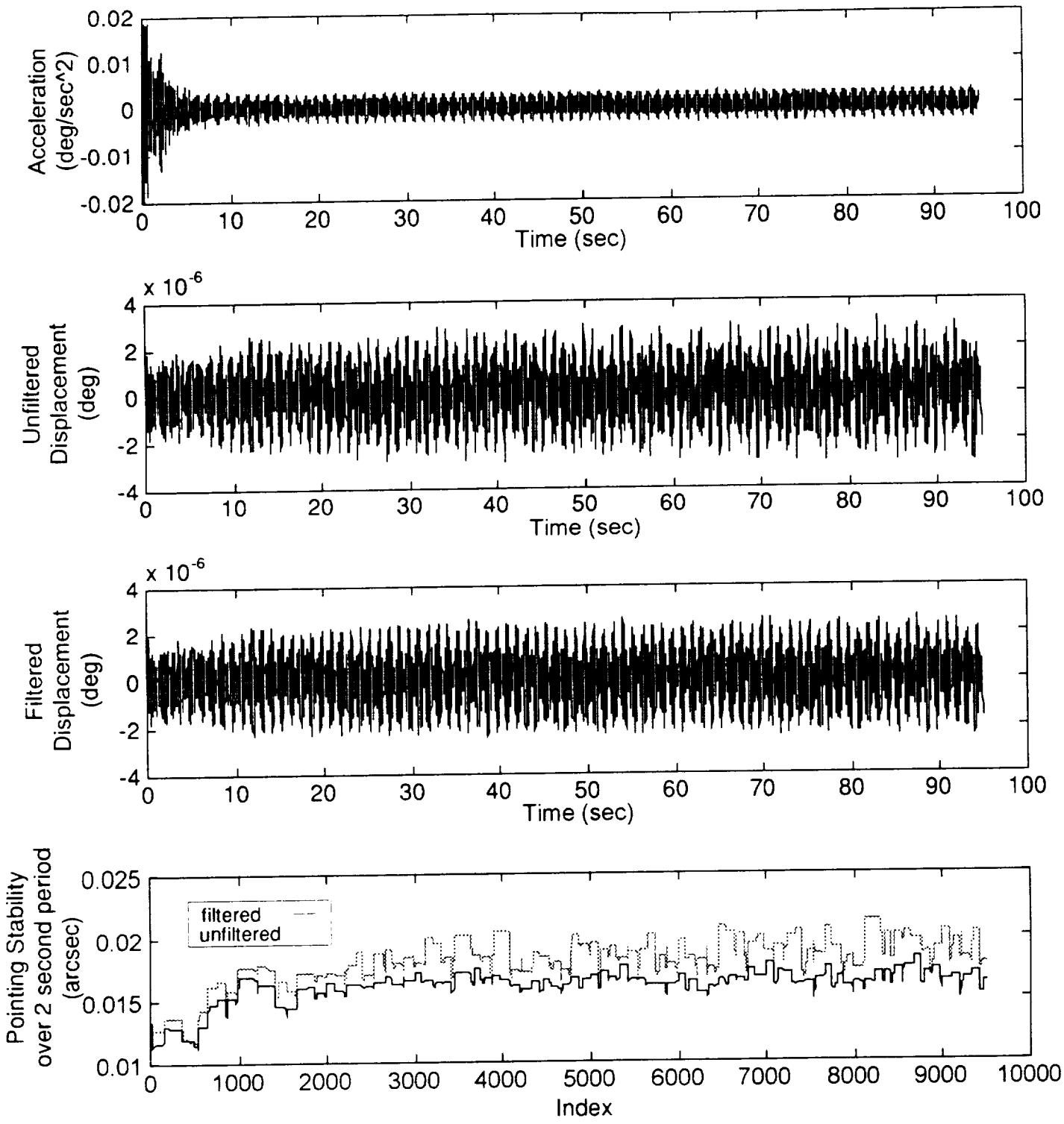

(b) Controlled response

Figure 3. - Concluded.

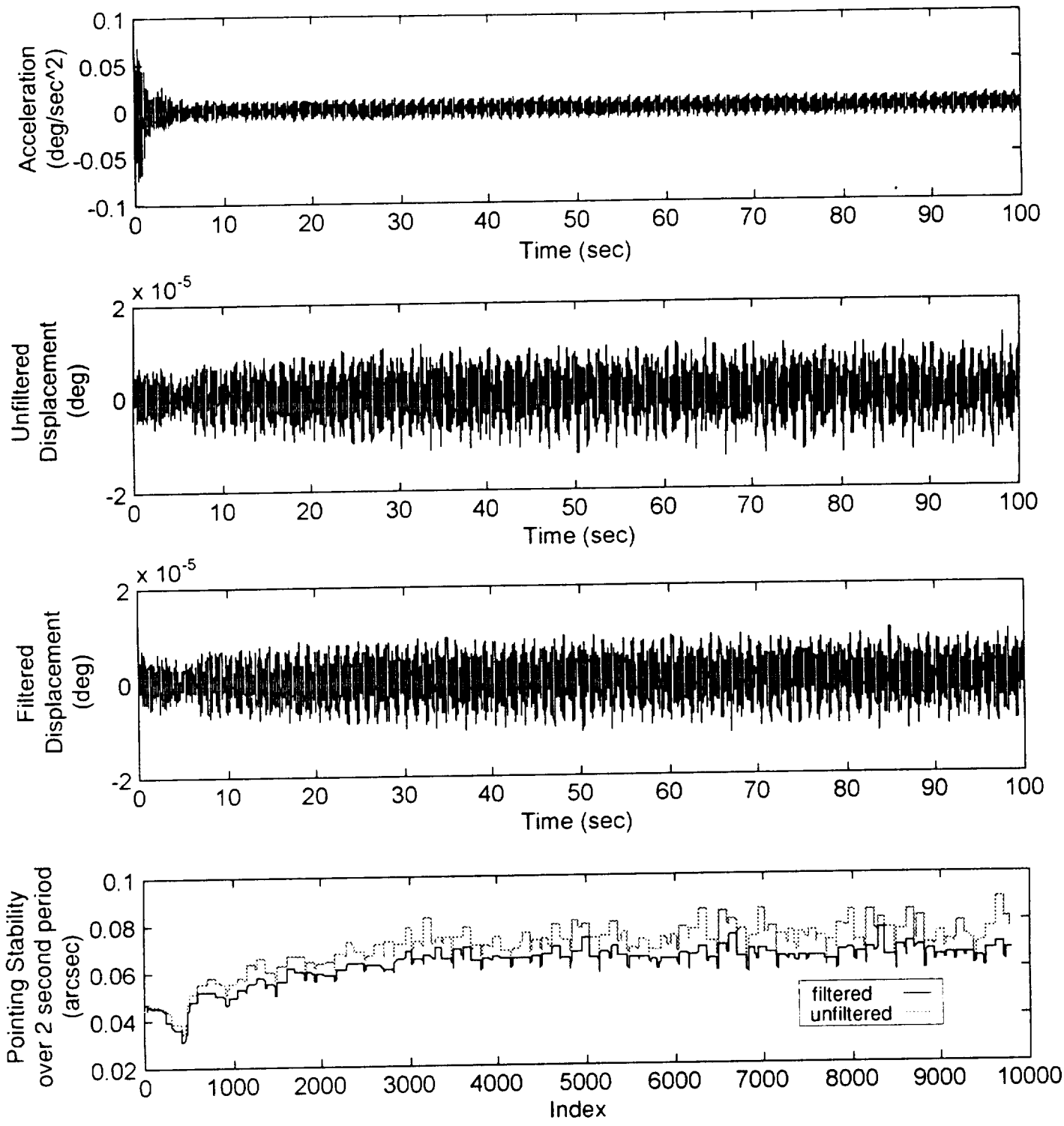

(a) Uncontrolled response

Figure 4. - Integration and pointing stability results at the SOU PAS in the -X ISS Axis for the response due to SARJ disturbance.

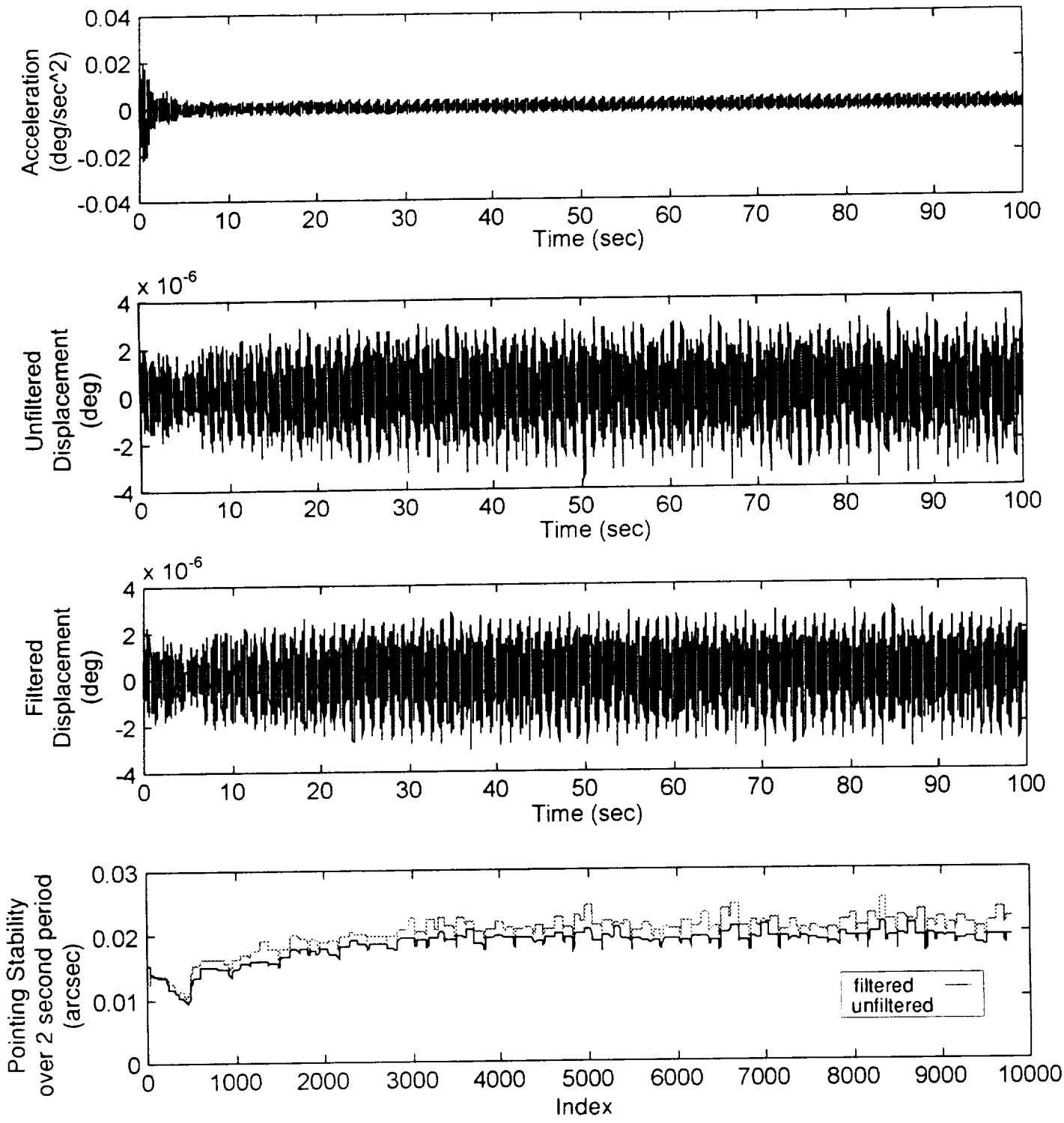

(b) Controlled response

Figure 4. - Concluded.

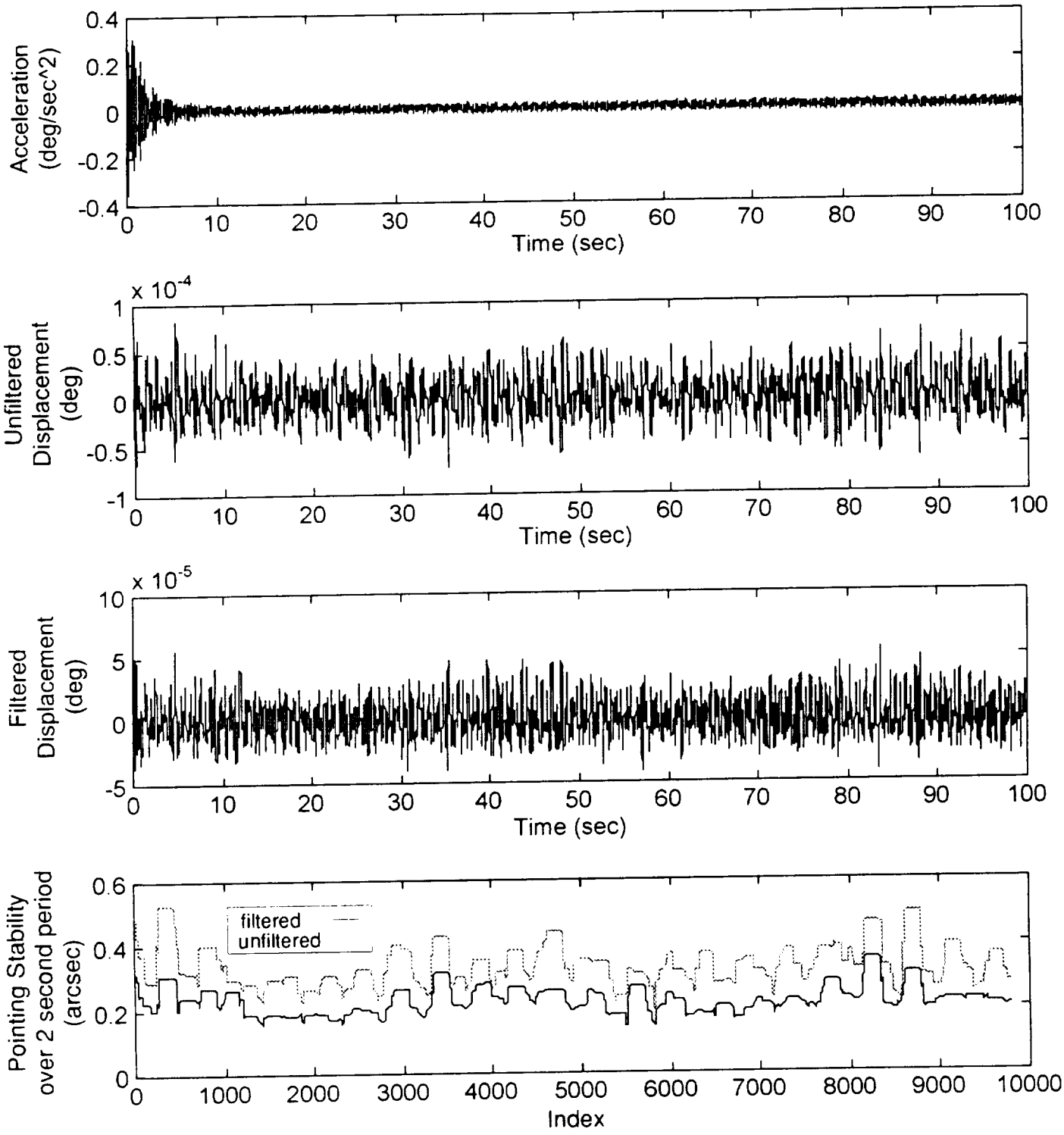

(a) Uncontrolled response

Figure 5.- Integration and pointing stability results at the SIL PAS in the Y ISS Axis for the response due to SARJ disturbance.

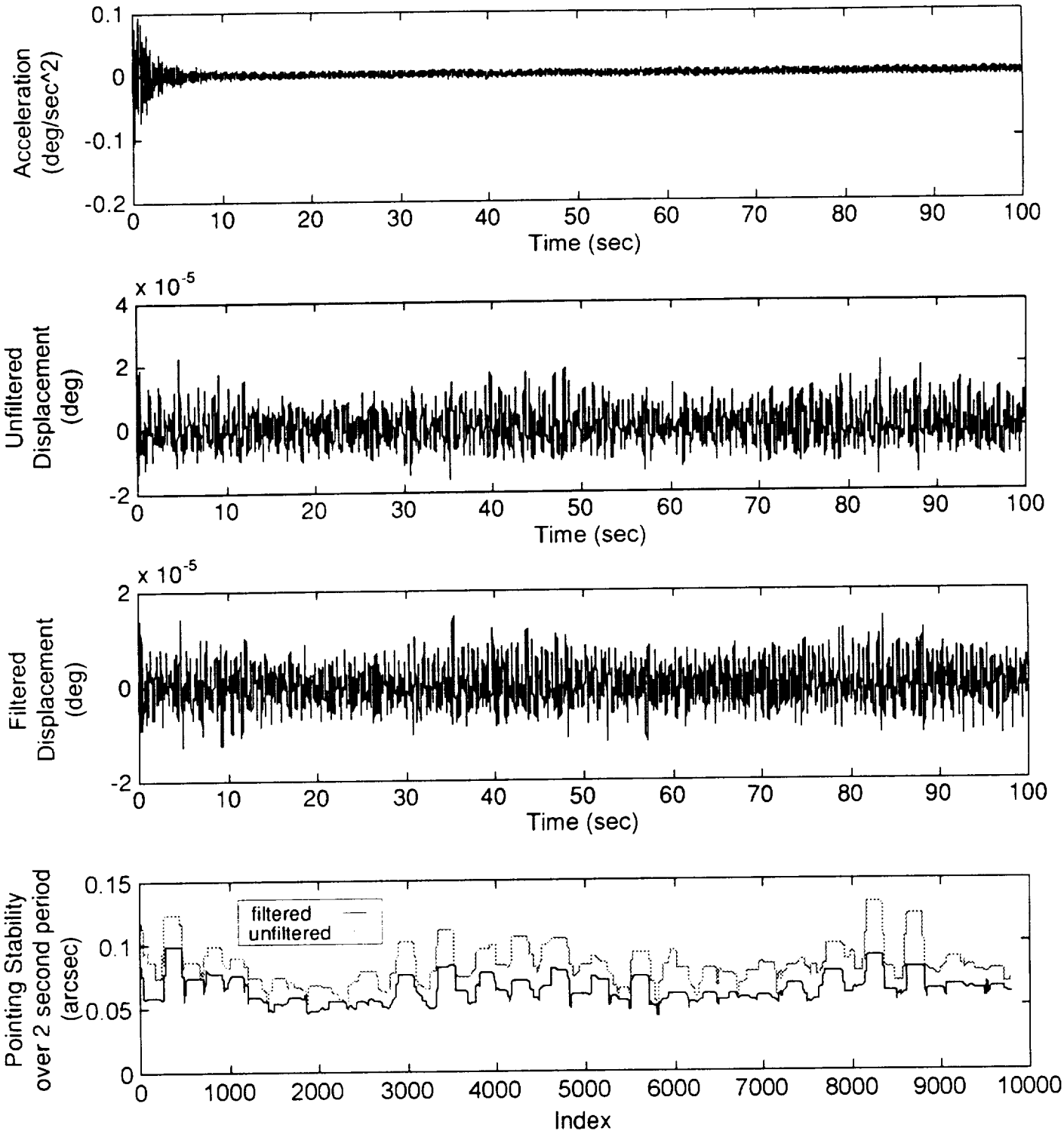

(b) Controlled response

Figure 5. - Concluded.

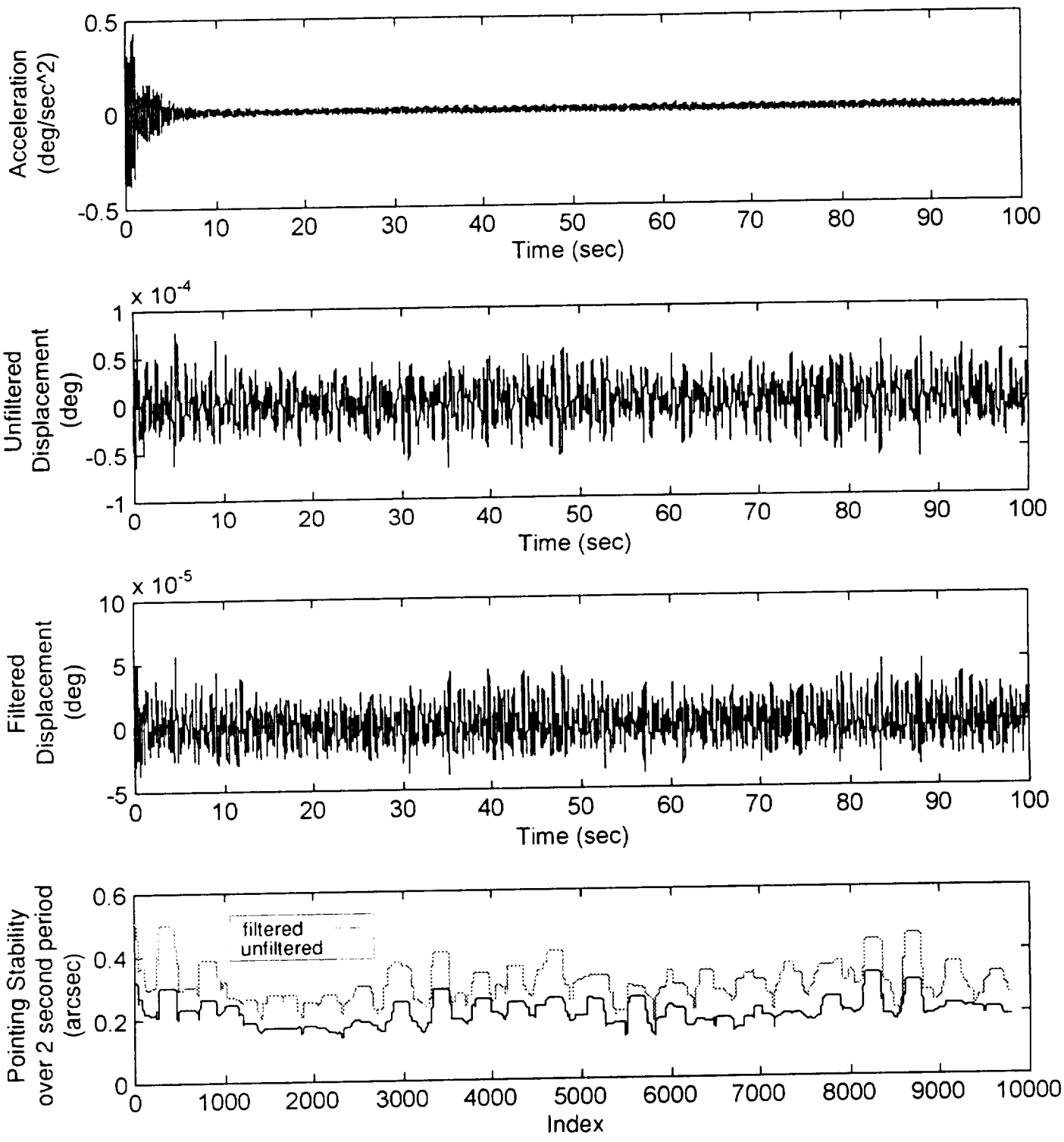

(a) Uncontrolled response

Figure 6. - Integration and pointing stability results at the SIU PAS in the Y ISS Axis for the response due to SARJ disturbance.

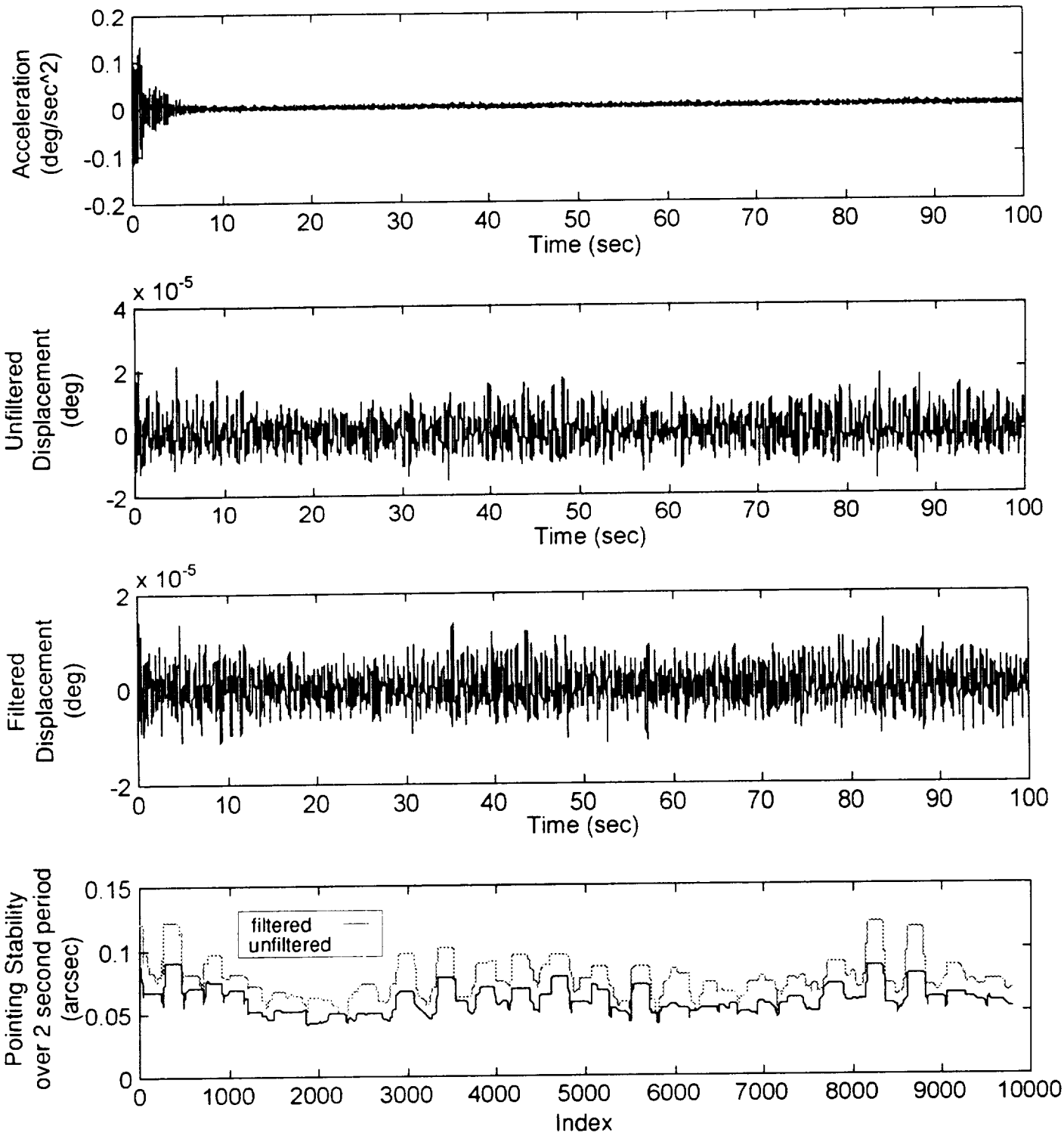

(b) Controlled response

Figure 6. - Concluded.

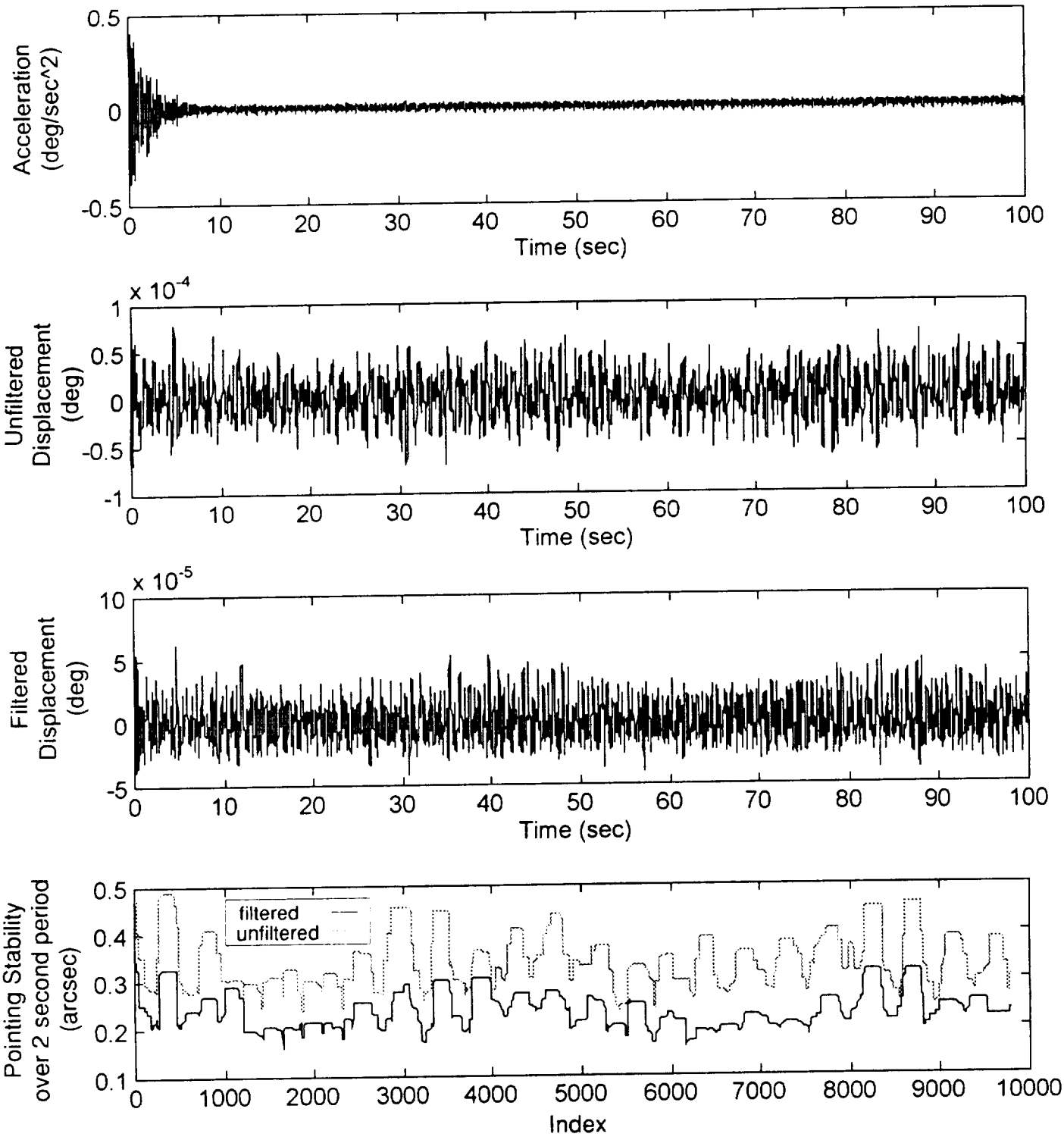

(a) Uncontrolled response

Figure 7. - Integration and pointing stability results at the SOL PAS in the Y ISS Axis for the response due to SARJ disturbance.

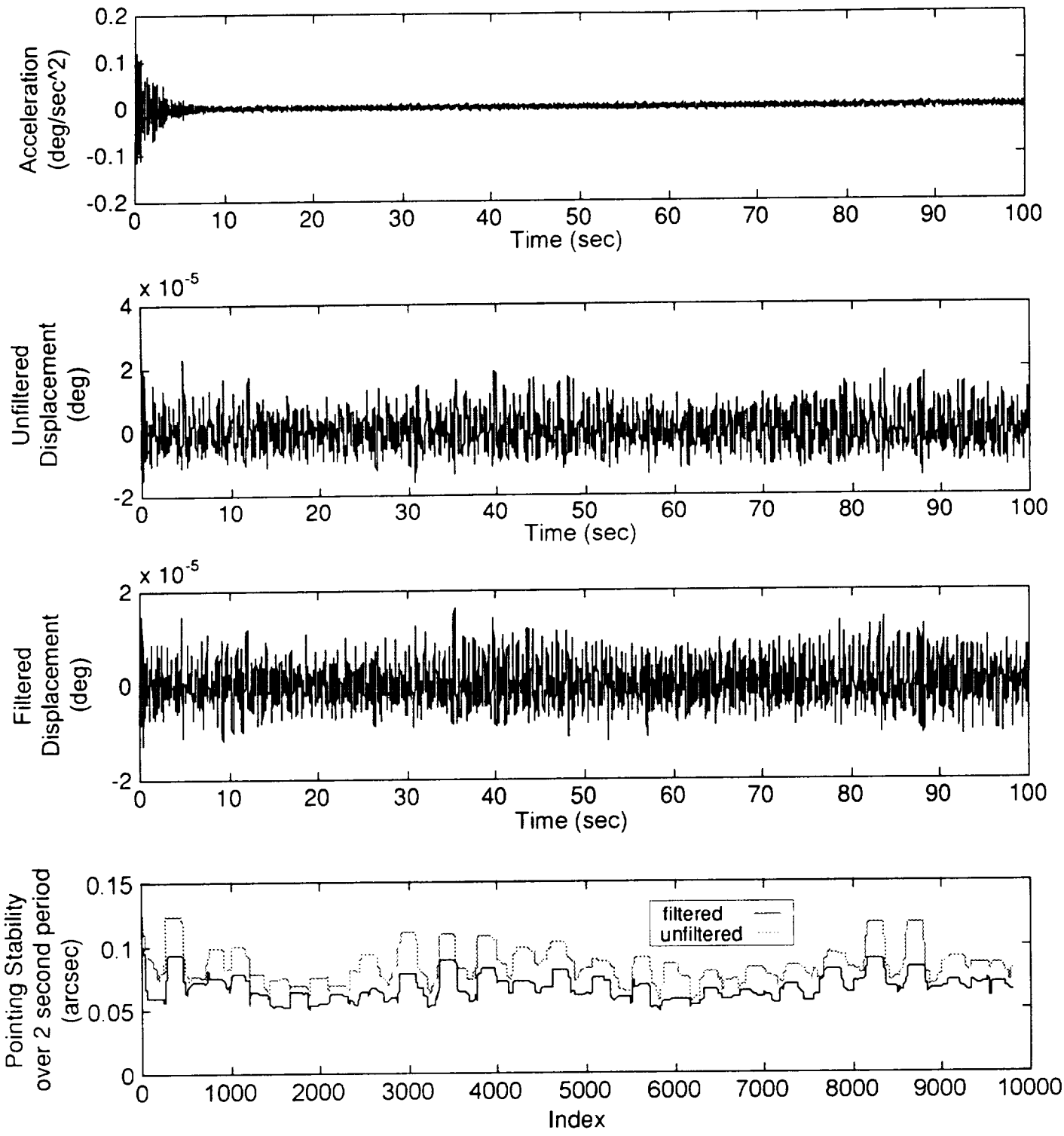

(b) Controlled response

Figure7. - Concluded.

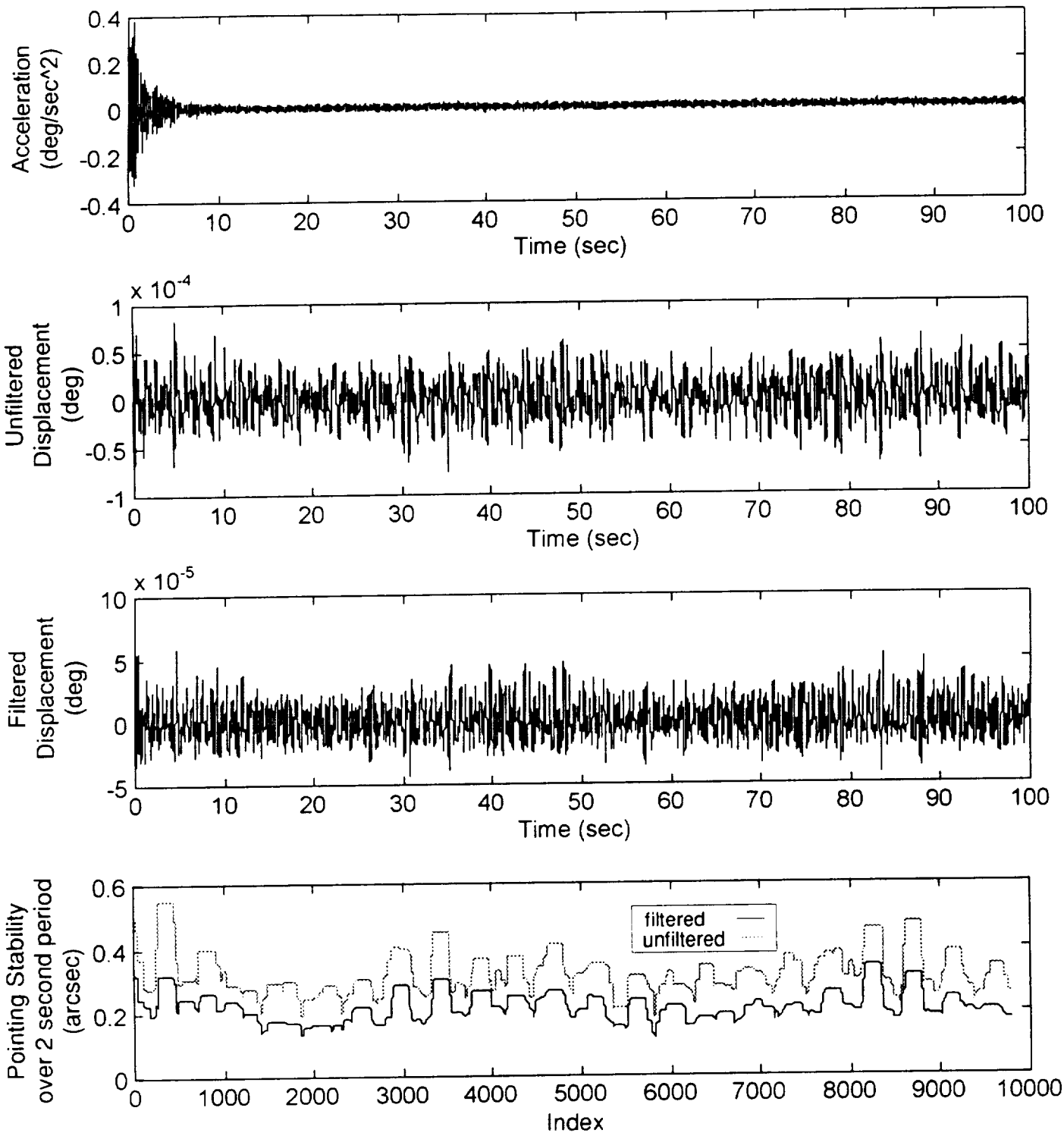

(a) Uncontrolled response

Figure 8. - Integration and pointing stability results at the SOU PAS in the -Z ISS Axis for the response due to SARJ disturbance.

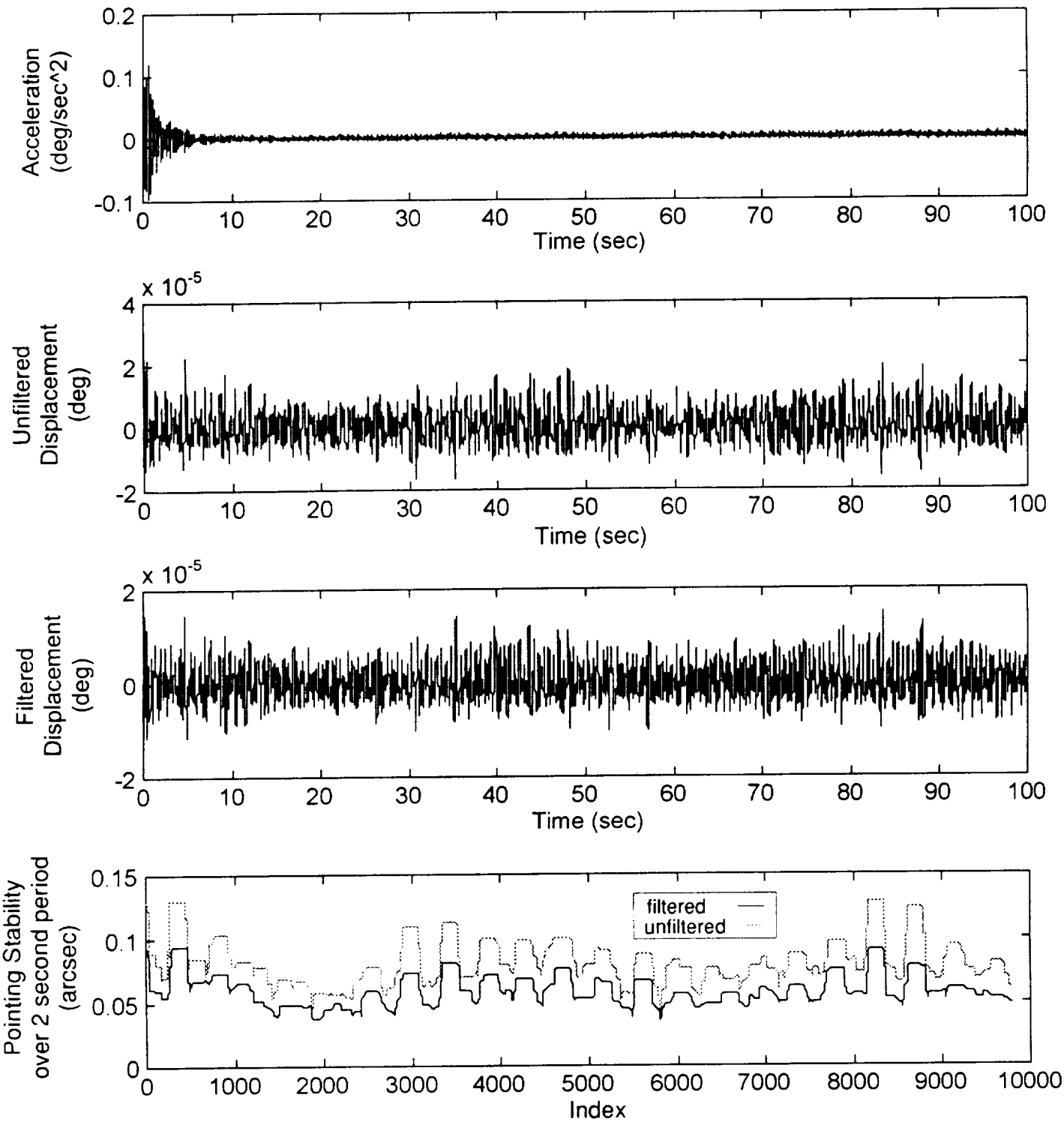

(b) Controlled response

Figure 8. - Concluded.

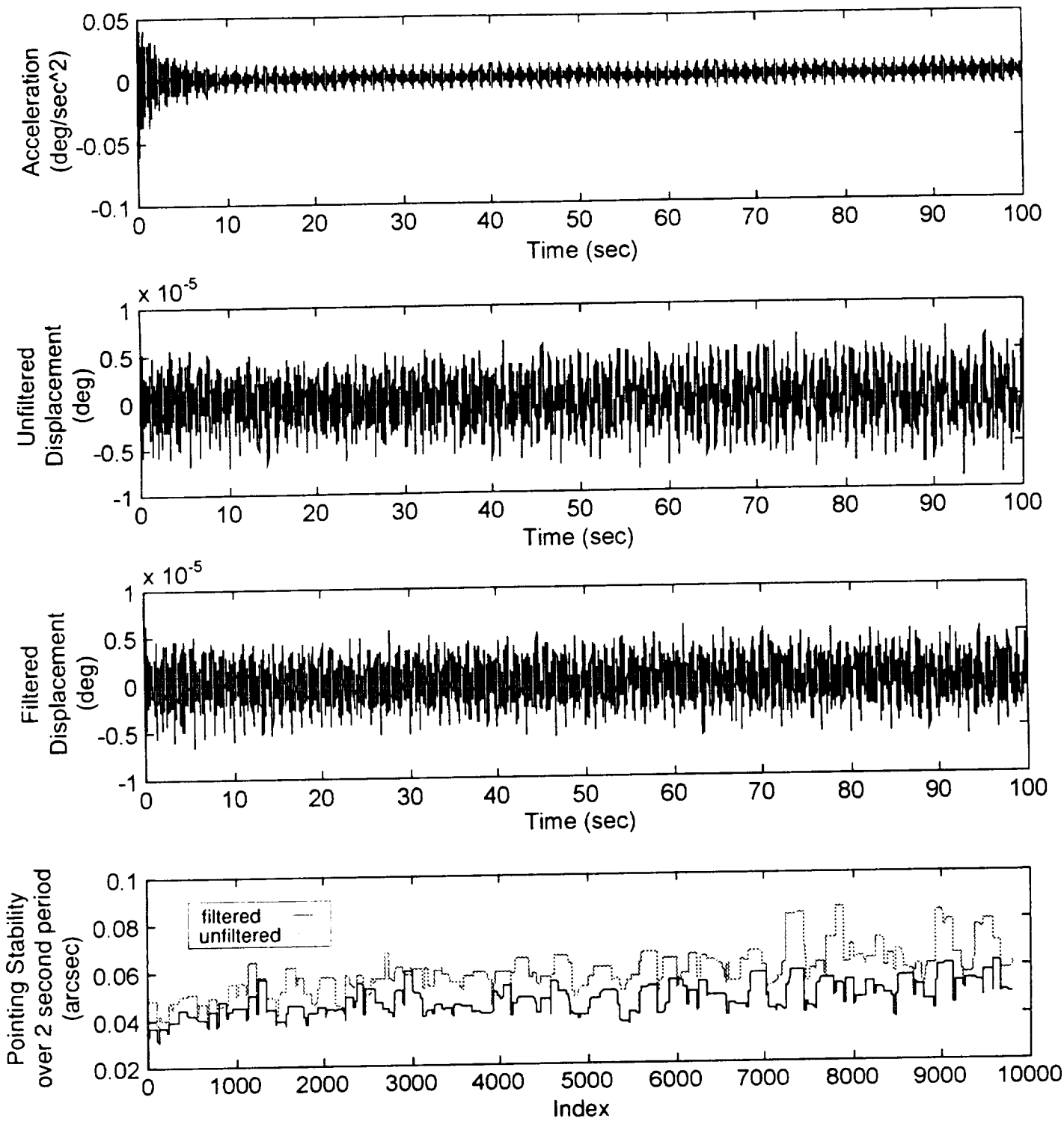

(a) Uncontrolled response

Figure 9. - Integration and pointing stability results at the SIL PAS in the -Z ISS Axis for the response due to SARJ disturbance.

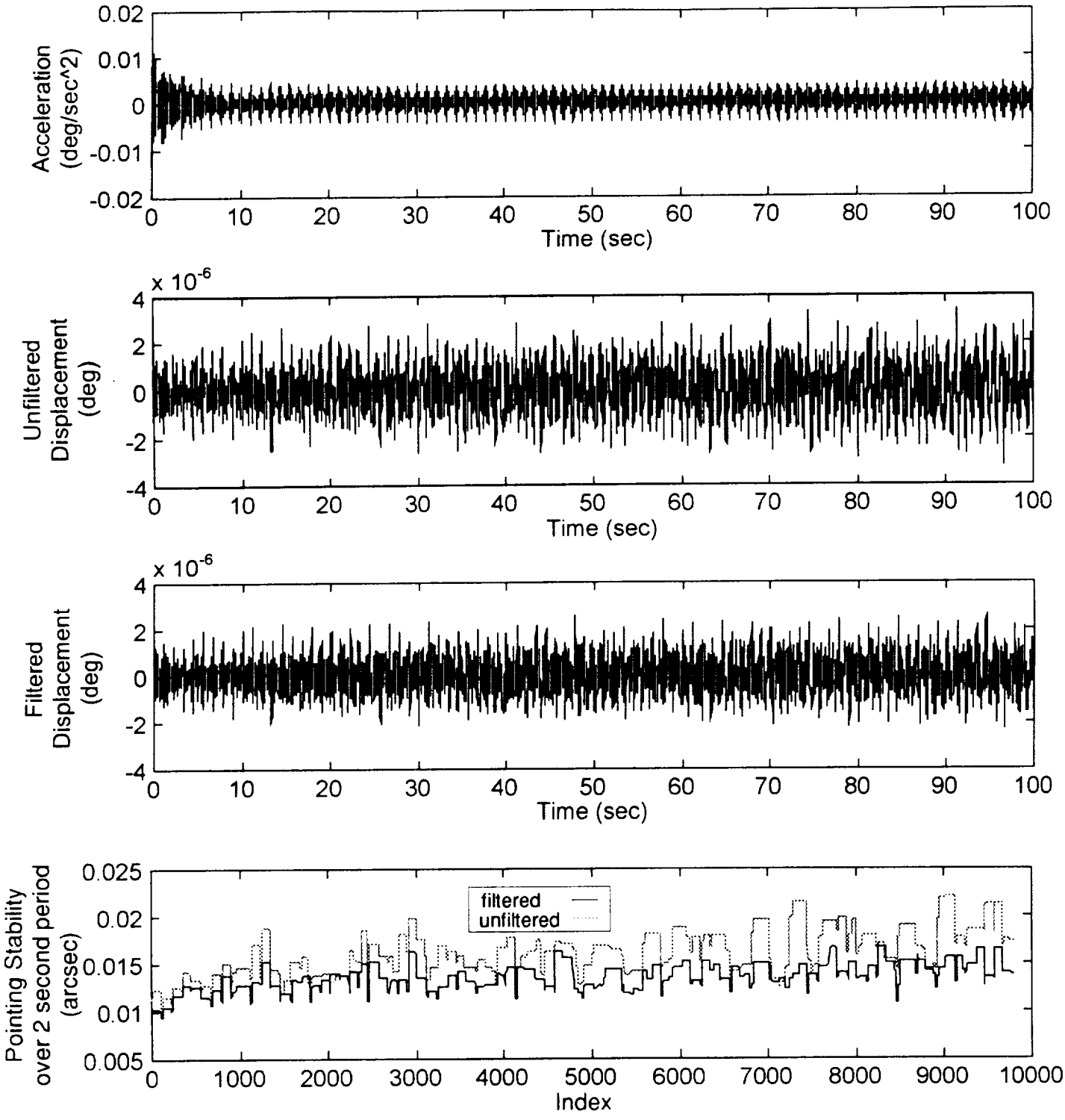

(b) Controlled response

Figure 9. - Concluded.

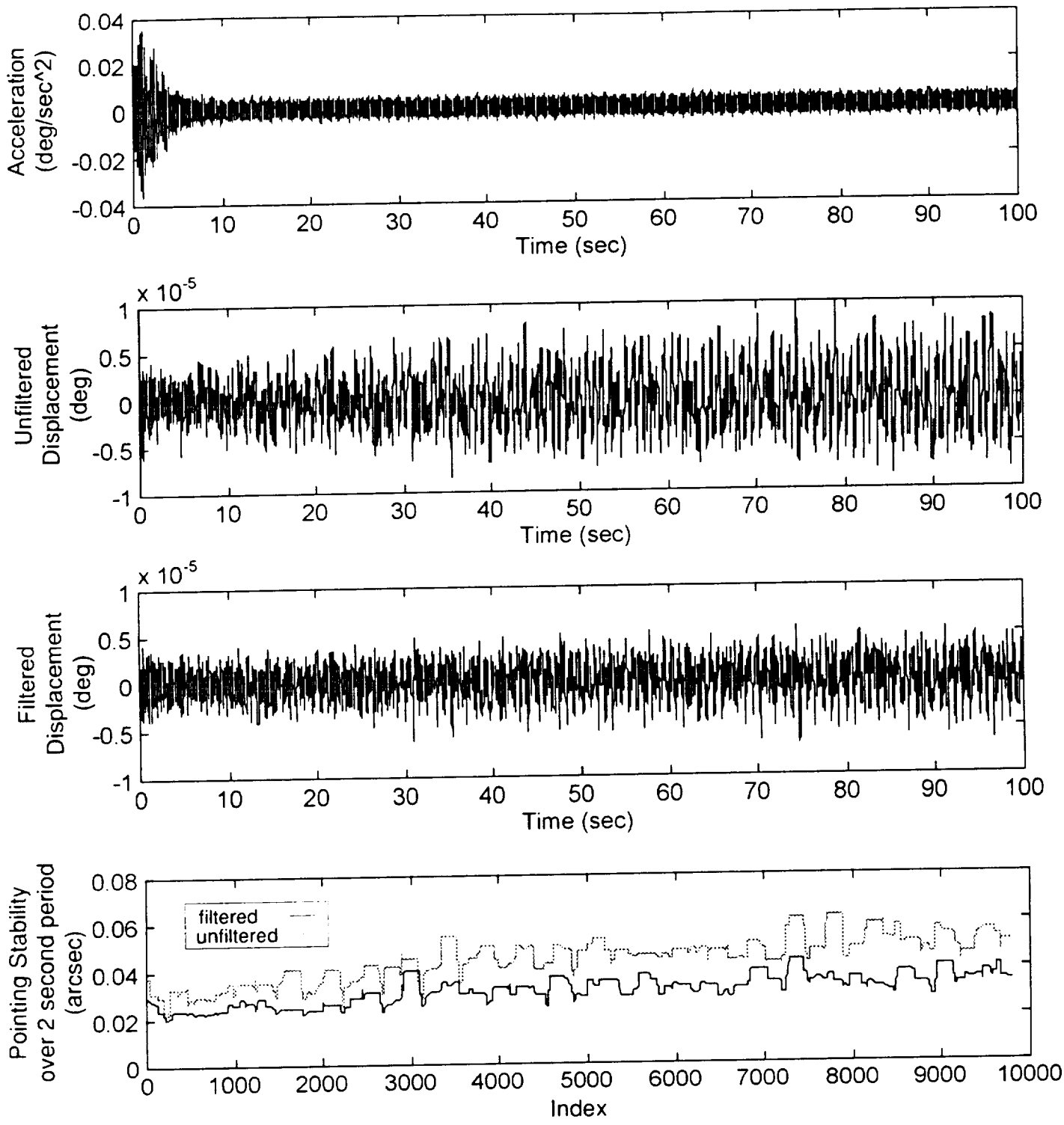

(a) Uncontrolled response

Figure 10. - Integration and pointing stability results at the SIU PAS in the -Z ISS Axis for the response due to SARJ disturbance.

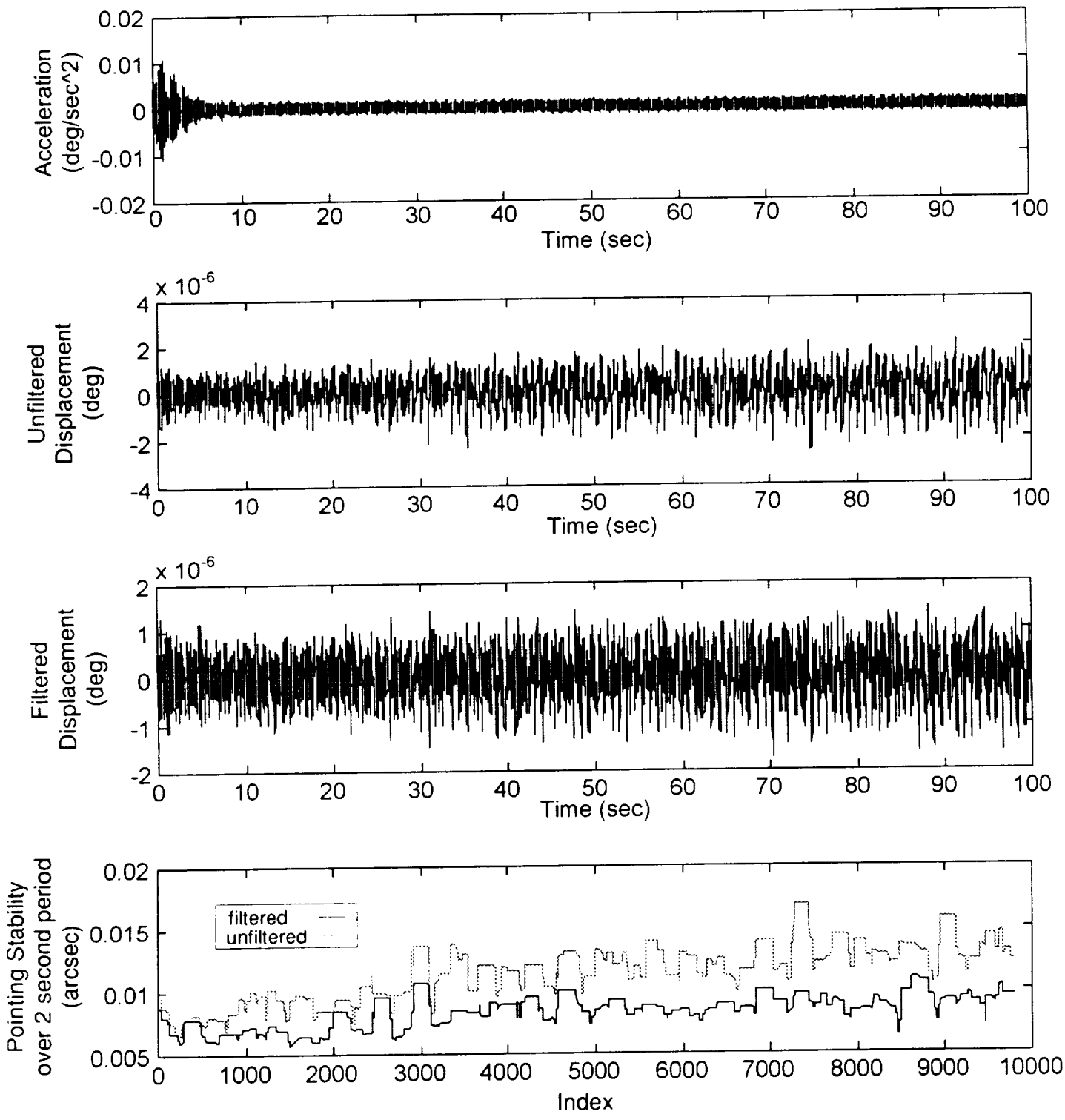

(b) Controlled response

Figure 10. - Concluded.

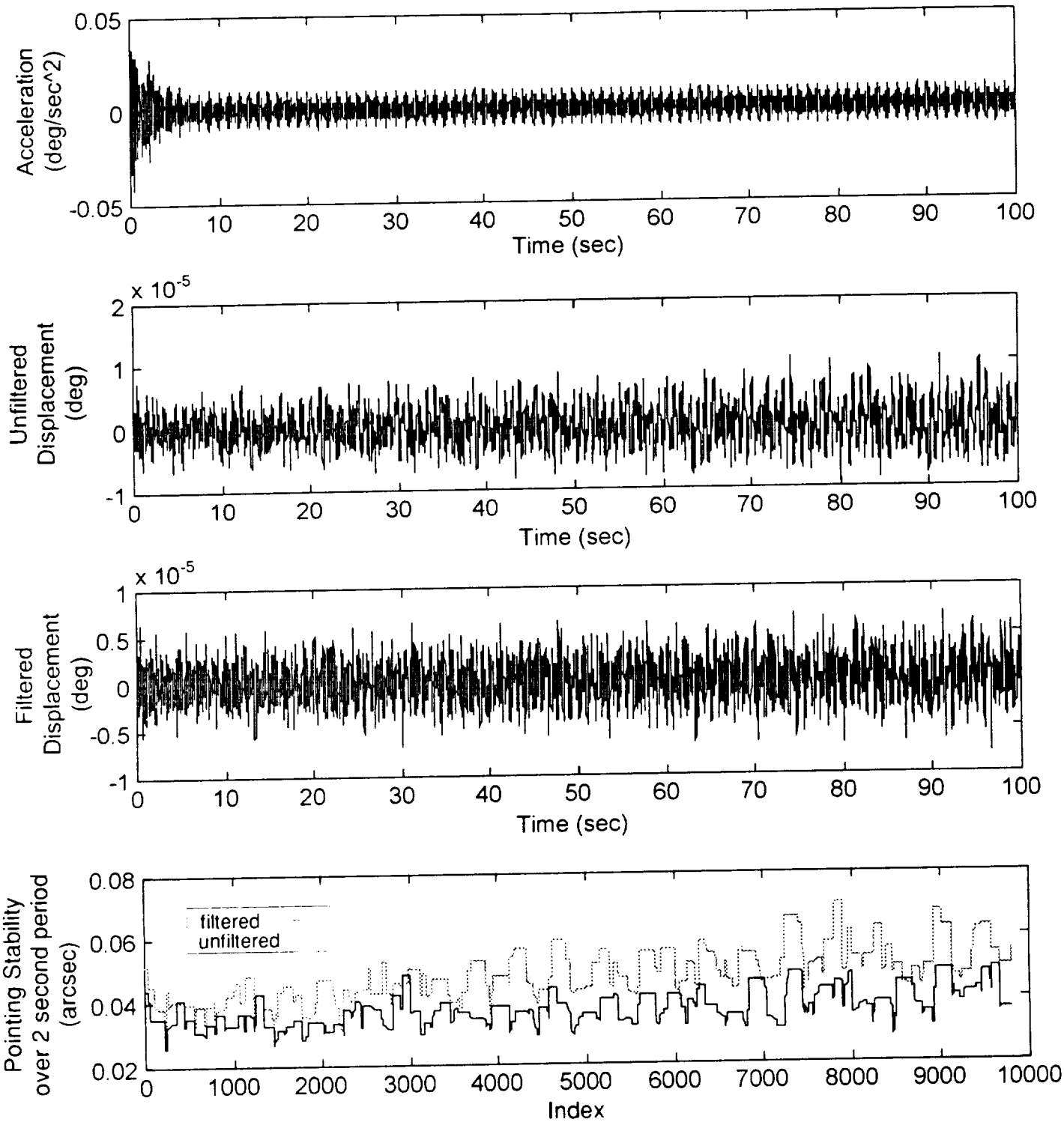

(a) Uncontrolled response

Figure 11. - Integration and pointing stability results at the SOL PAS in the -Z ISS Axis for the responses due to SARJ disturbance.

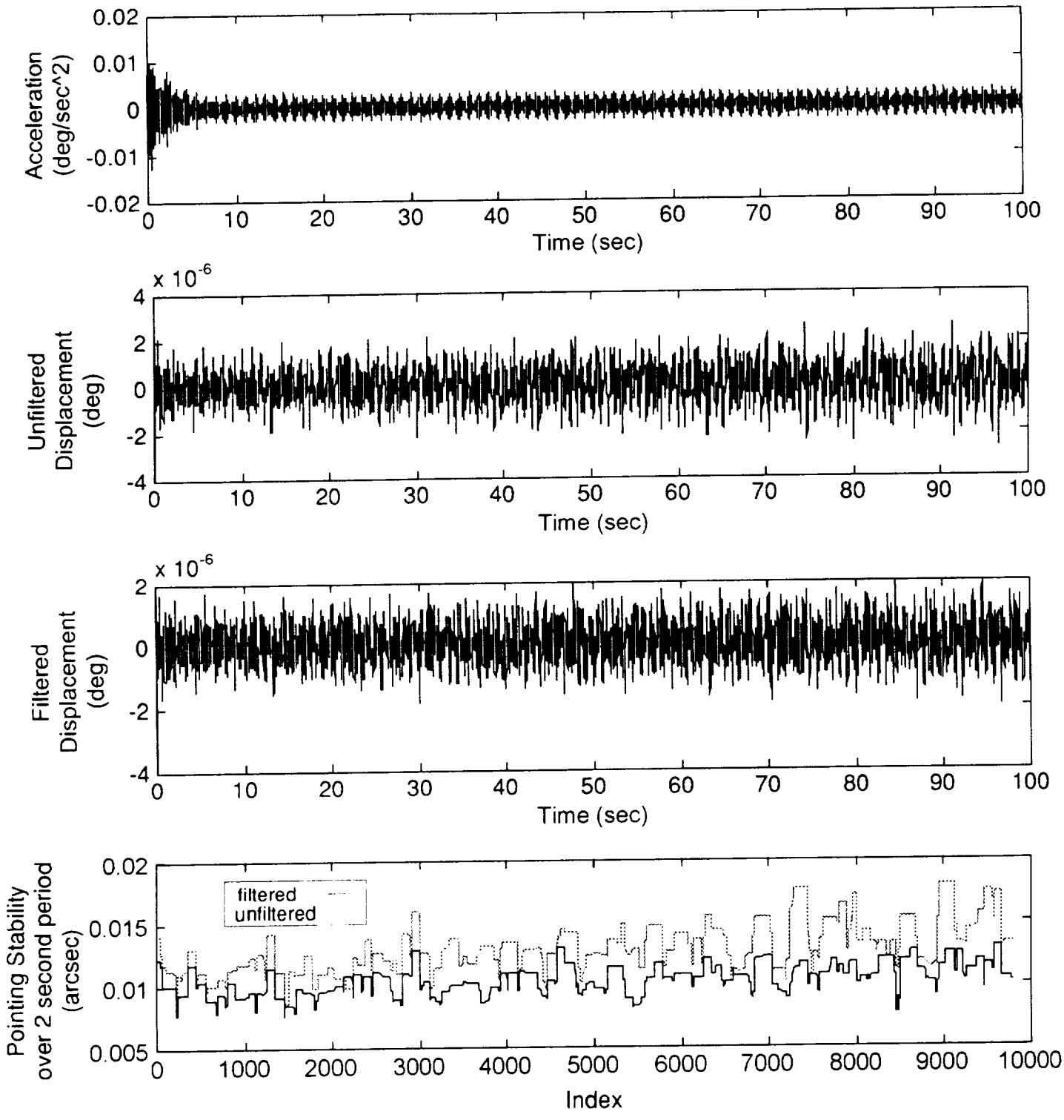

(b) Controlled response

Figure 11. - Concluded

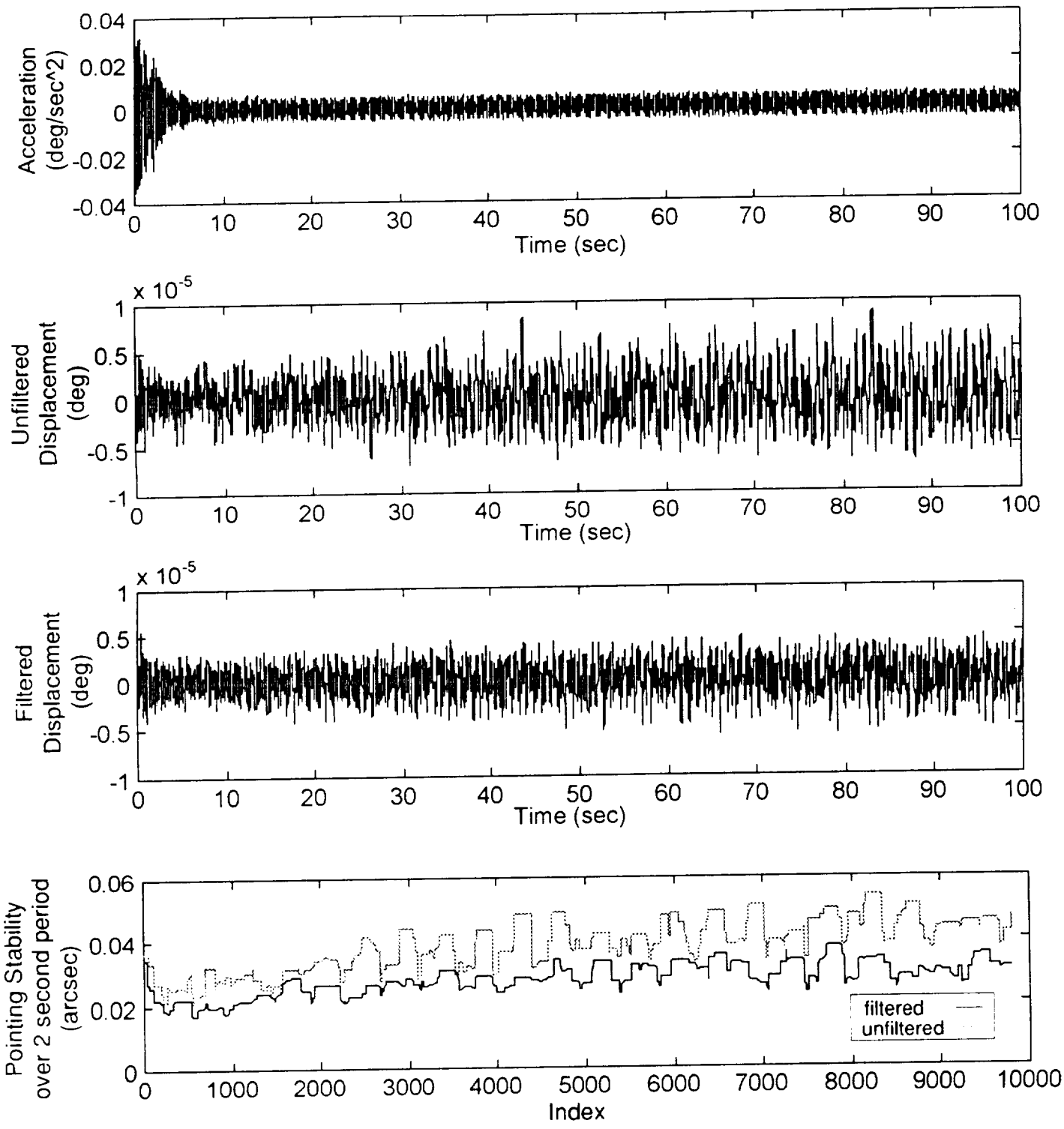

(a) Uncontrolled response

Figure 12. - Integration and pointing stability results at the SOU PAS in the -Z ISS Axis for the response due to SARJ disturbance.

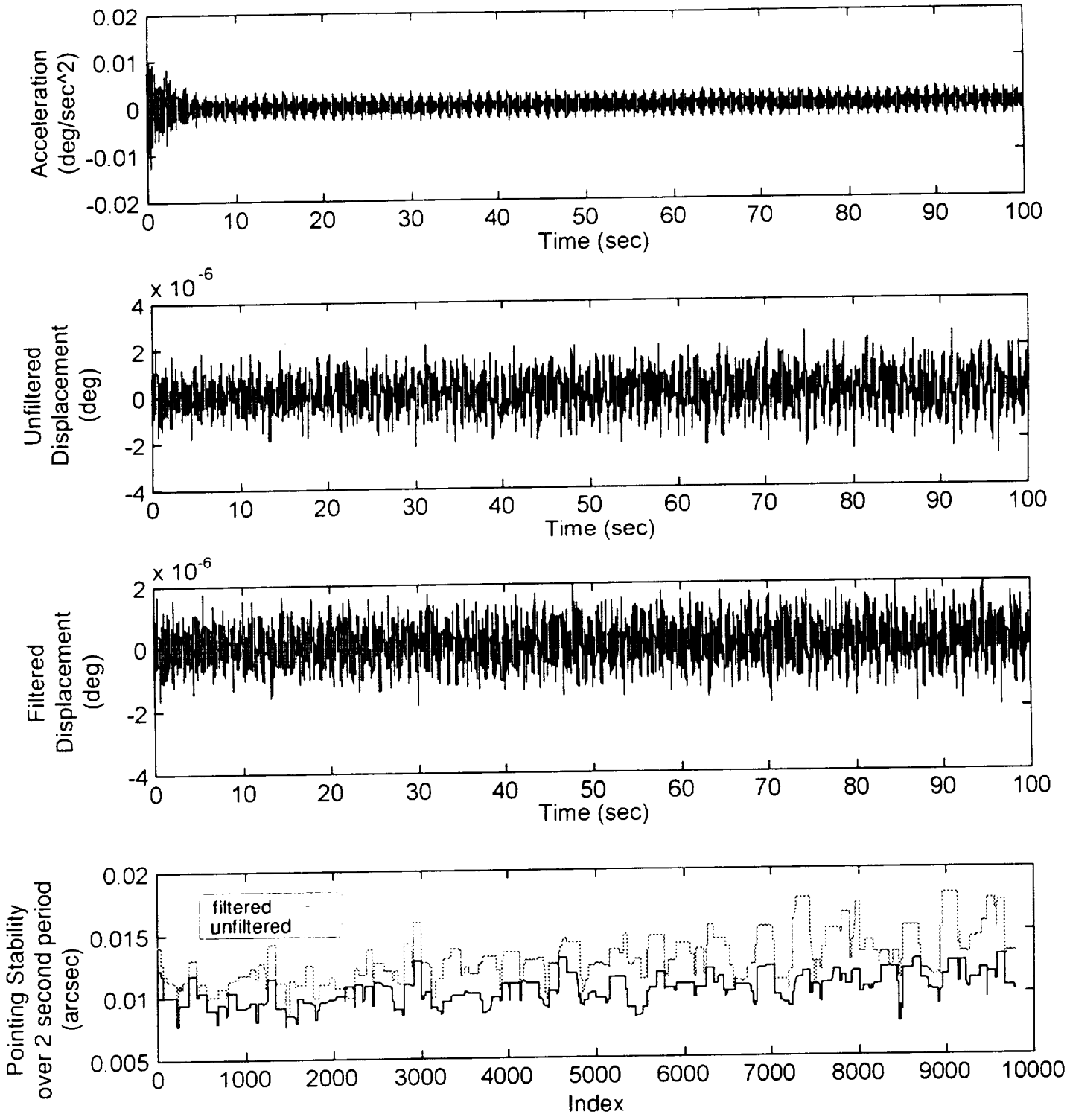

(b) Controlled response

Figure 12. - Concluded.

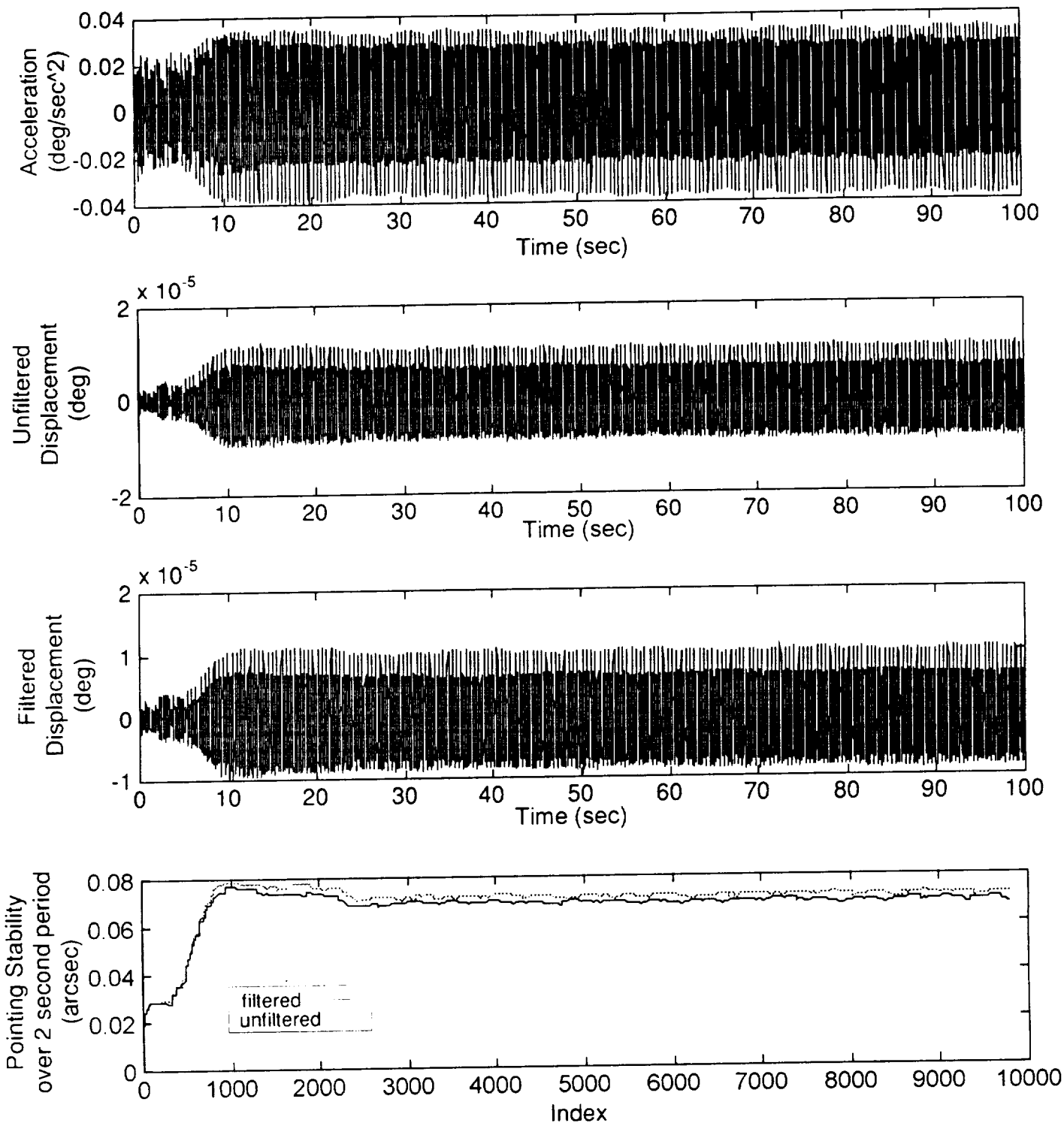

(a) Uncontrolled response

Figure 13. - Integration and pointing stability results at the SIL PAS in the -X ISS Axis for the response due to TRRJ disturbance .

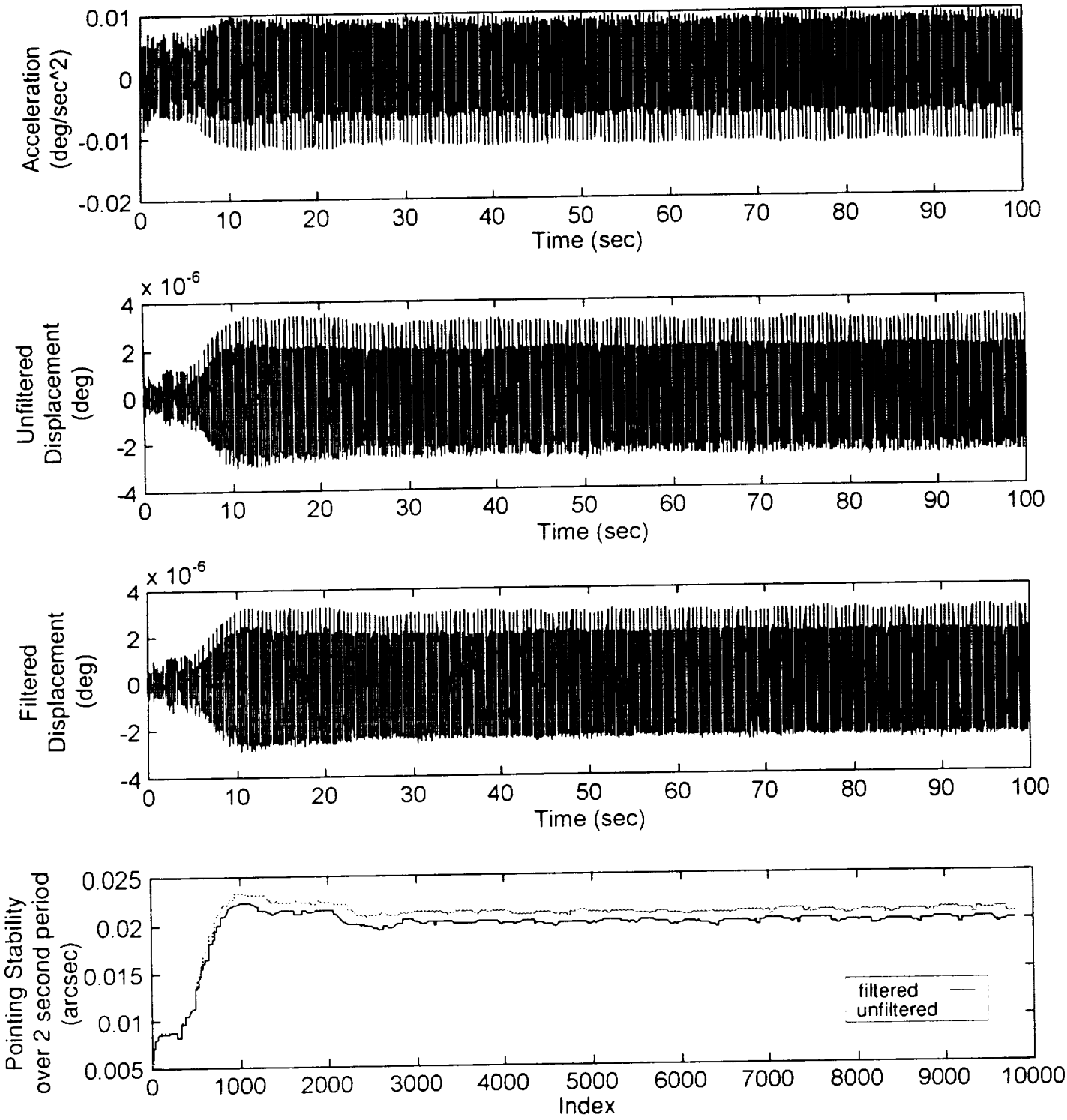

(b) Controlled response

Figure 13. Concluded.

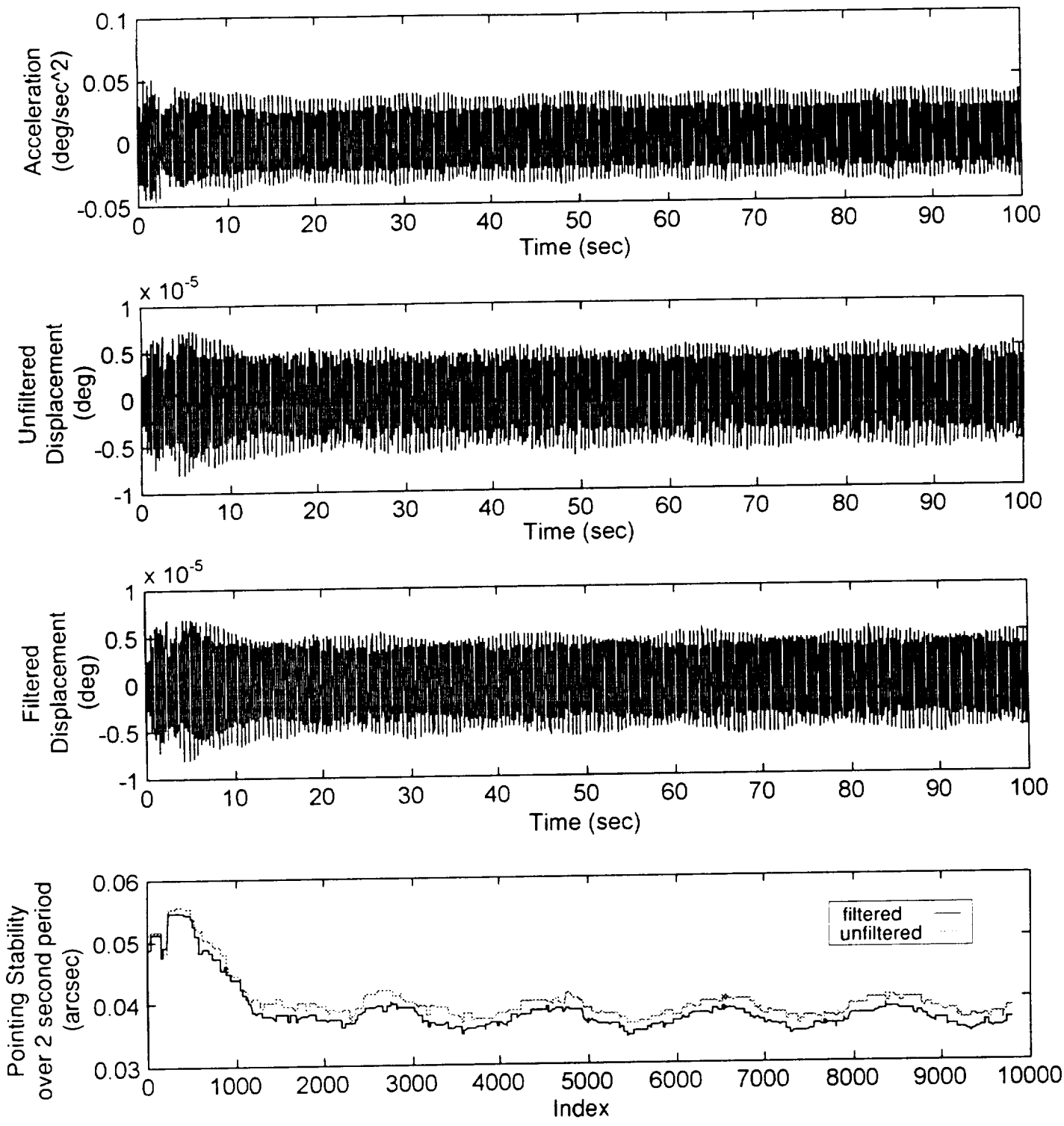

(a) Uncontrolled response

Figure 14. - Integration and pointing stability for the response at the SIU PAS in the -X ISS Axis due to TRRJ disturbance.

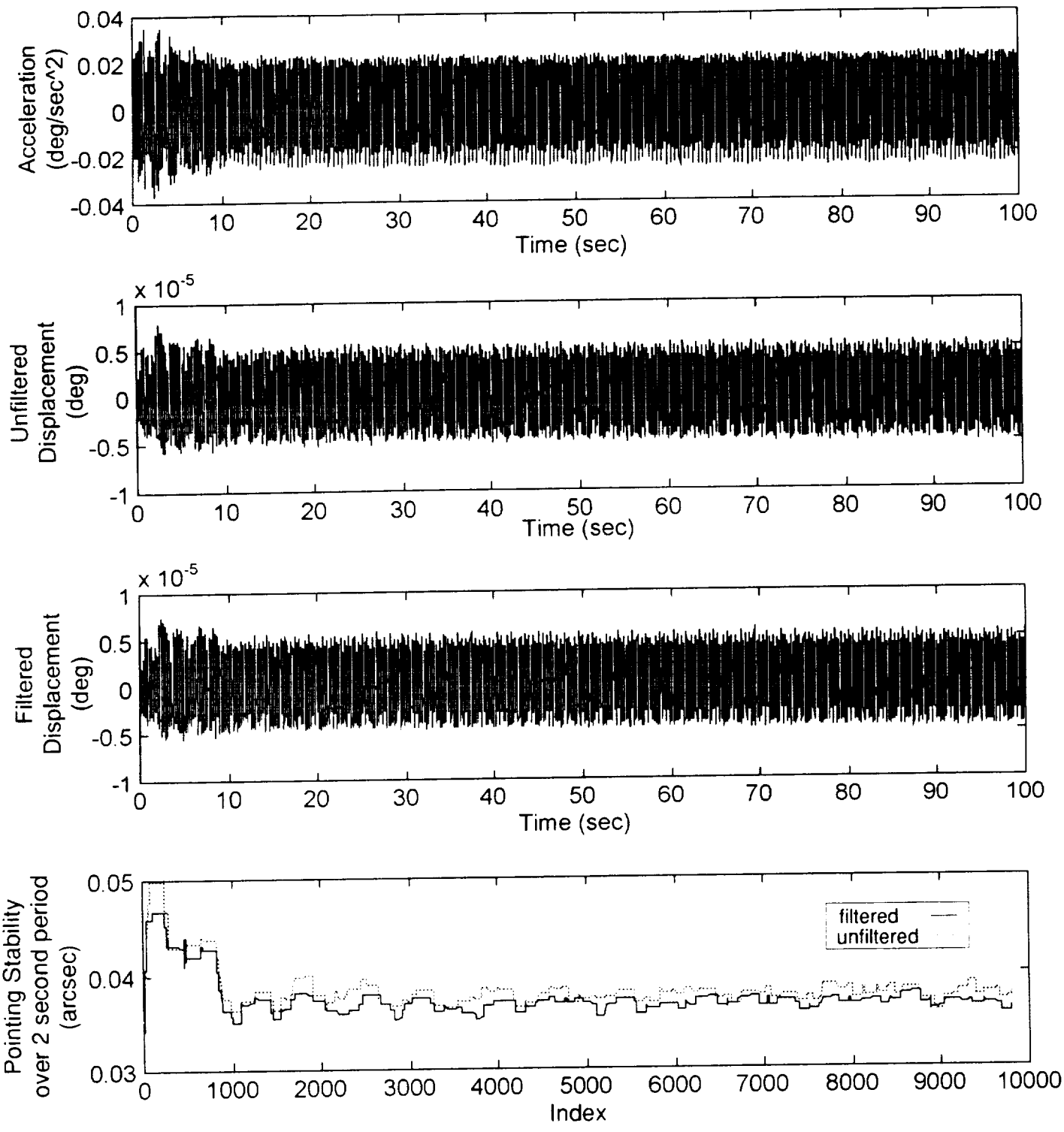

(a) Uncontrolled response

Figure 15. - Integration and pointing stability at the SOL PAS in the -X ISS Axis for the response due to TRRJ disturbance.

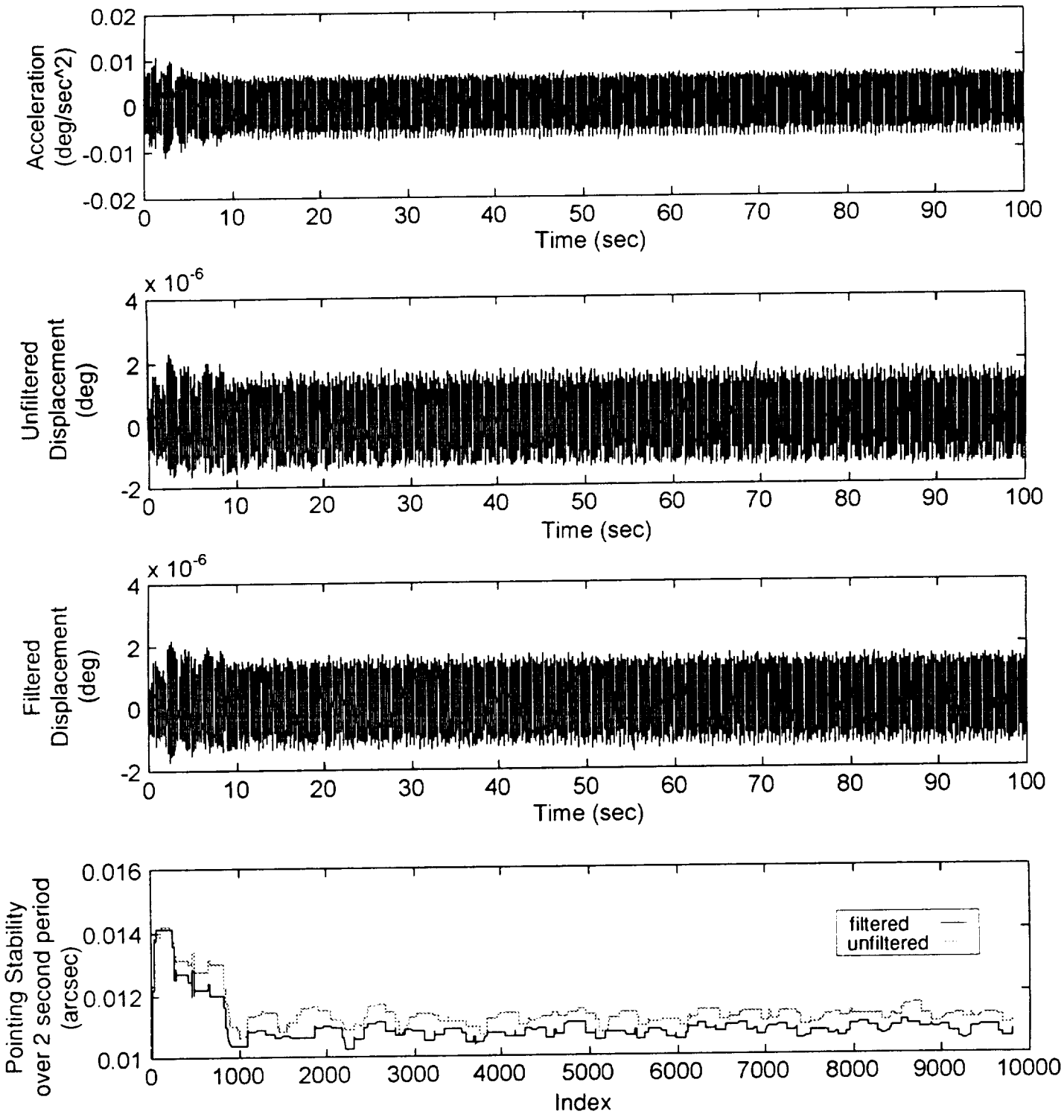

(b) Controlled response

Figure 15. - Concluded.

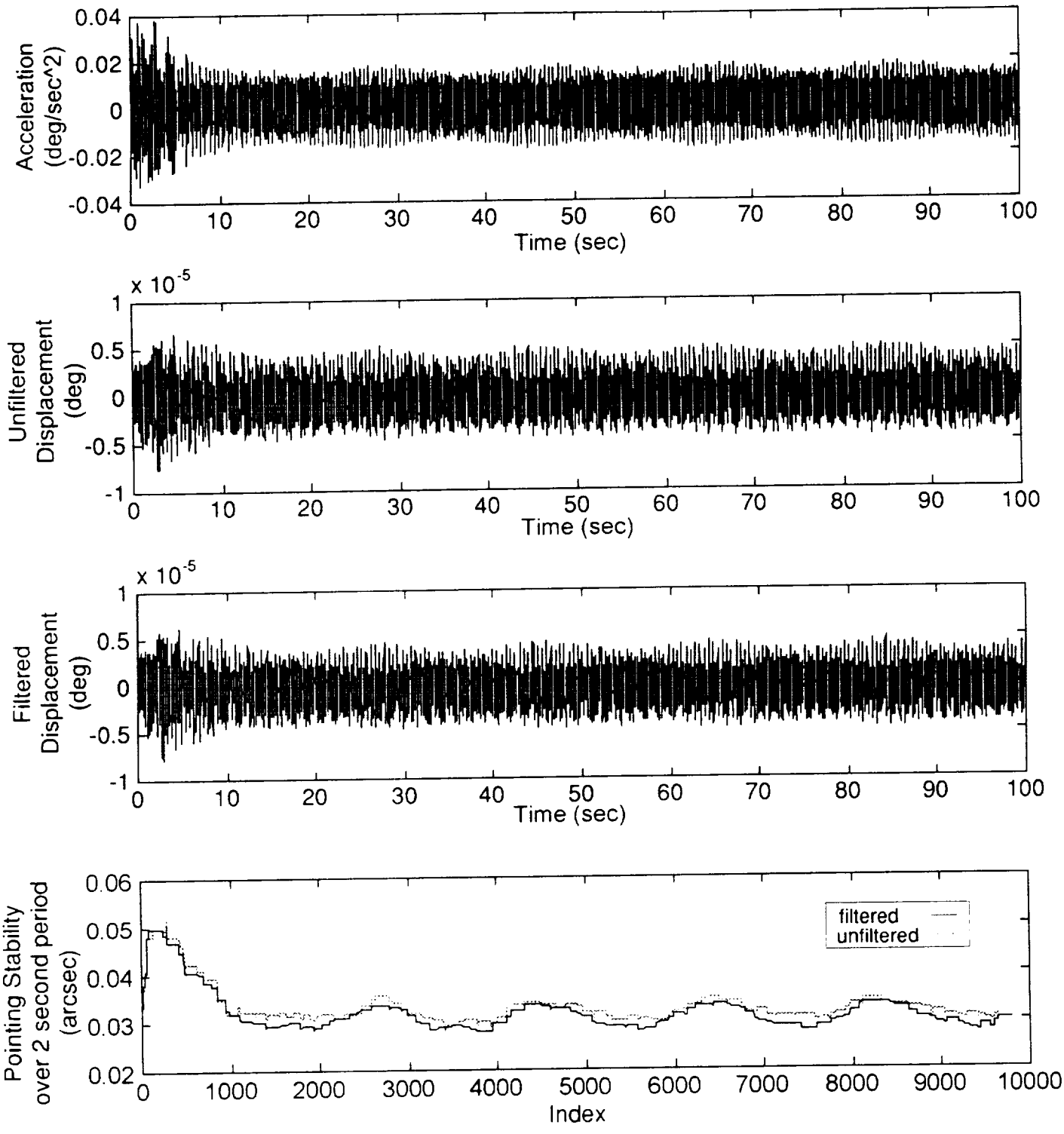

(a) Uncontrolled response

Figure 16. - Integration and pointing stability at the SOU PAS in the -X ISS Axis for the response due to TRRJ disturbance.

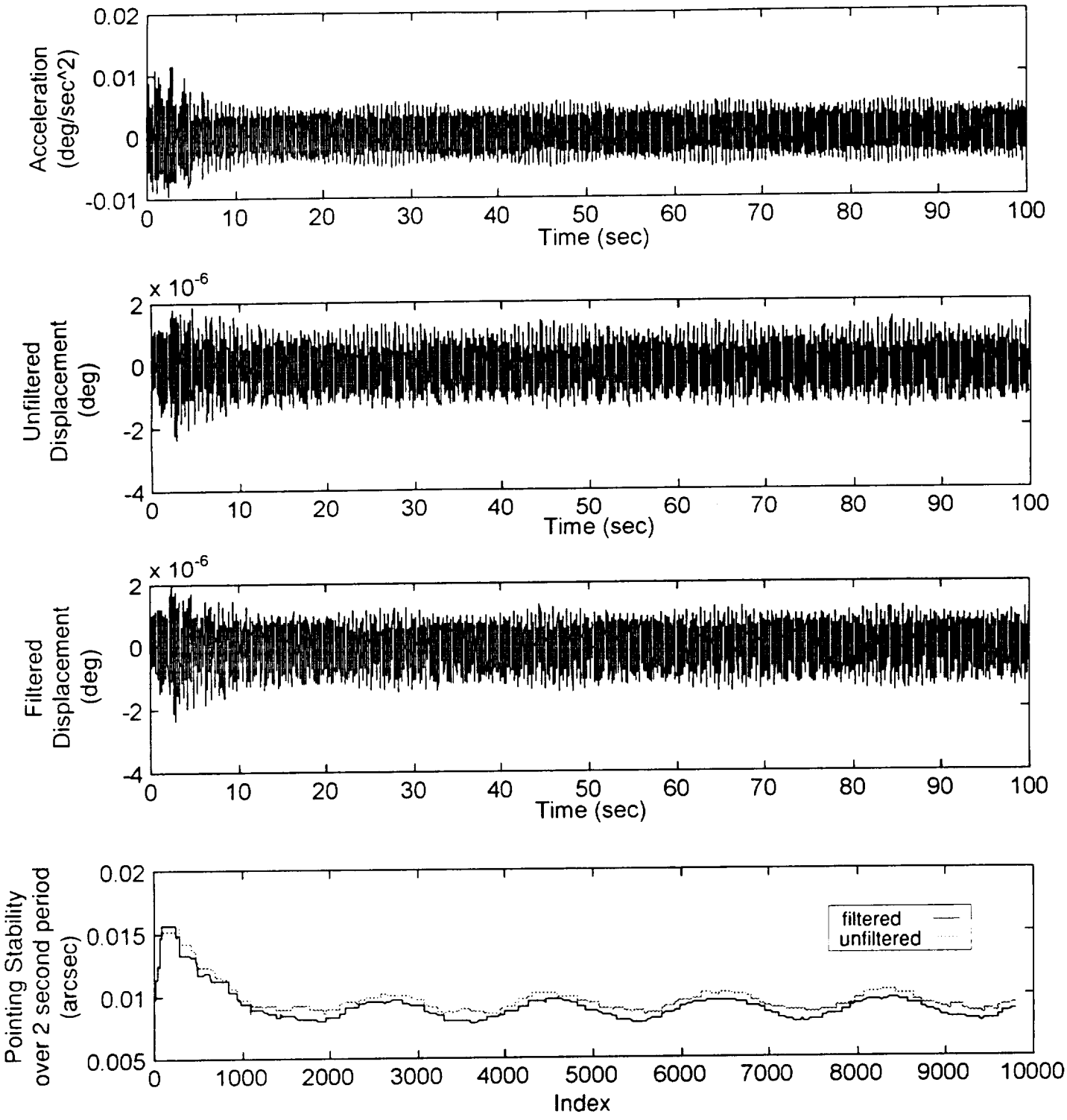

(b) Controlled response

Figure 16. - Concluded.

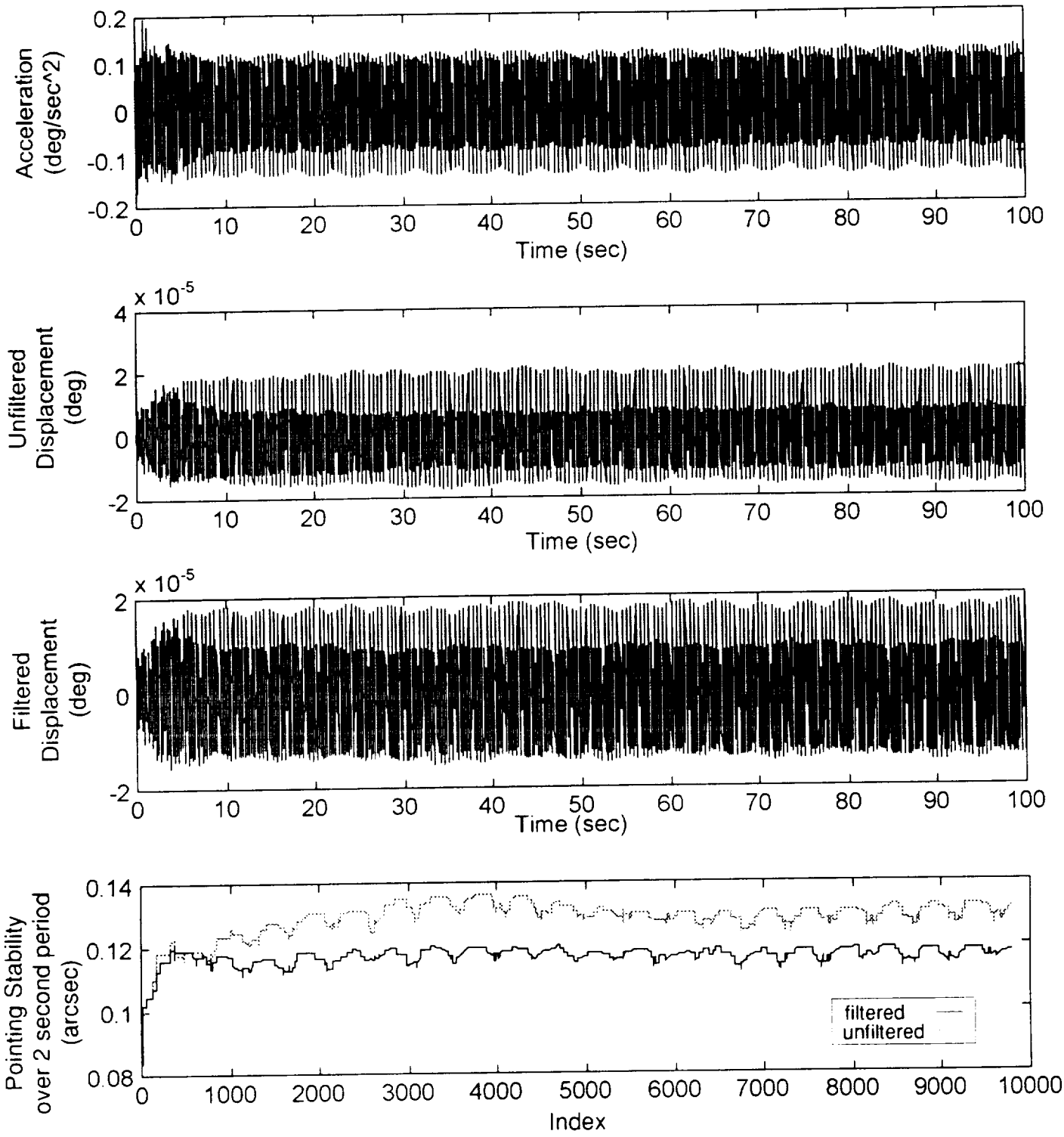

(a) Uncontrolled response

Figure 17. - Integration and pointing stability for the response at the SIL PAS in the Y ISS Axis due to TRRJ disturbance.

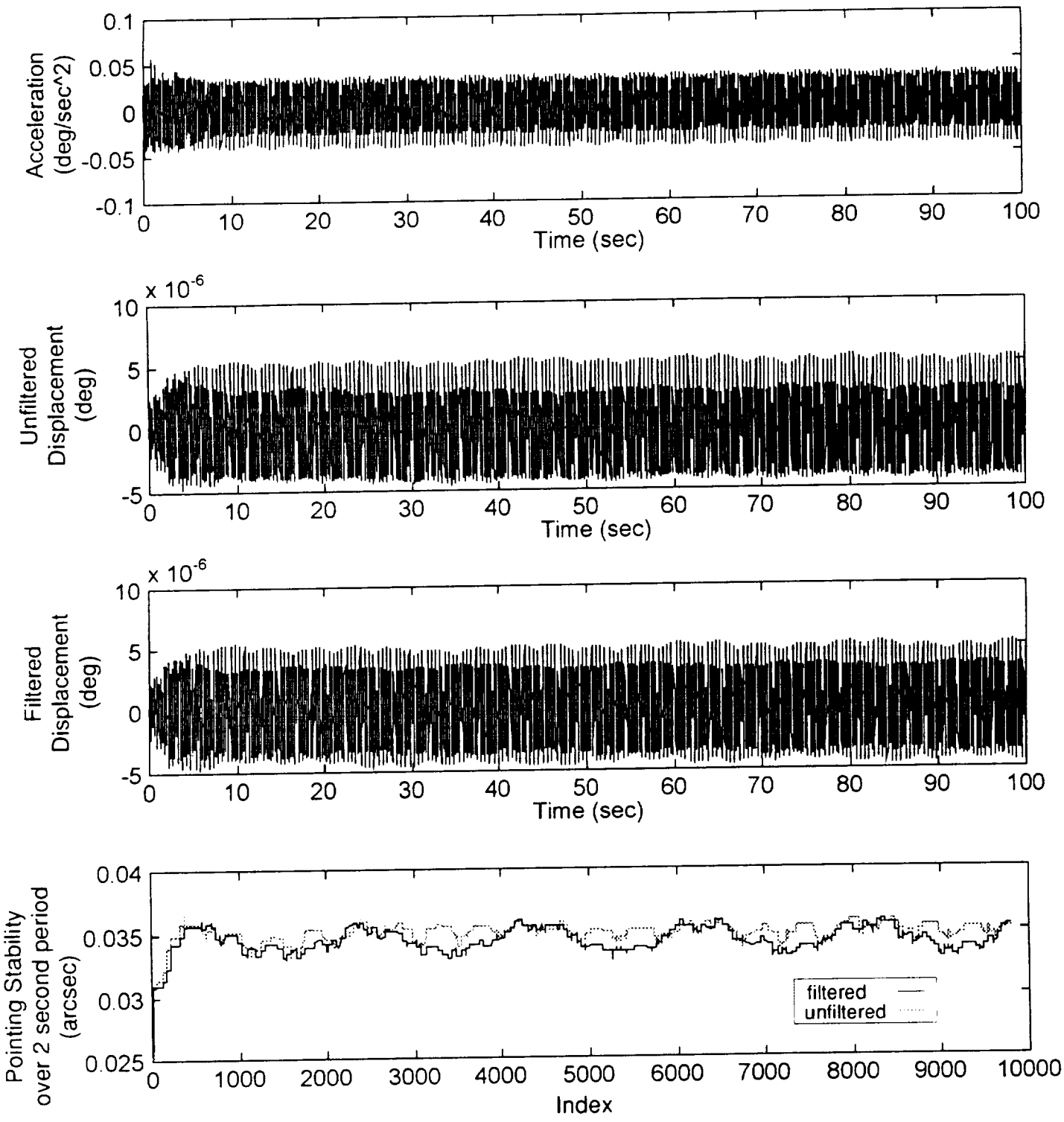

(b) Controlled response

Figure 17. - Concluded.

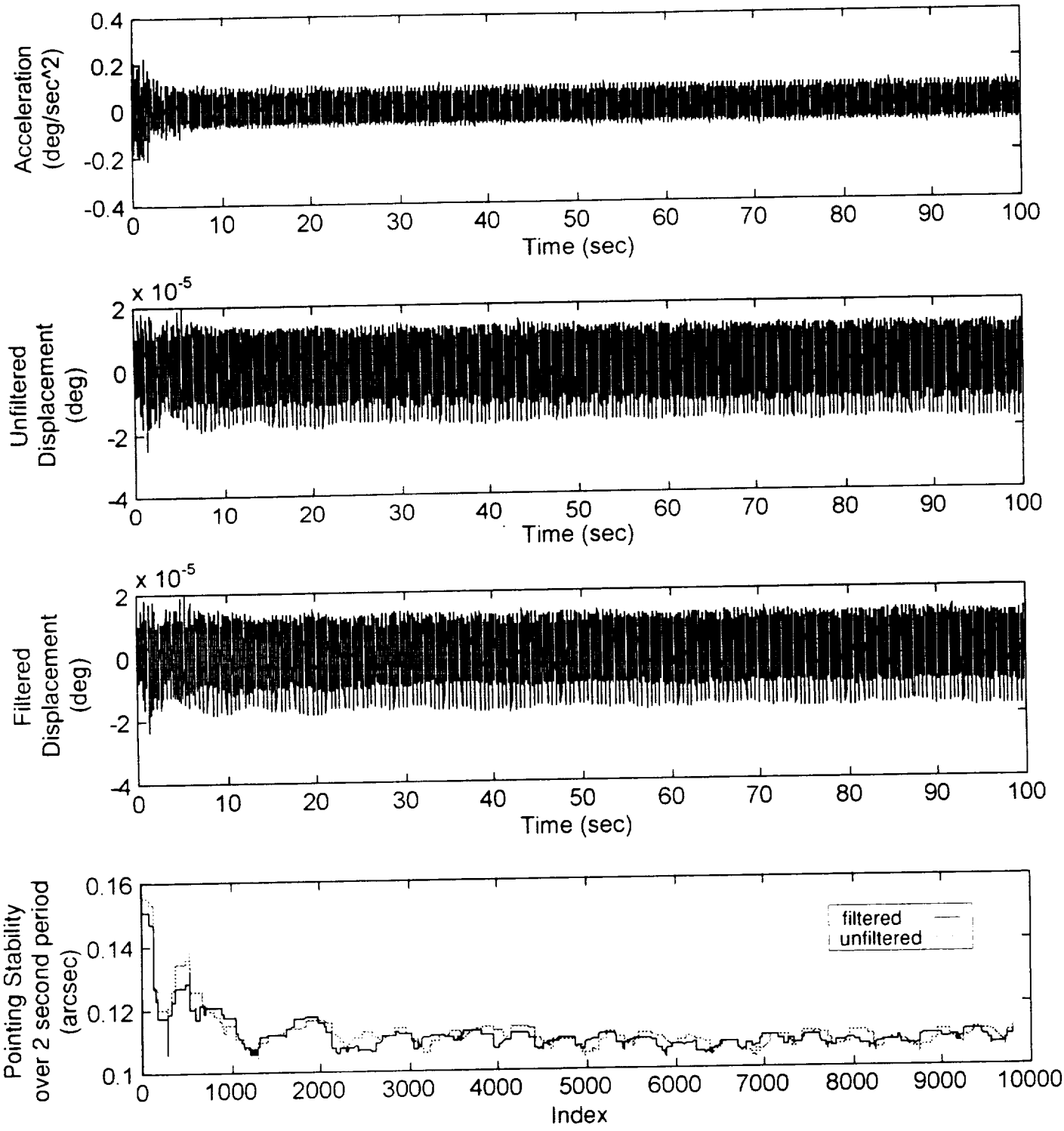

(a) Uncontrolled response

Figure 18. - Integration and pointing stability for the response at the SIU PAS in the Y ISS Axis due to TRRJ disturbance.

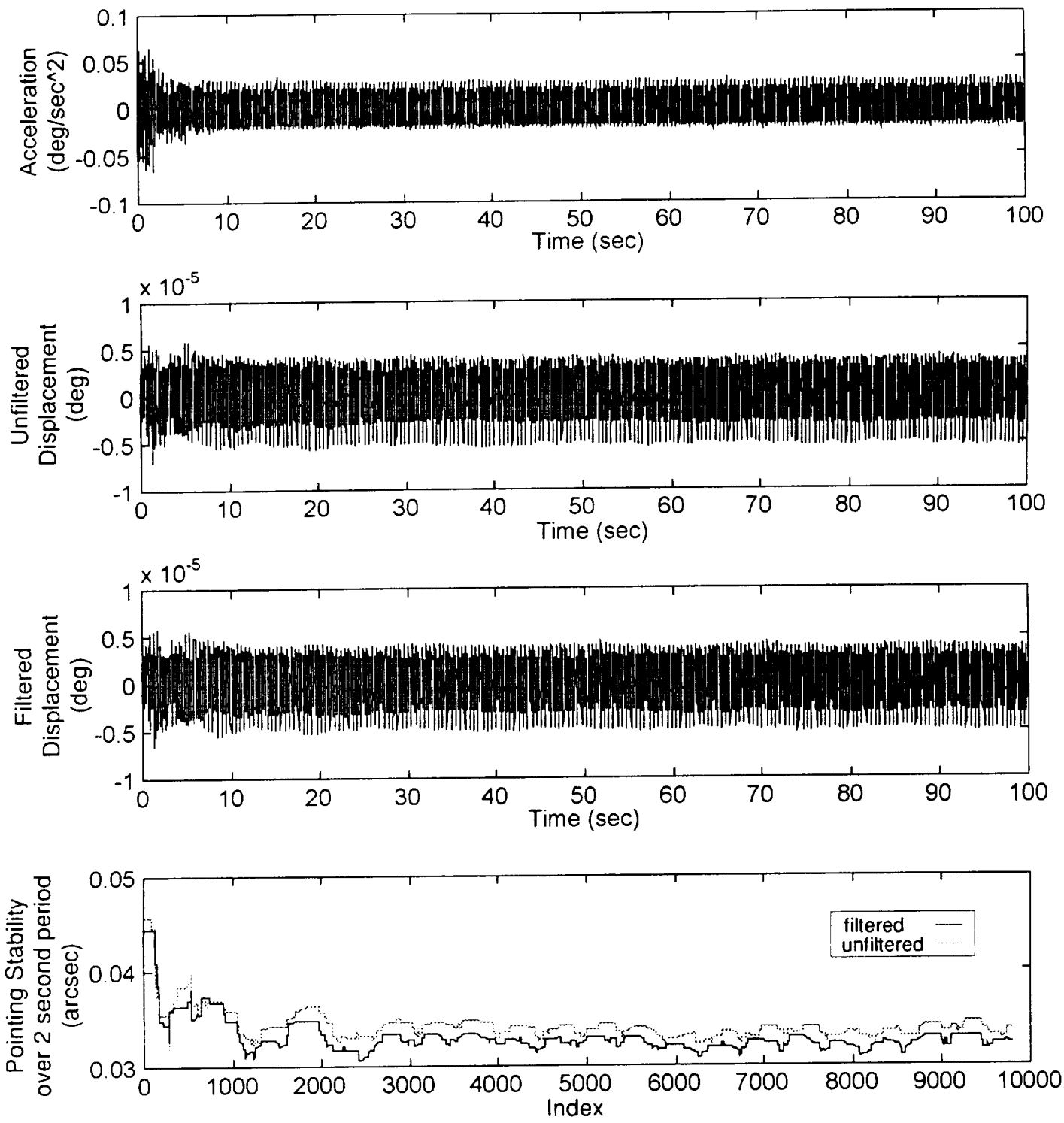

(b) Controlled response

Figure 18. - Concluded.

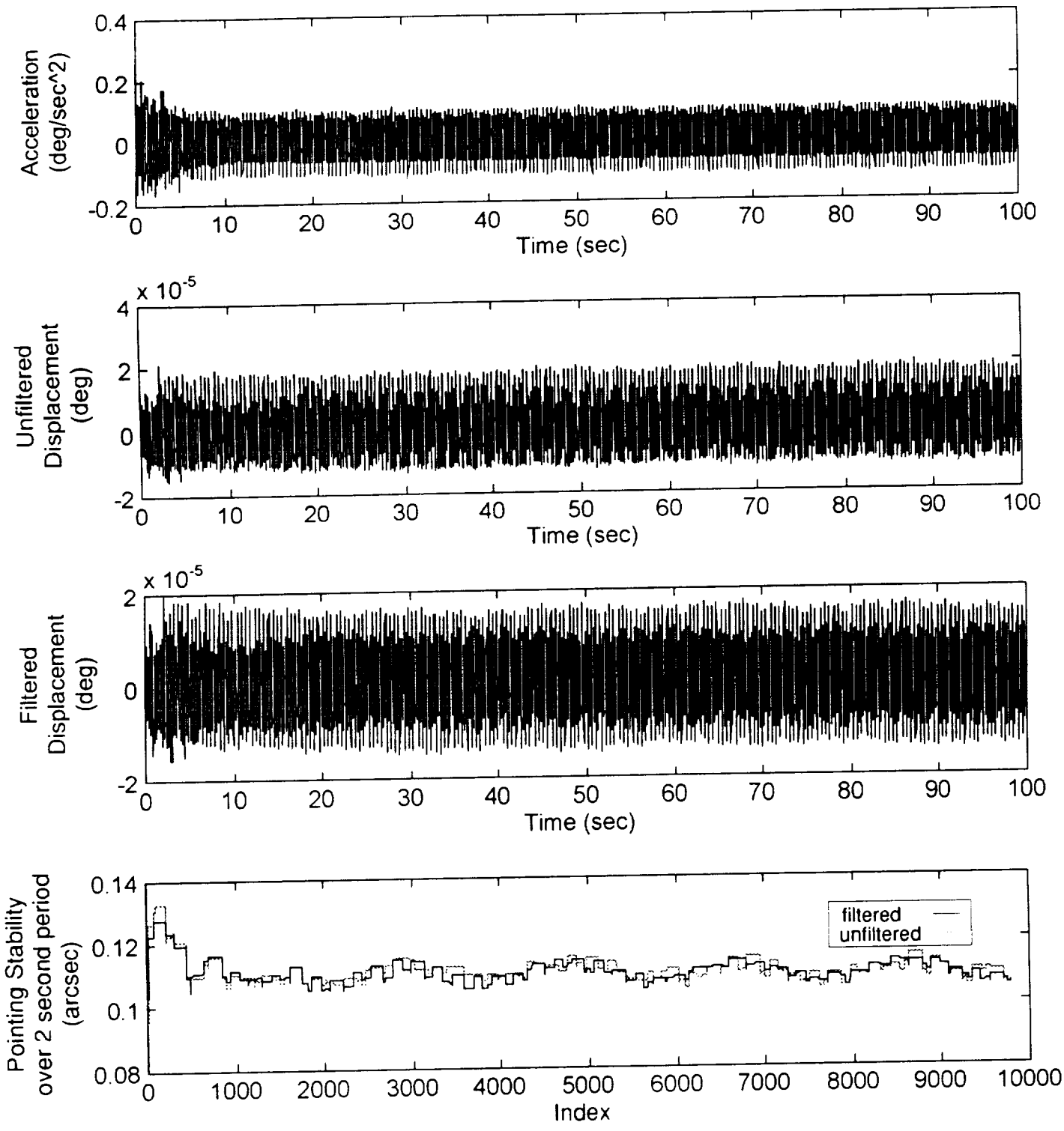

(a) Uncontrolled response

Figure 19. - Integration and pointing stability results at the SOL PAS in the Y ISS Axis for the response due to TRRJ disturbance.

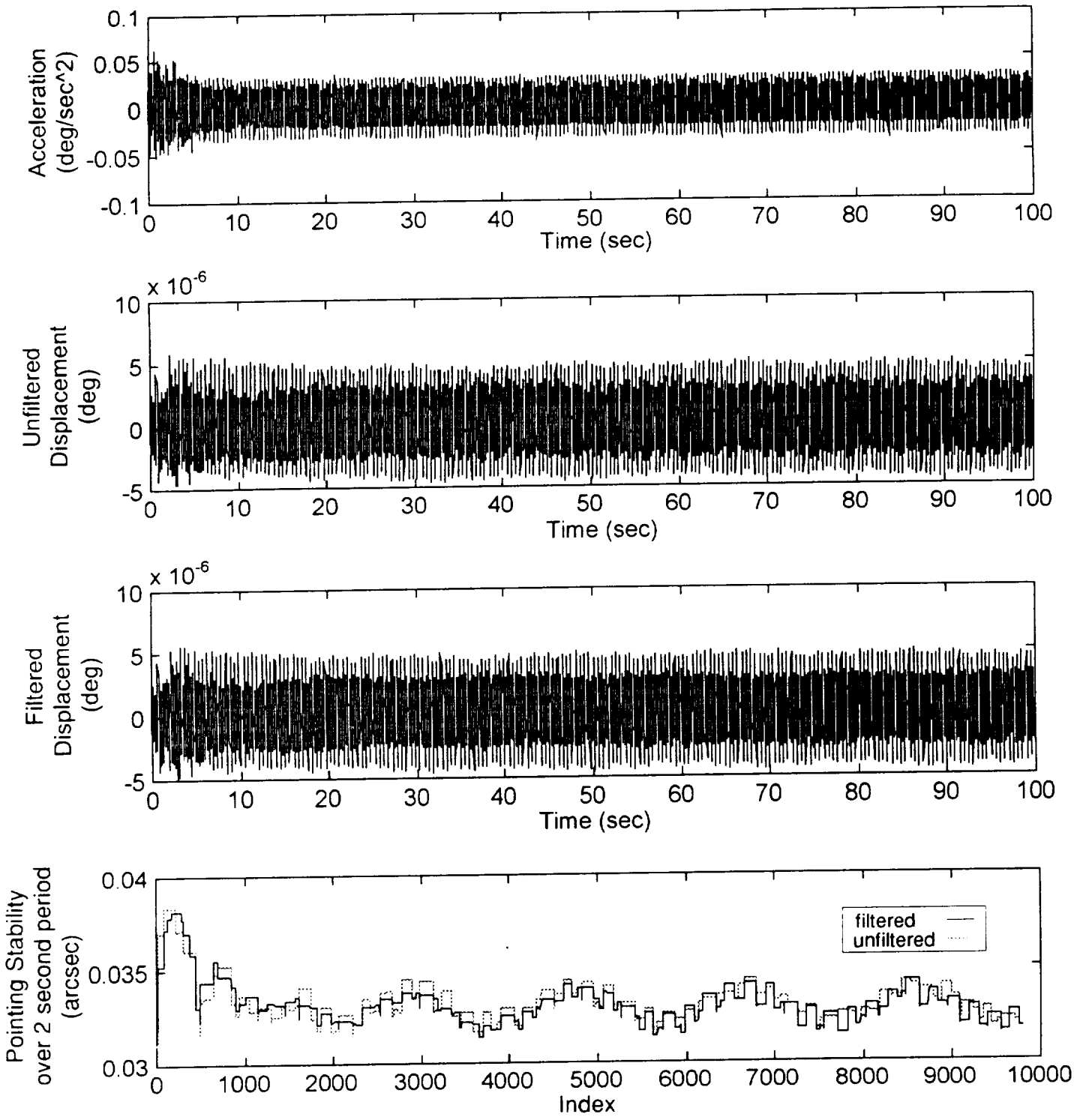

(b) Controlled response

Figure 19. - Concluded.

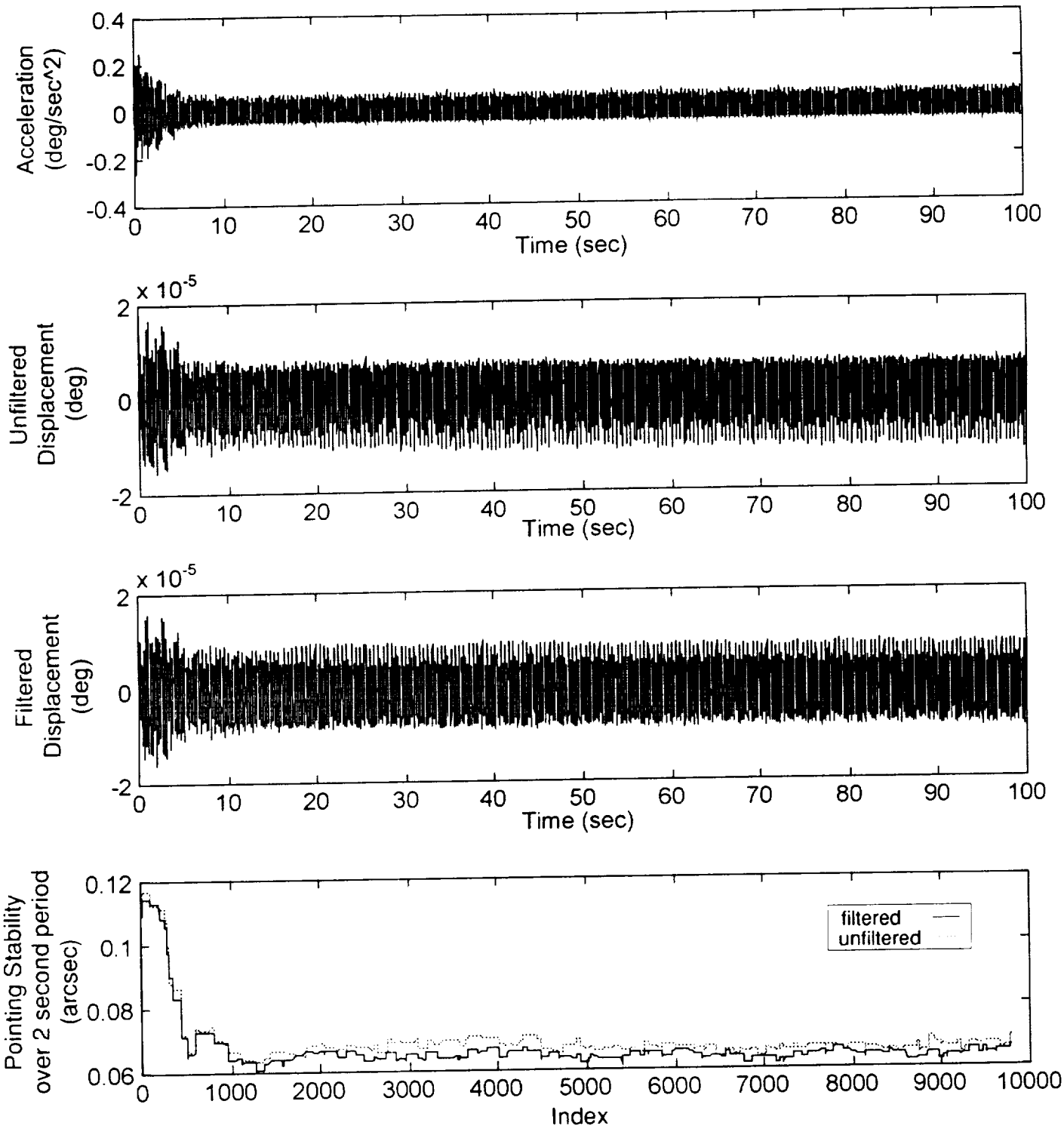

(a) Uncontrolled response

Figure 20. - Integration and pointing stability results at the SOL PAS in the Y ISS Axis for the response due to SARJ disturbance.

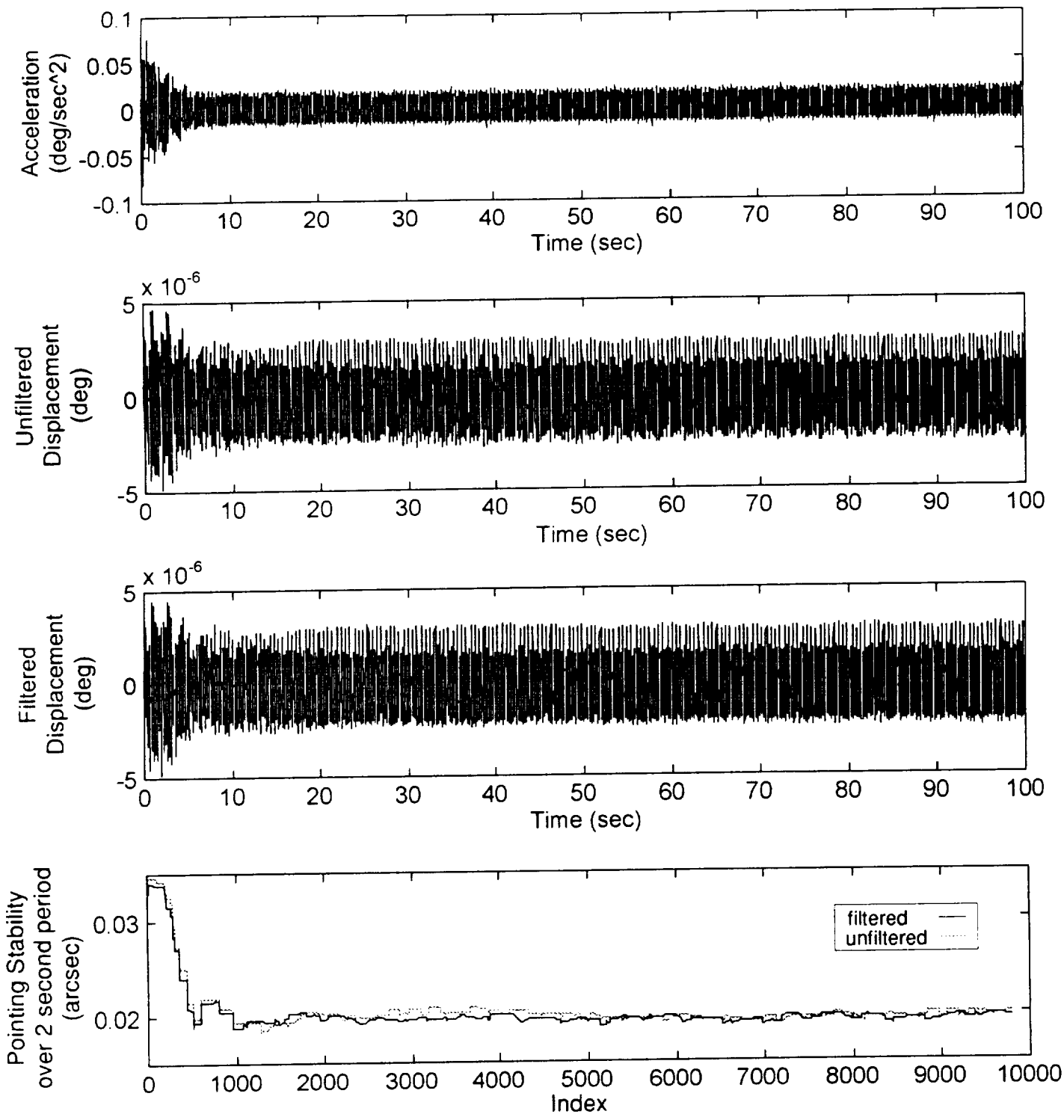

(b) Controlled response

Figure 20. - Concluded.

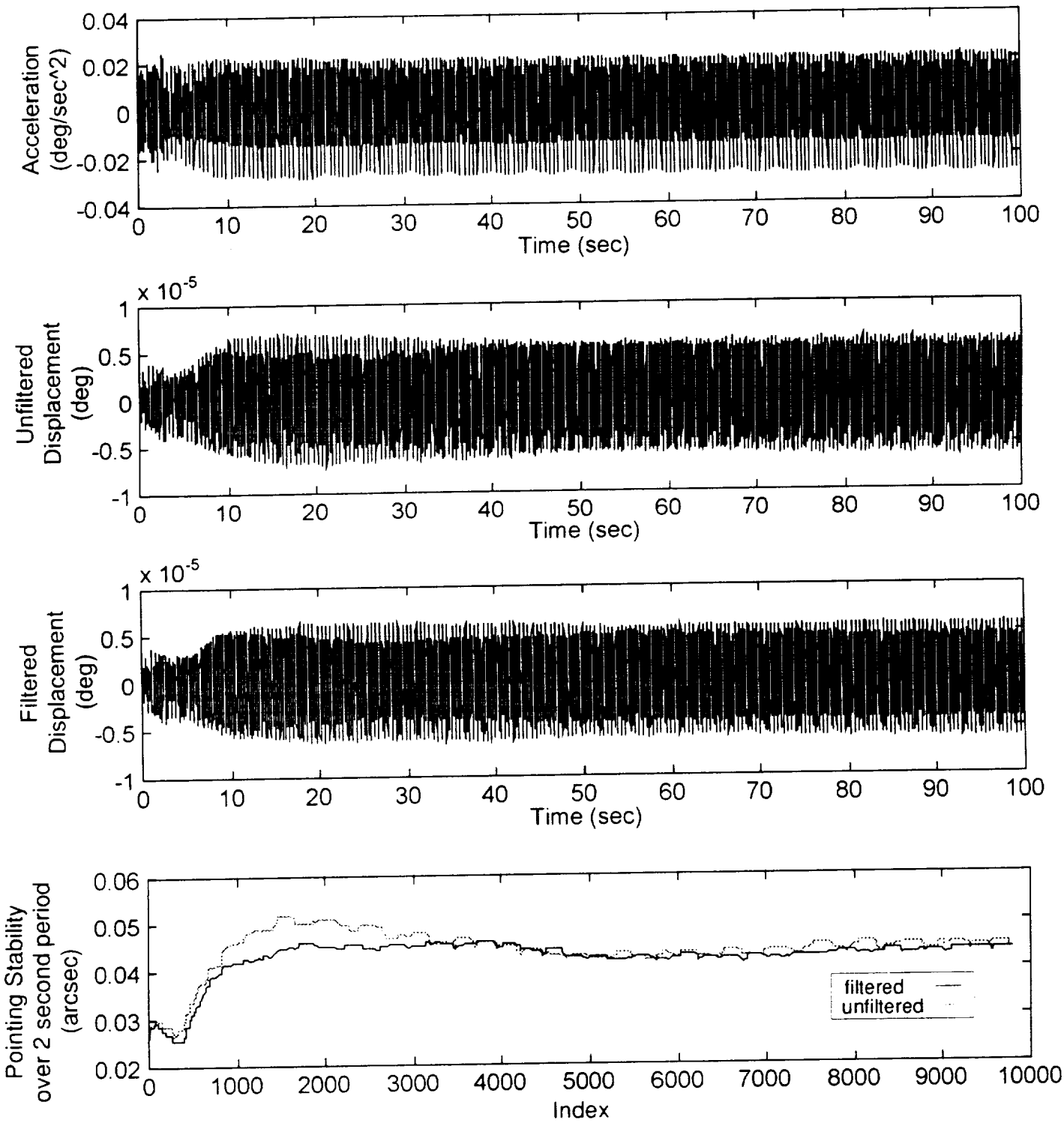

(a) Uncontrolled response

Figure 21. - Integration and pointing stability results at the SIL PAS in the -Z ISS Axis for the response due to TRRJ disturbance.

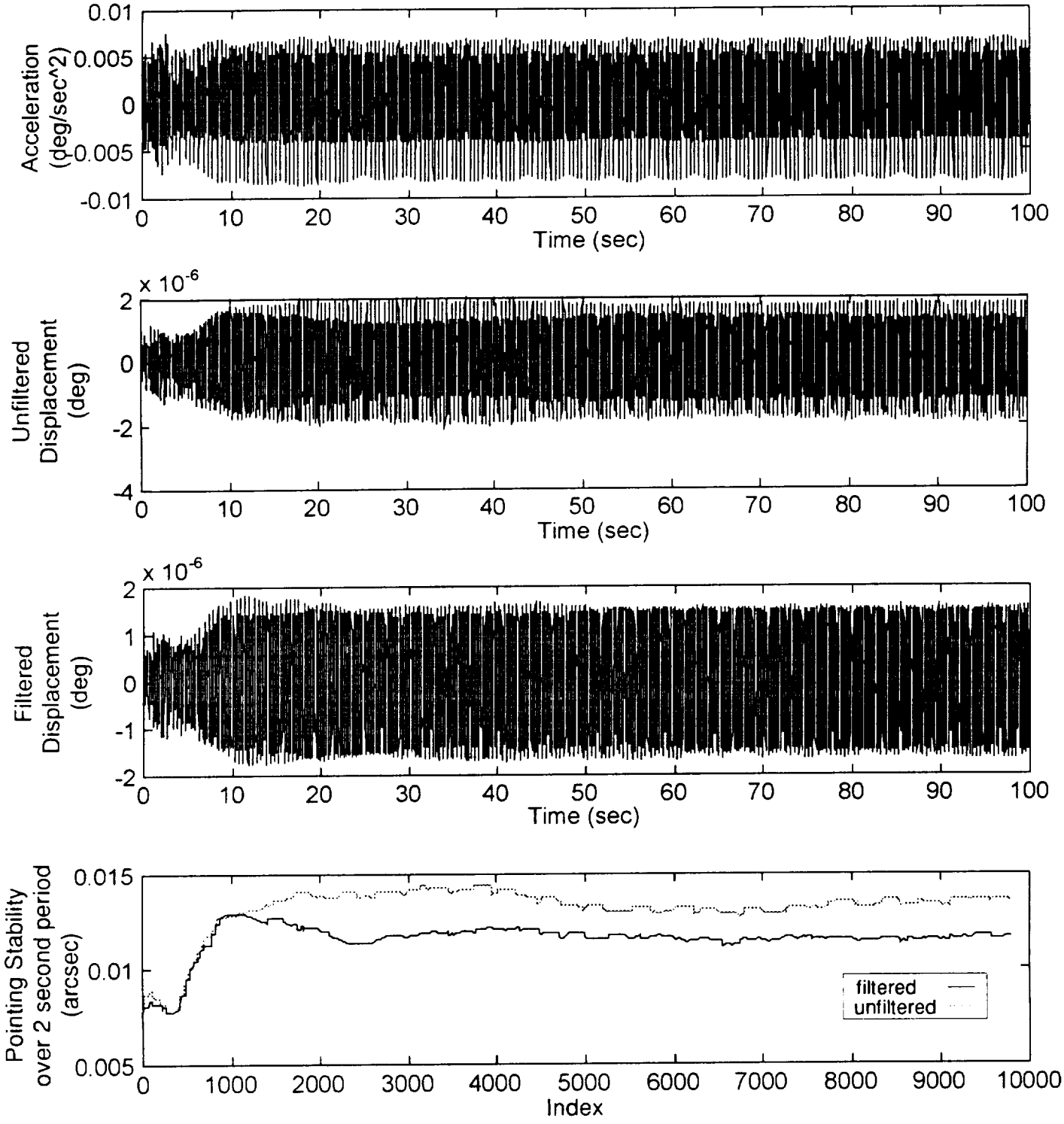

(b) Controlled response

Figure 21. - Concluded.

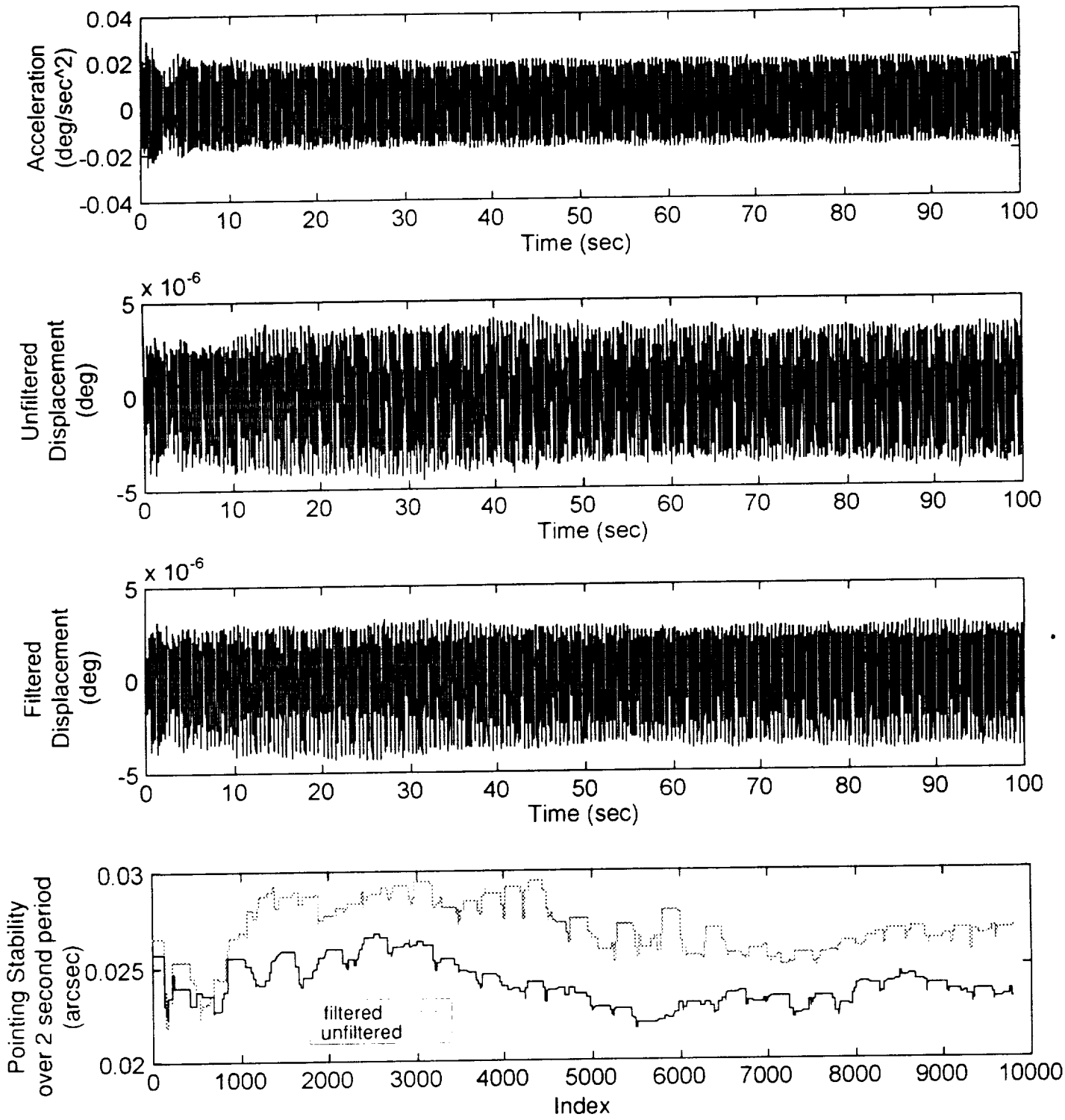

(a) Uncontrolled response

Figure 22. - Integration and pointing stability results at the SOL PAS in the -Z ISS Axis for the response due to TRRJ disturbance.

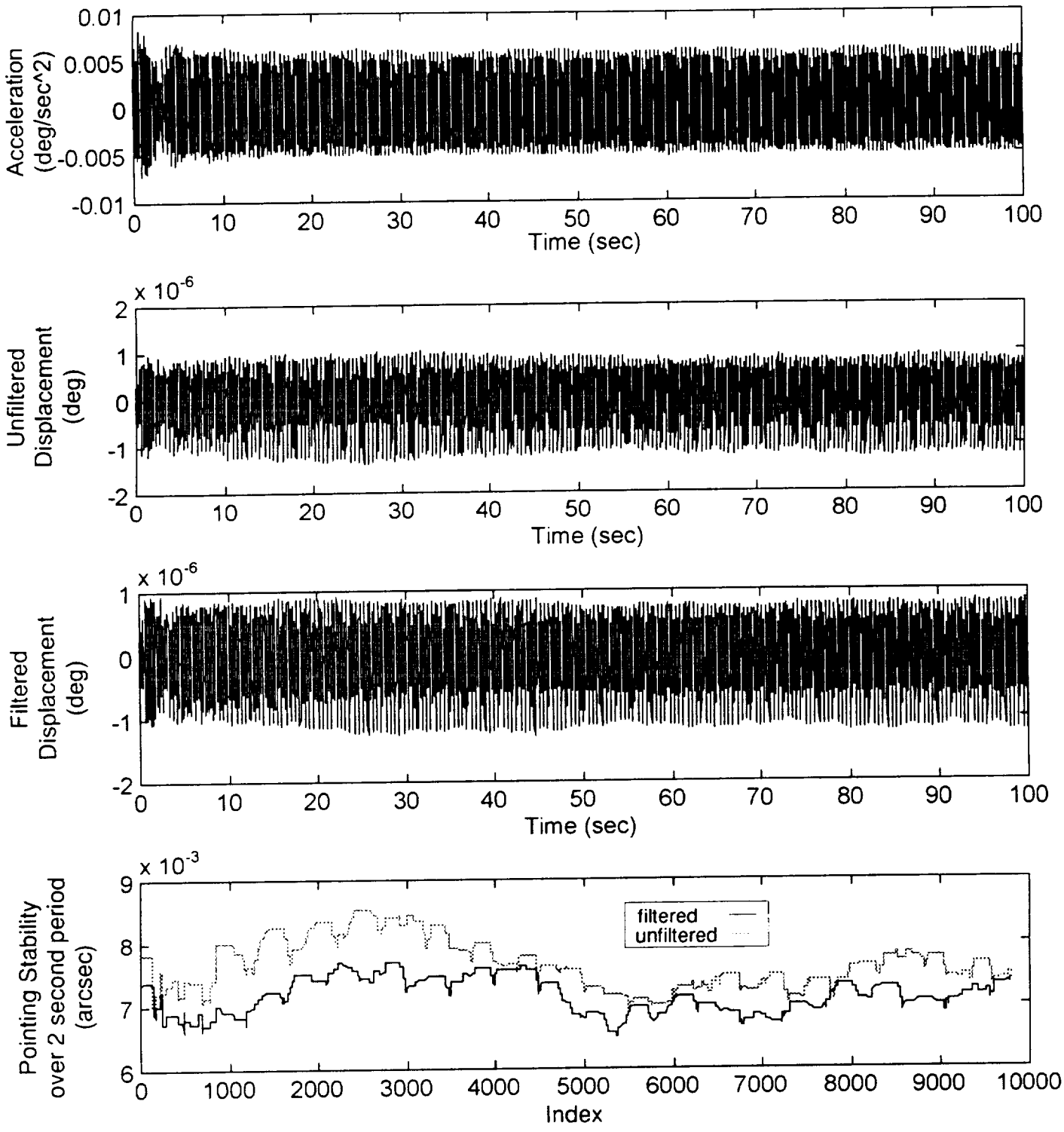

(b) Controlled response

Figure 22. - Concluded.

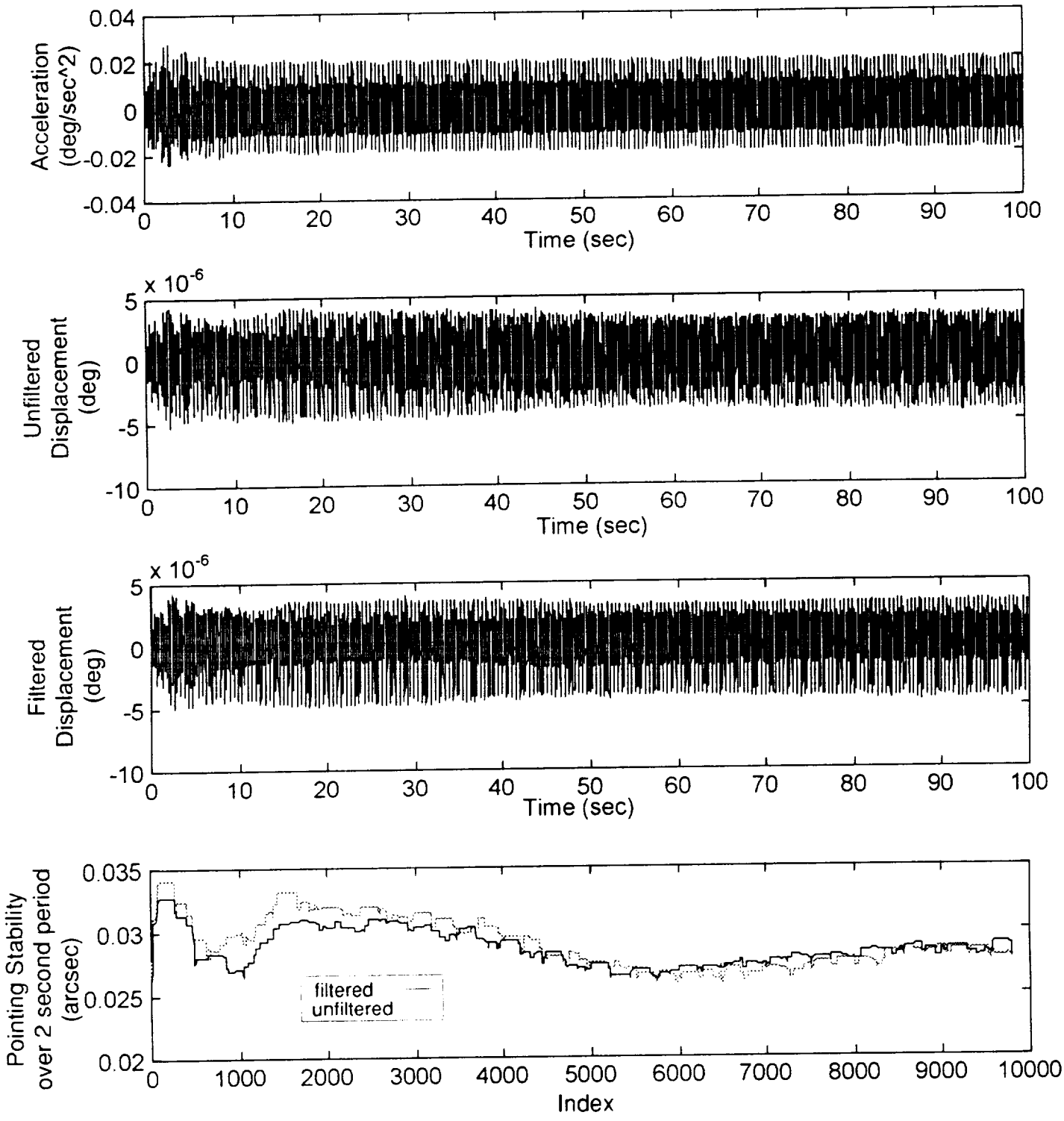

(a) Uncontrolled response

Figure 23. - Integration and pointing stability results at the SOL PAS in the -Z ISS Axis for the response due to TRRJ disturbance.

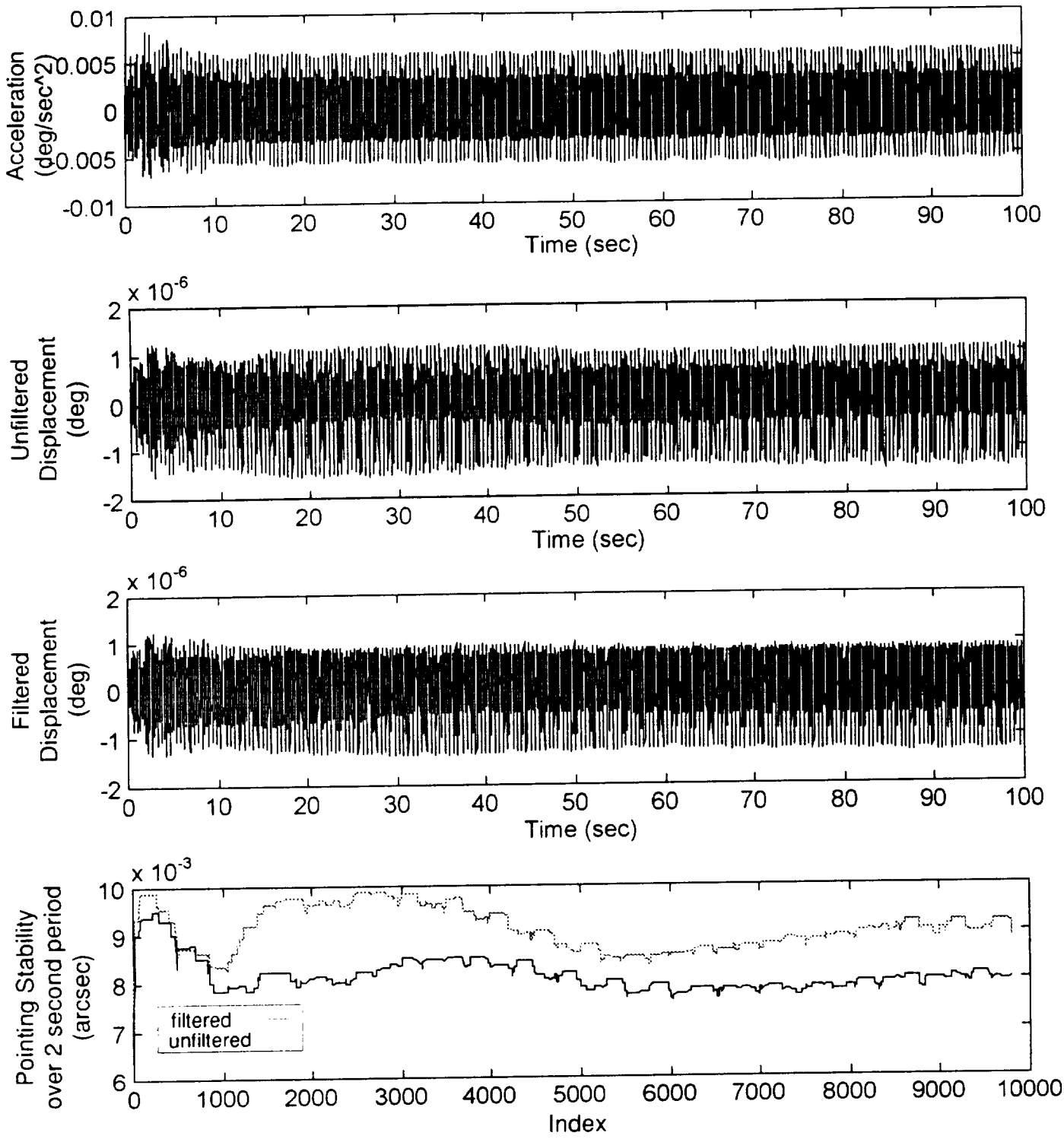

(b) Controlled response

Figure 23. - Concluded.

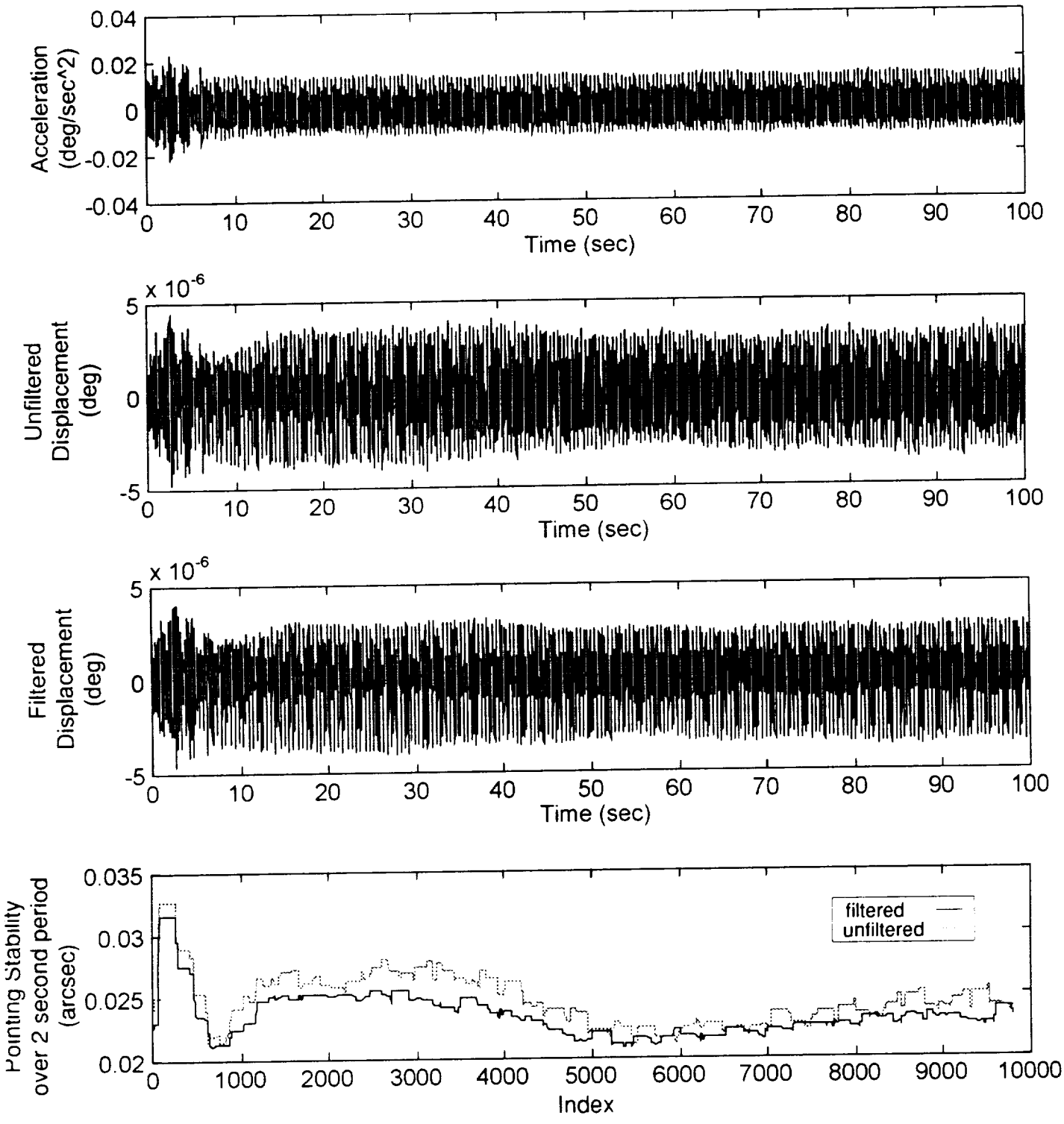

(a) Uncontrolled response

Figure 24. - Integration and pointing stability results at the SOU PAS in the -Z ISS Axis for the response due to TRRJ disturbance.

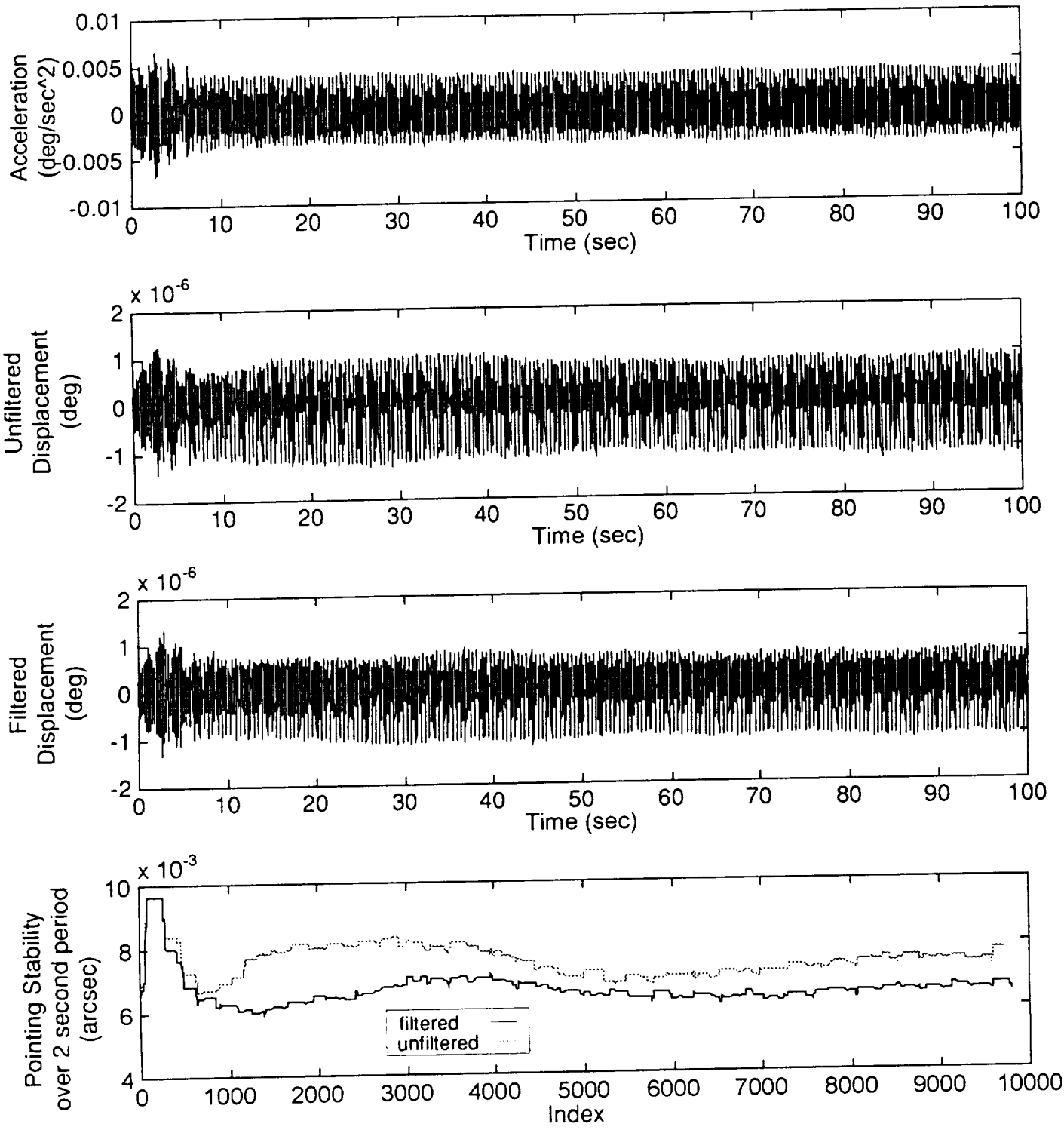

(b) Controlled response

Figure 24. - Concluded.

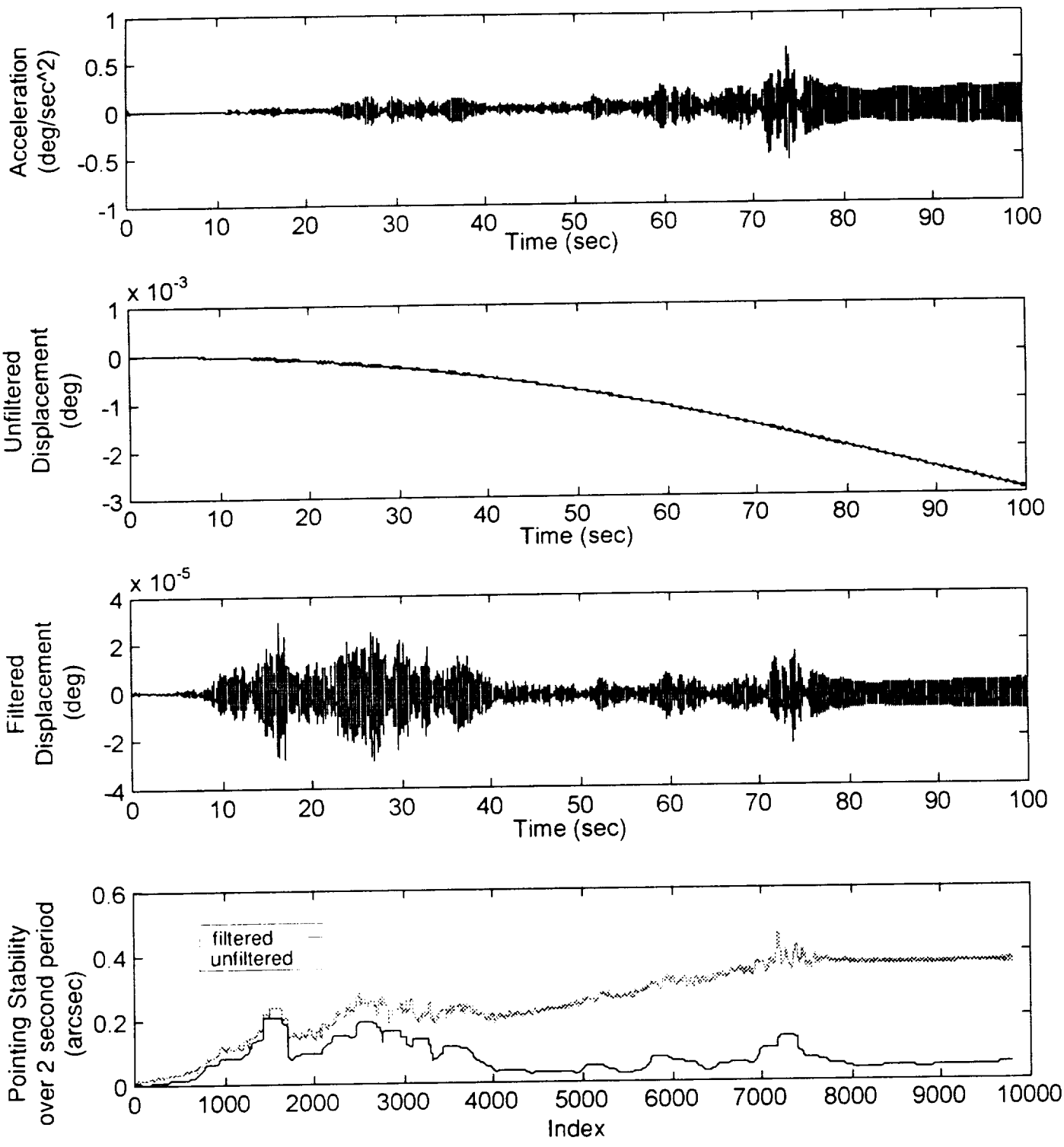

(a) Uncontrolled response

Figure 25. - Integration and pointing stability results at the SIL PAS in the -X ISS Axis for the response due to TRRJ Slew disturbance.

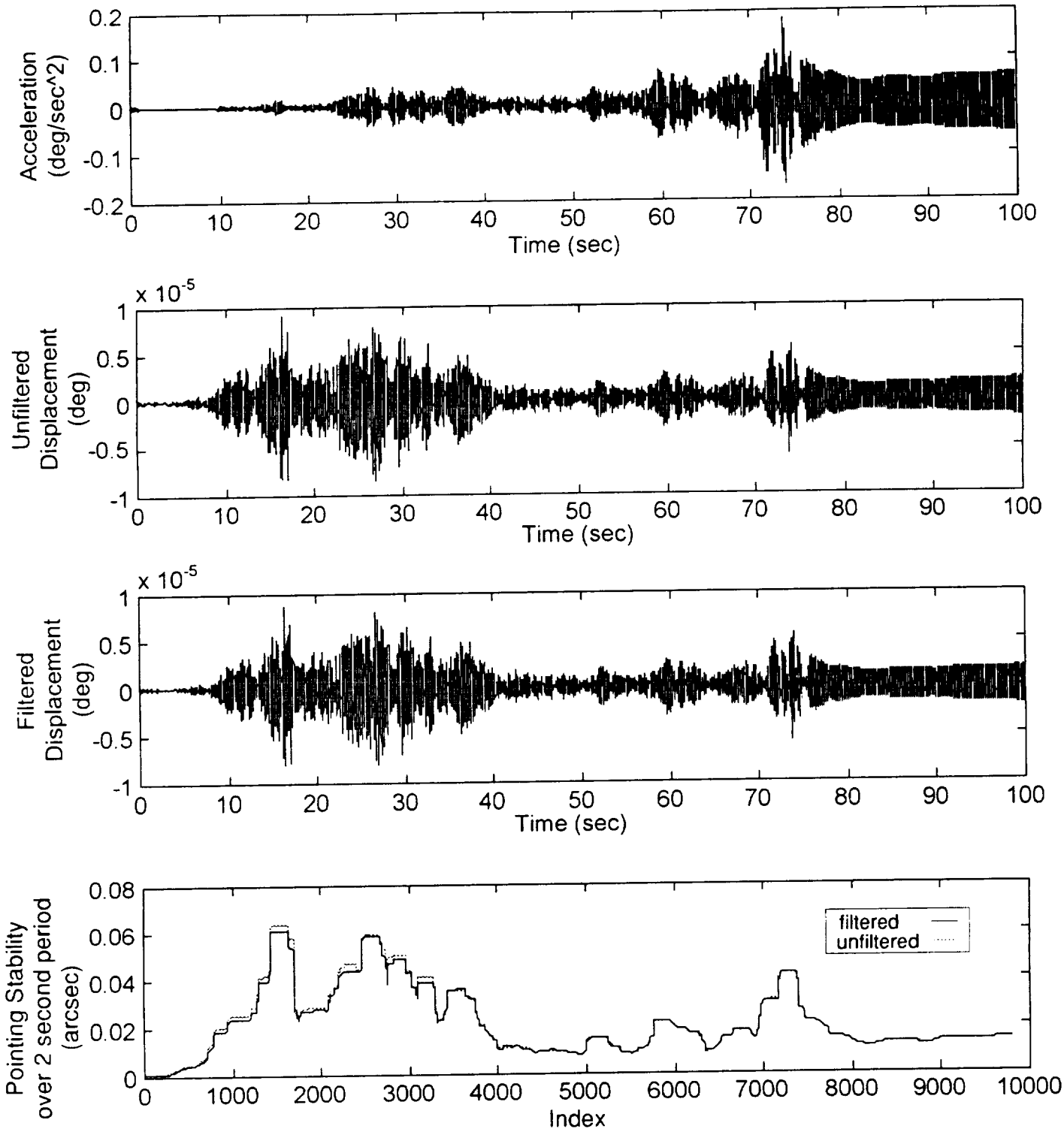

(b) Controlled response

Figure 25. - Concluded.

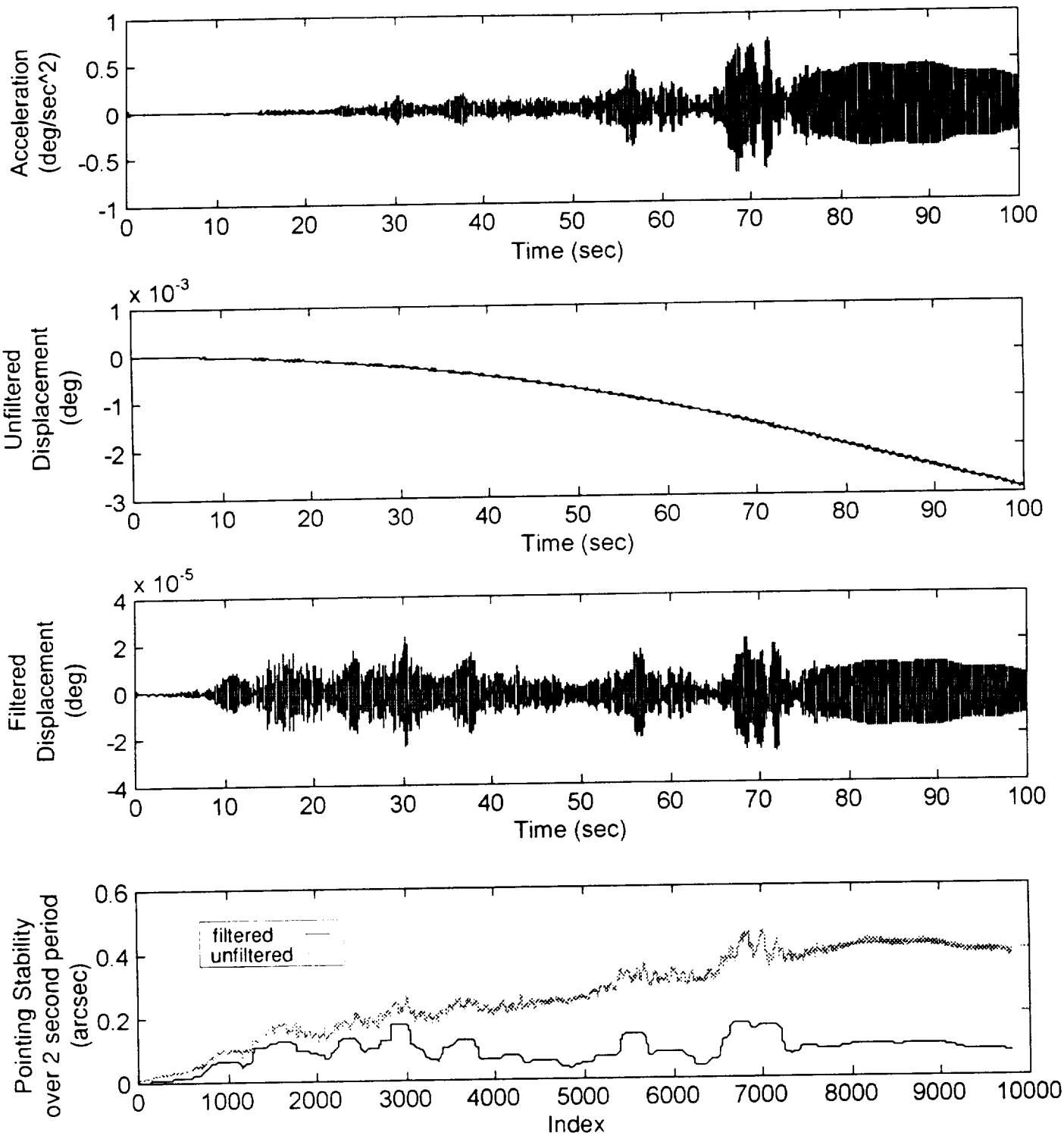

(a) Uncontrolled response

Figure 26. - Integration and pointing stability results at the SIU PAS in the -X ISS Axis for the response due to TRRJ Slew disturbance.

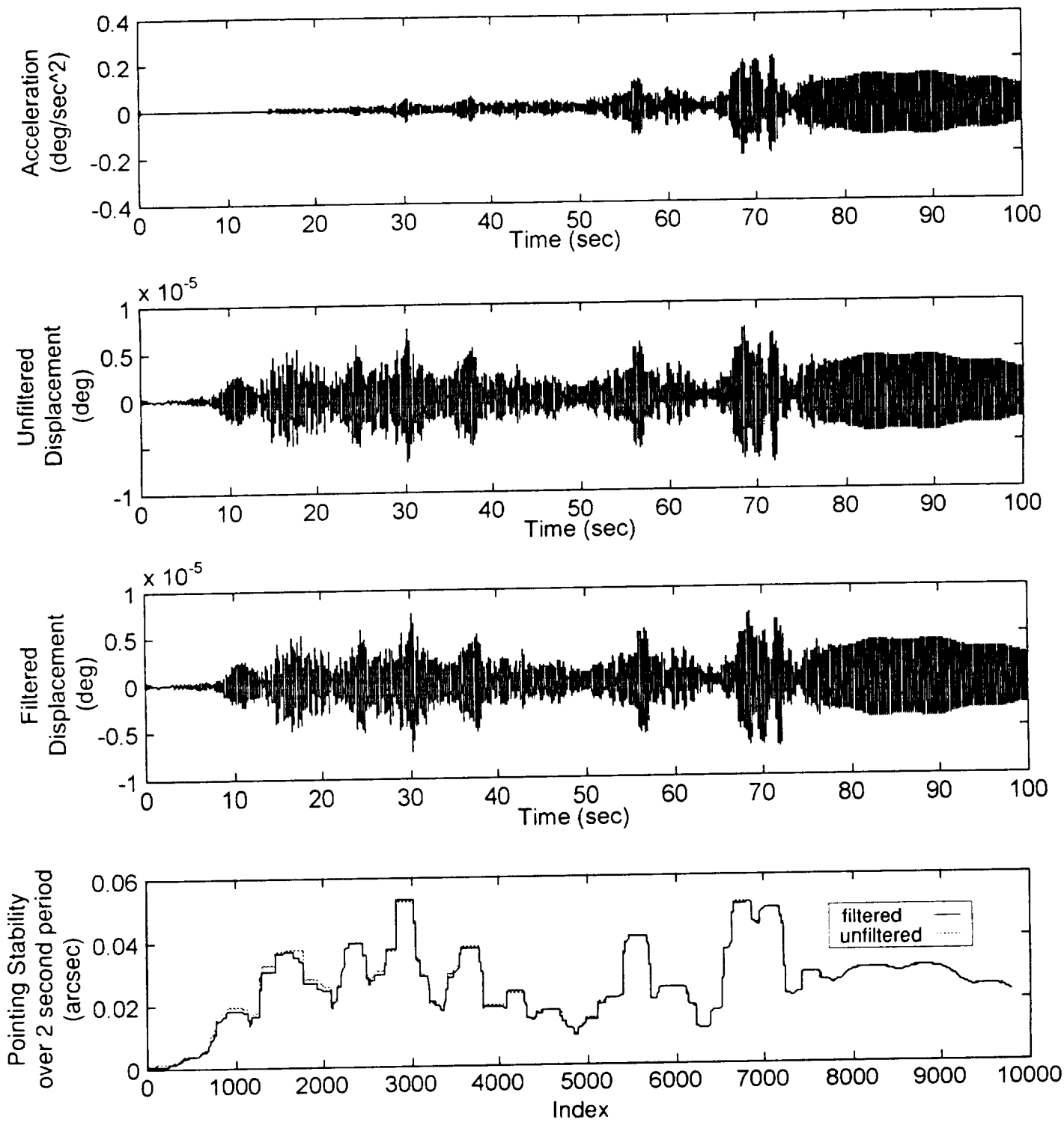

(b) Controlled response

Figure 26. - Concluded.

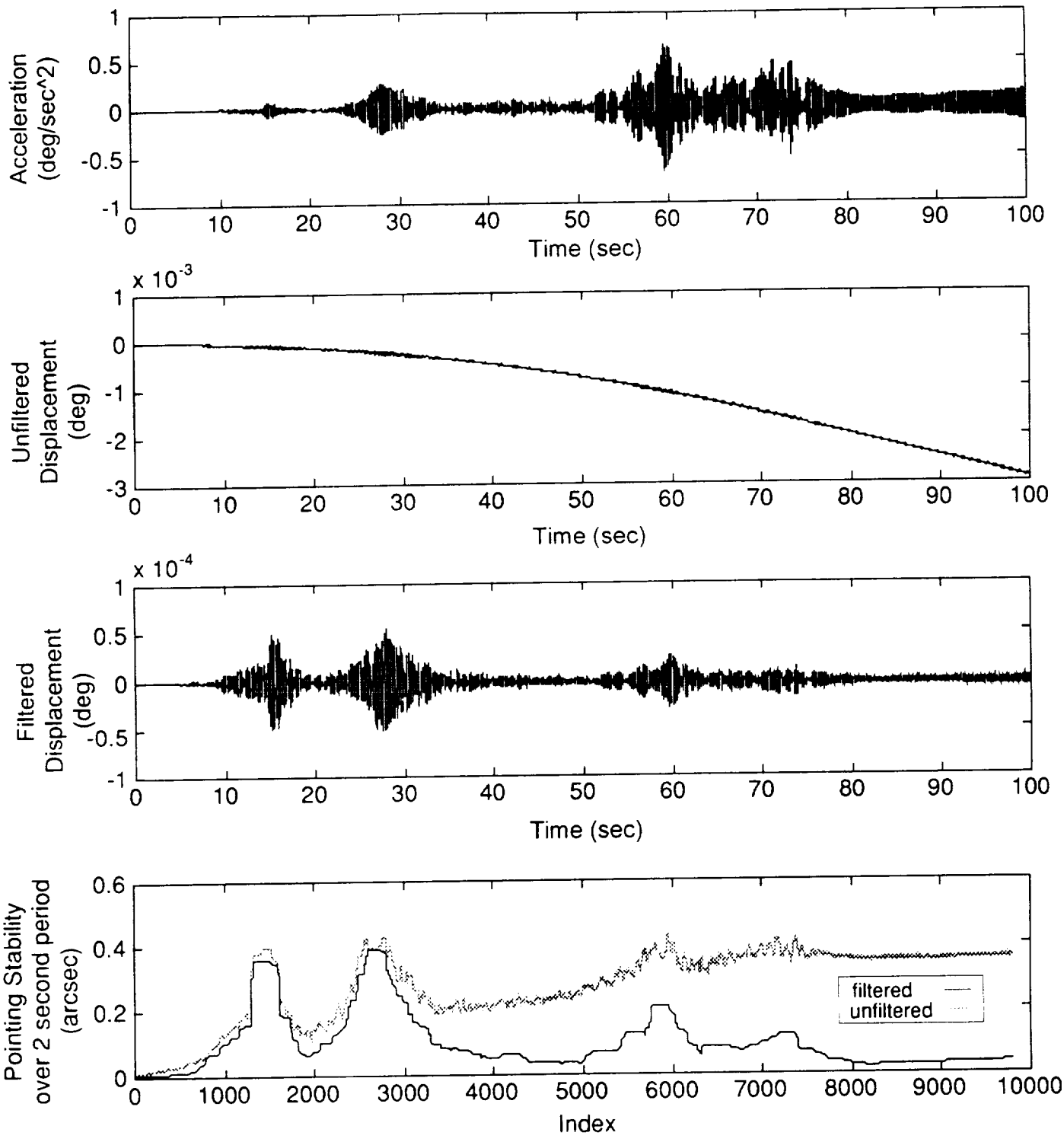

(a) Uncontrolled response

Figure 27. - Integration and pointing stability results at the SOL PAS in the -X ISS Axis for the response due to TRRJ slew disturbance.

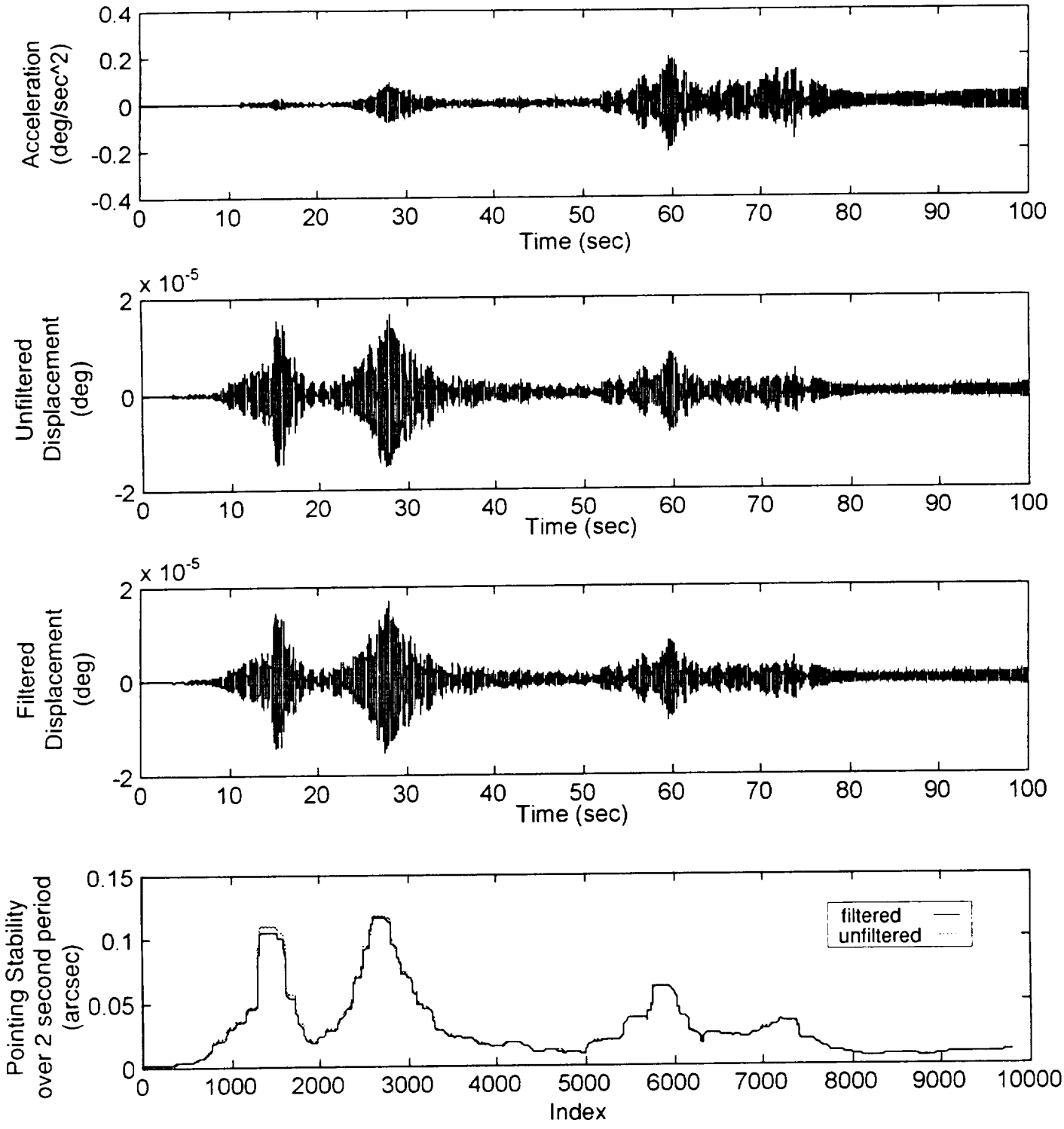

(b) Controlled response

Figure 27. - Concluded.

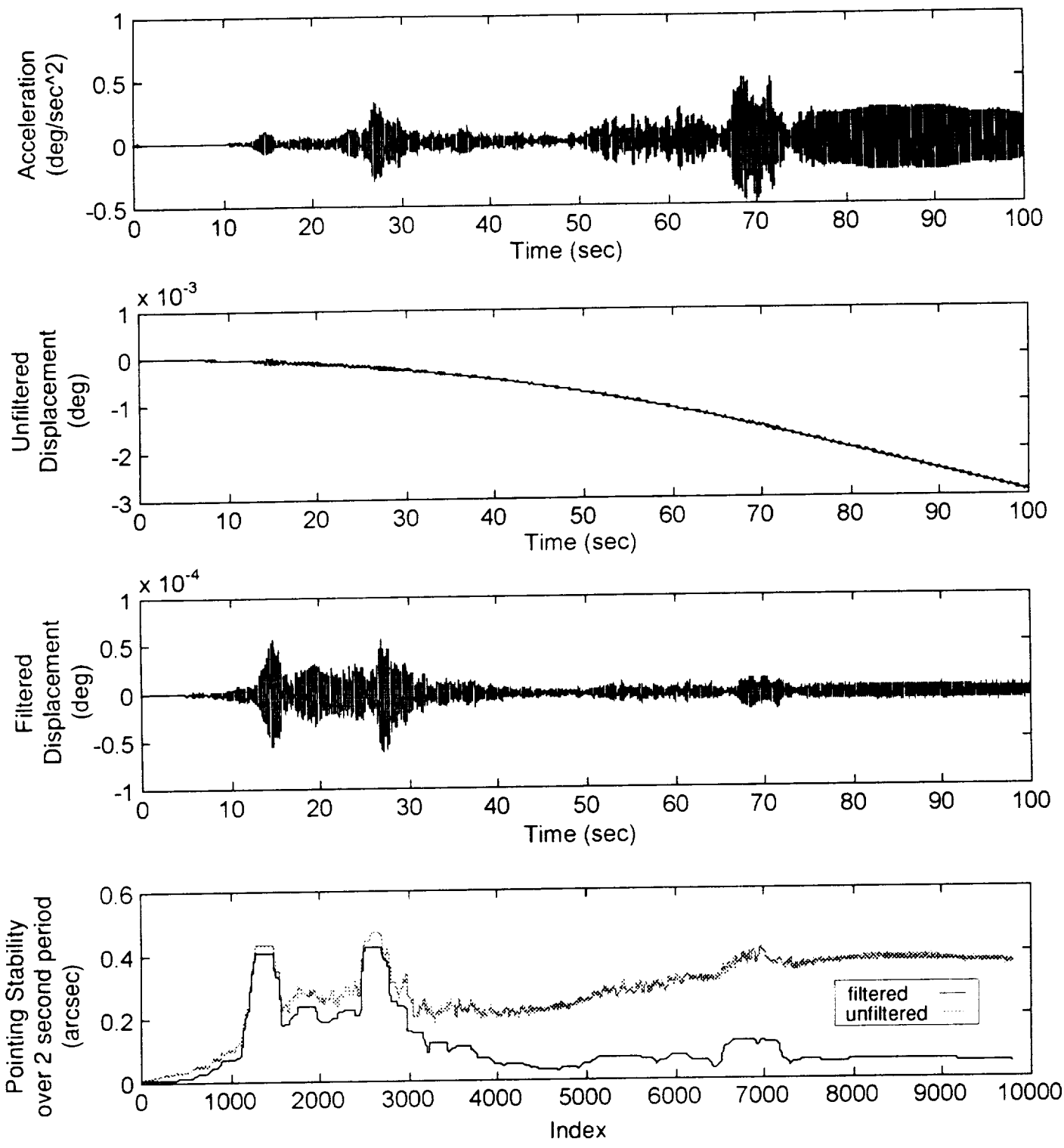

(a) Uncontrolled response

Figure 28. - Integration and pointing stability results at the SOU PAS in the -X ISS Axis for the response due to TRRJ Slew disturbance.

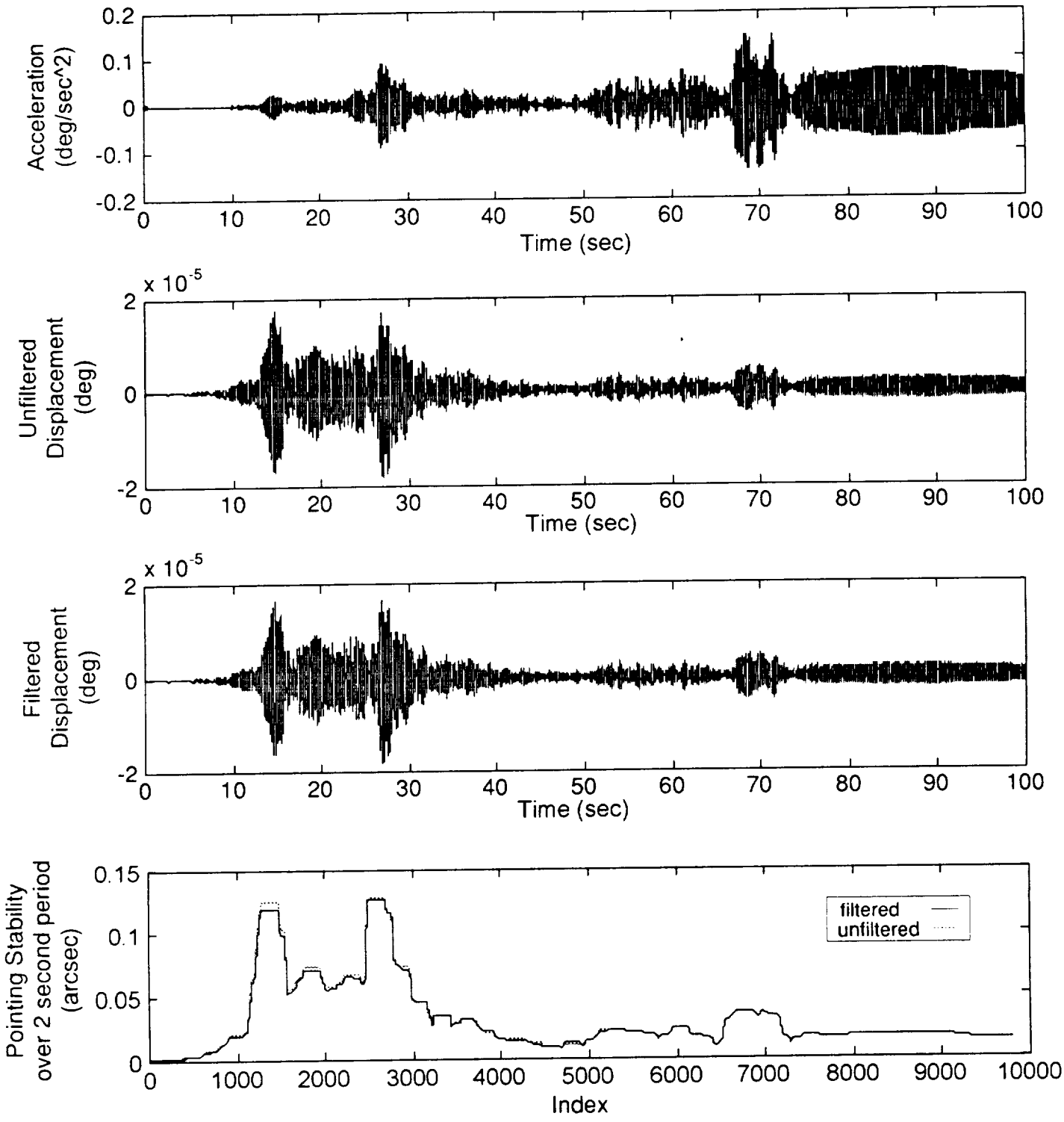

(b) Controlled response

Figure 28. - Concluded.

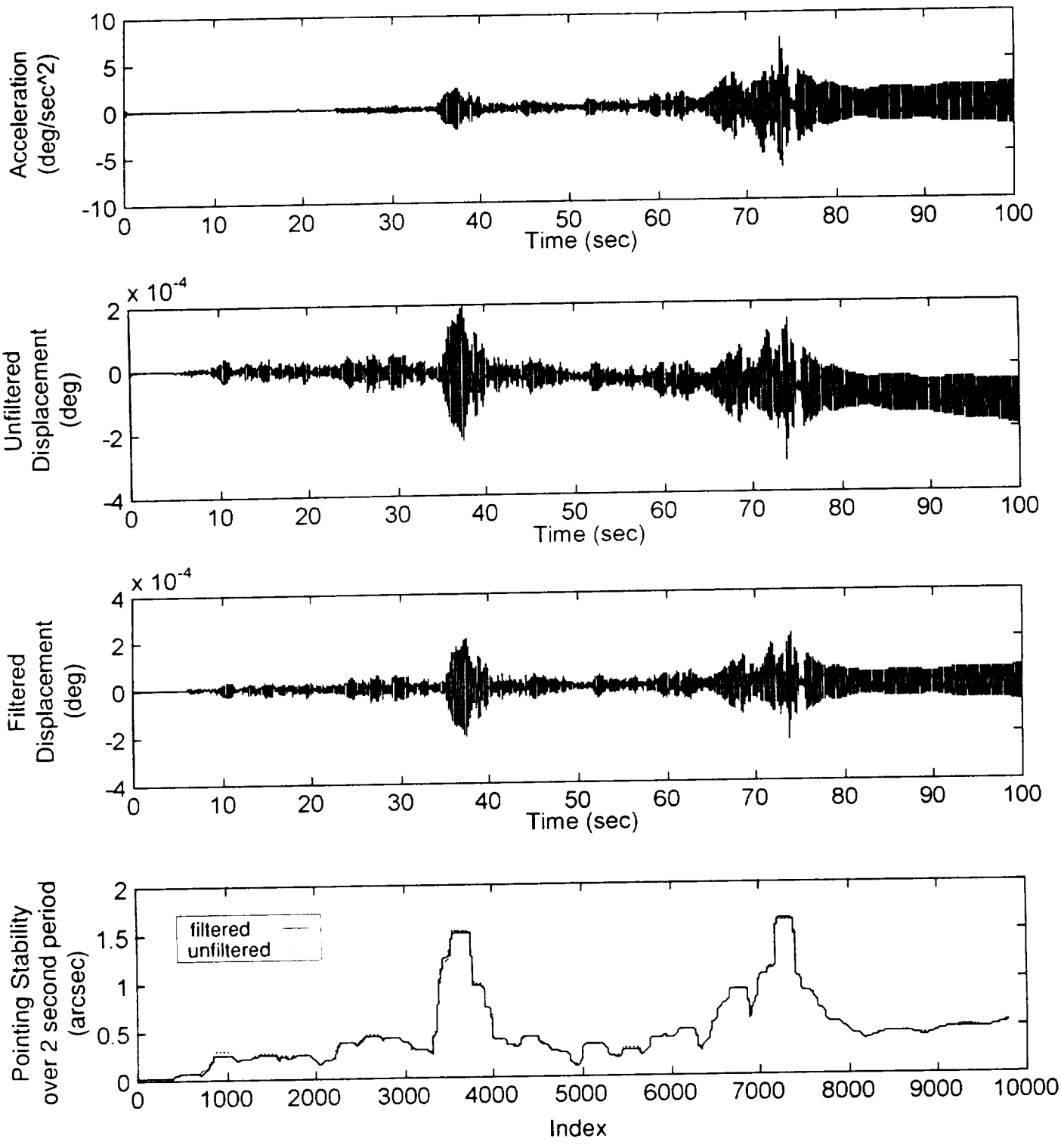

(a) Uncontrolled response

Figure 29. - Integration and pointing stability results at the SIL PAS in the Y ISS Axis for the response due to TRRJ Slew disturbance.

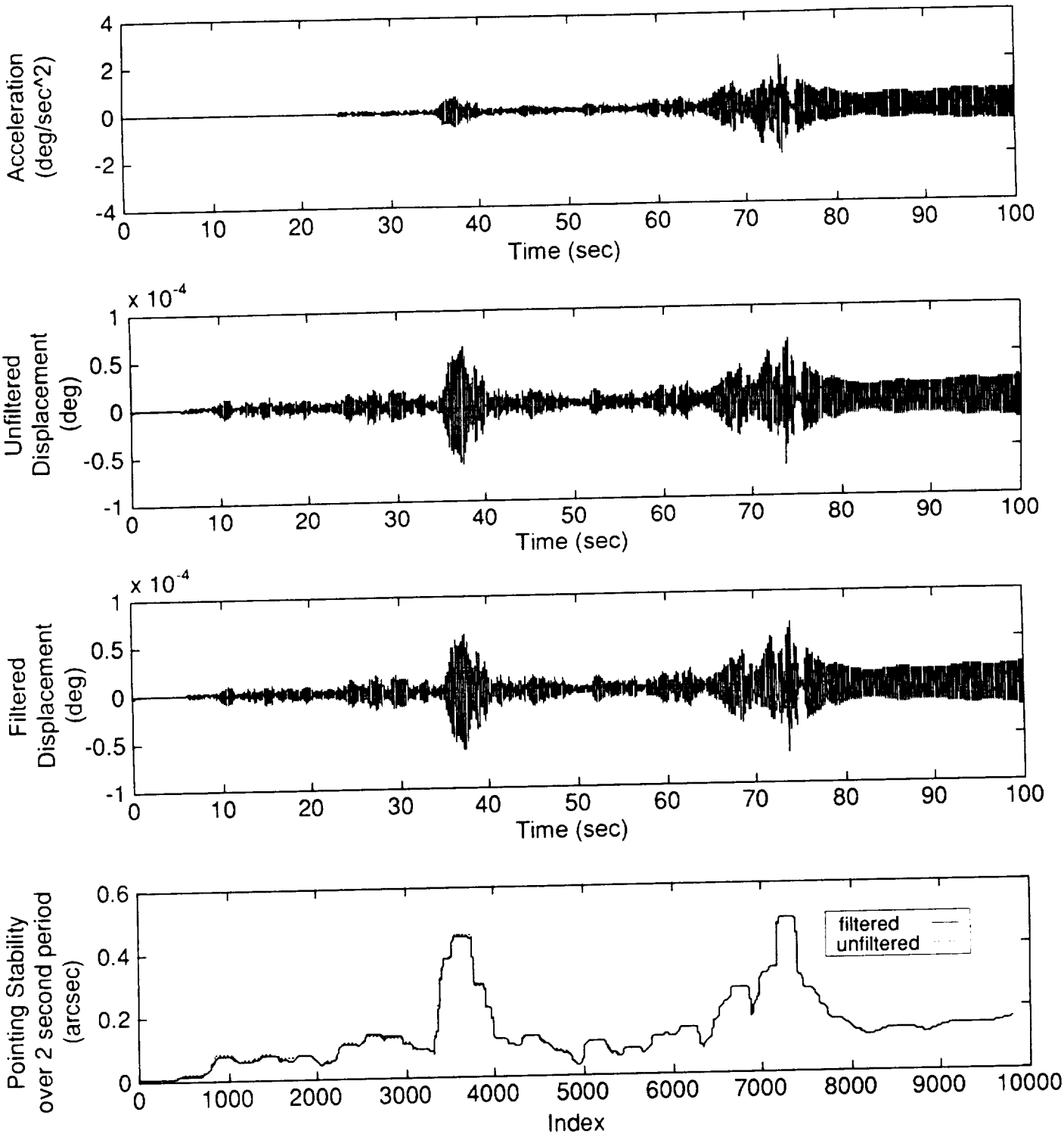

(b) Controlled response

Figure 29. - Concluded.

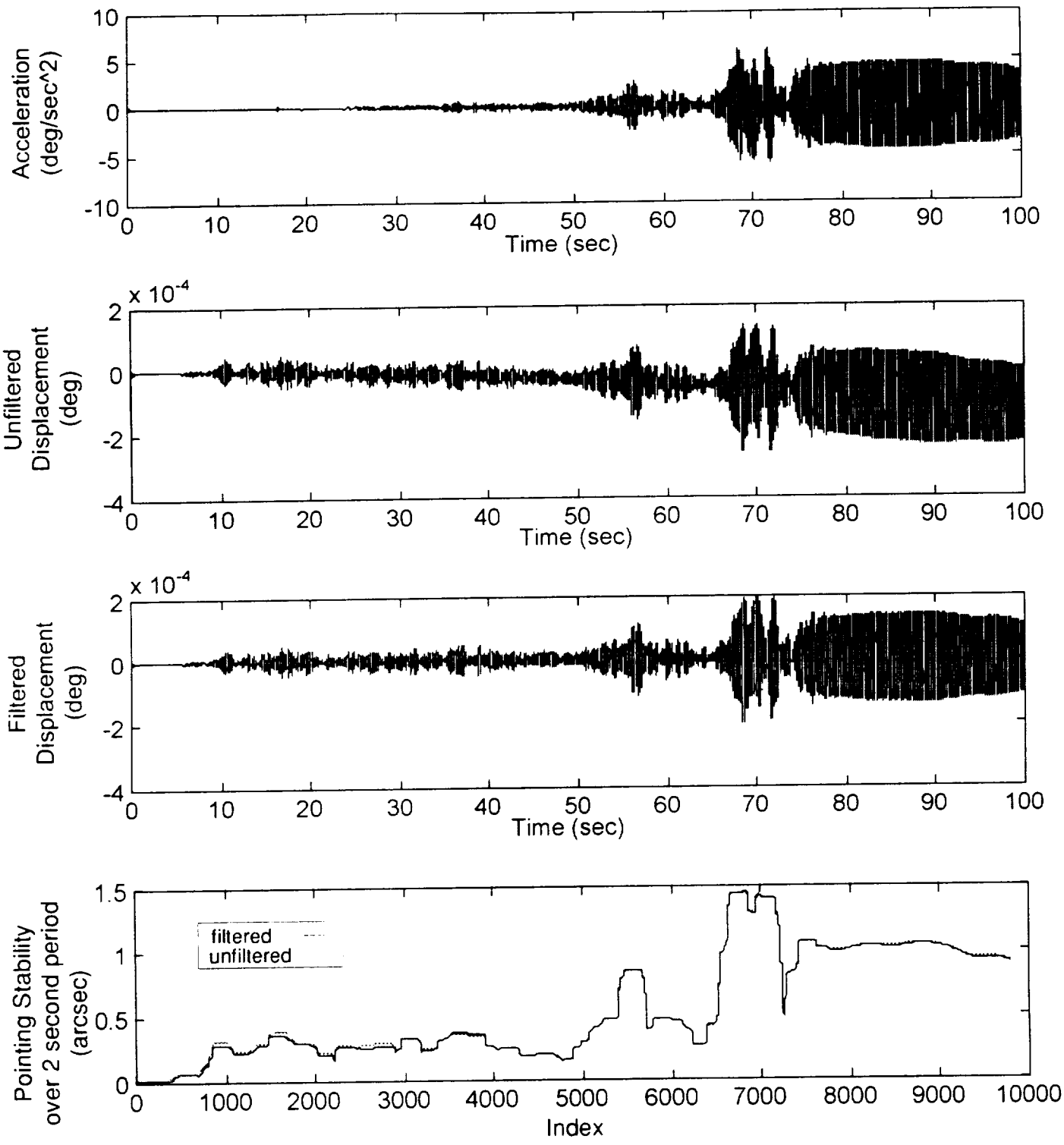

(a) Uncontrolled response

Figure 30. - Integration and pointing stability results at the SIU PAS in the Y ISS Axis for the response due to TRRJ Slew disturbance.

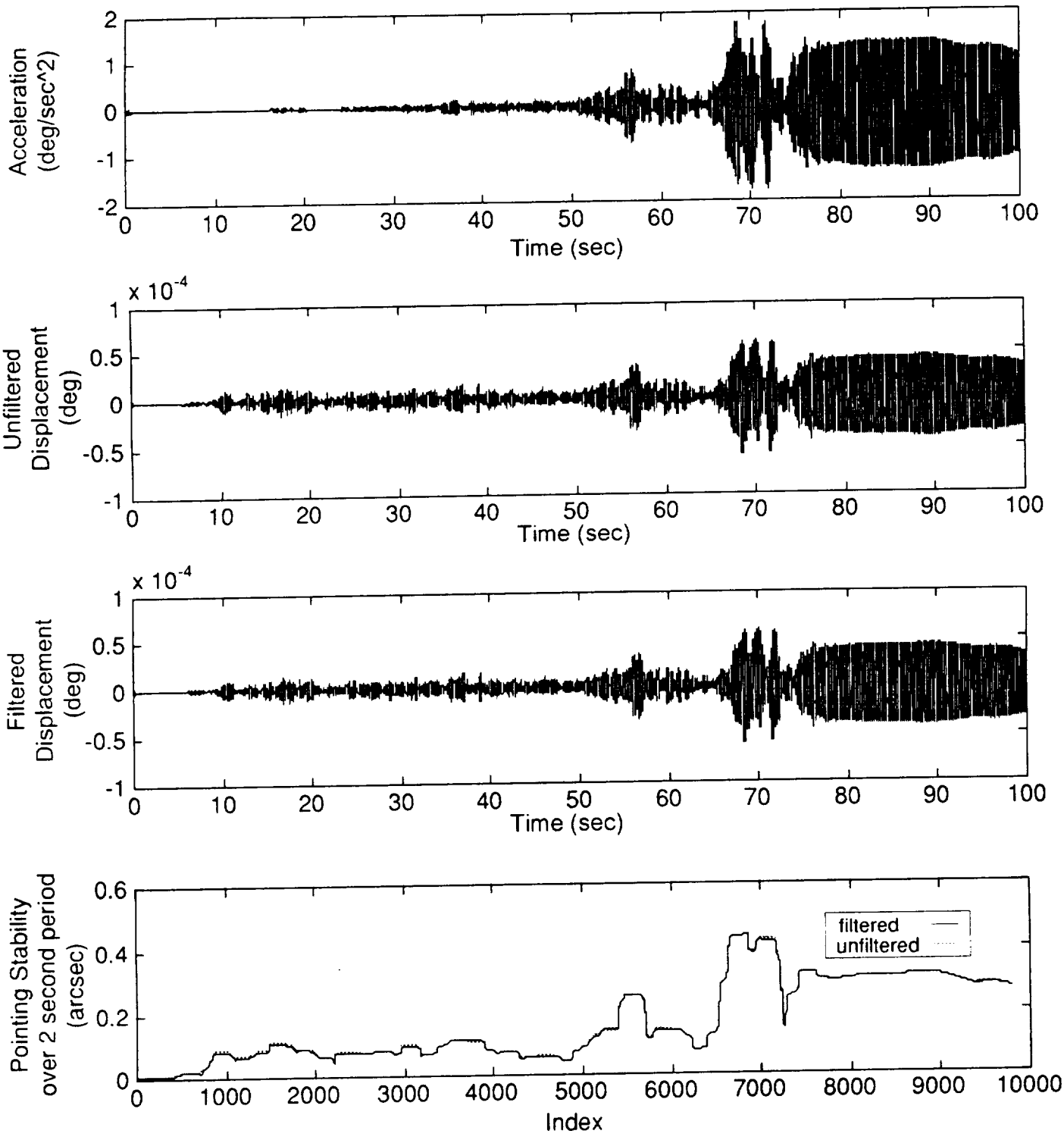

(b) Controlled response

Figure 30. - Concluded.

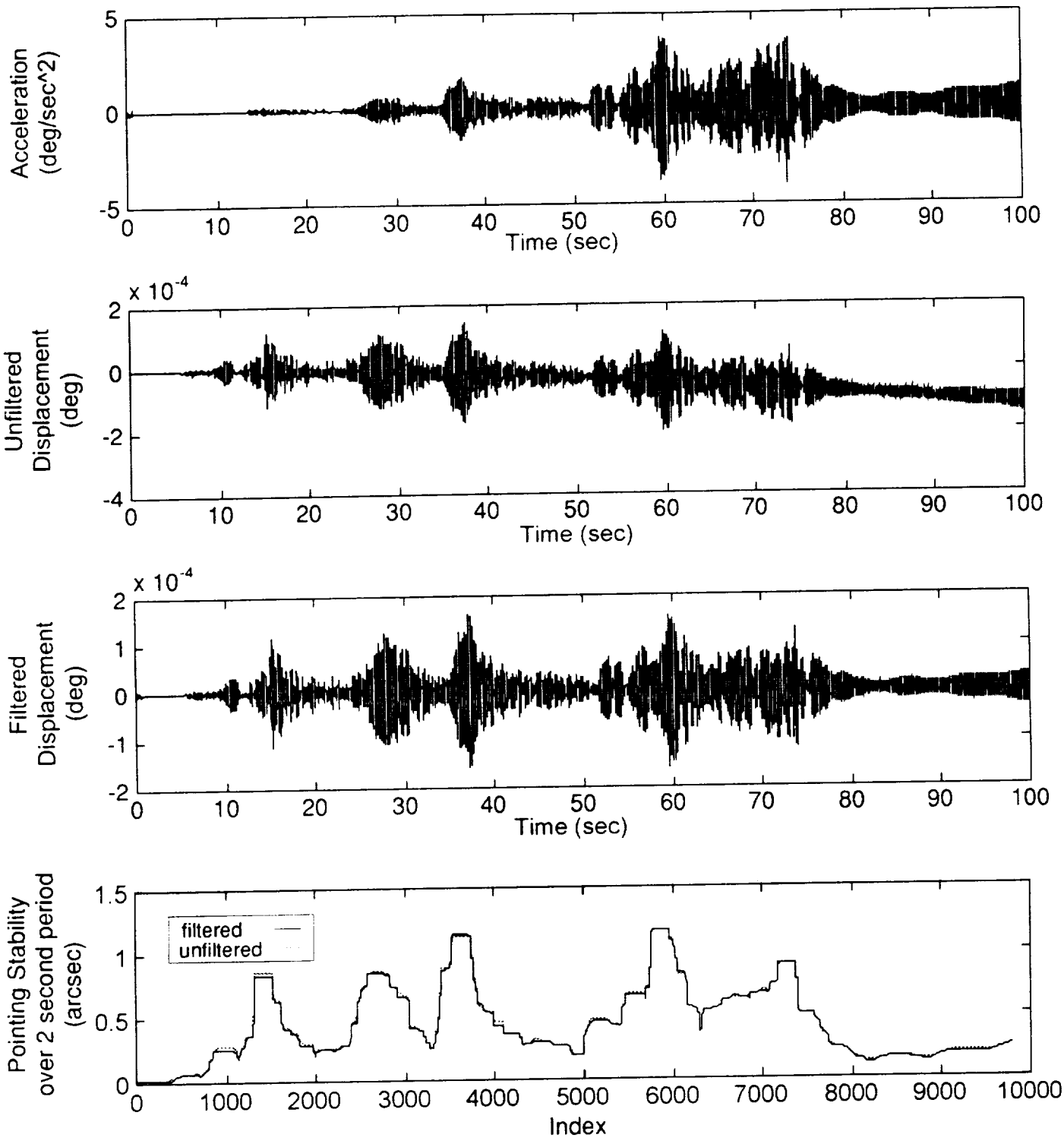

(a) Uncontrolled response

Figure 31. - Integration and pointing stability results at the SOL PAS in the Y ISS Axis for the response due to TRRJ Slew disturbance.

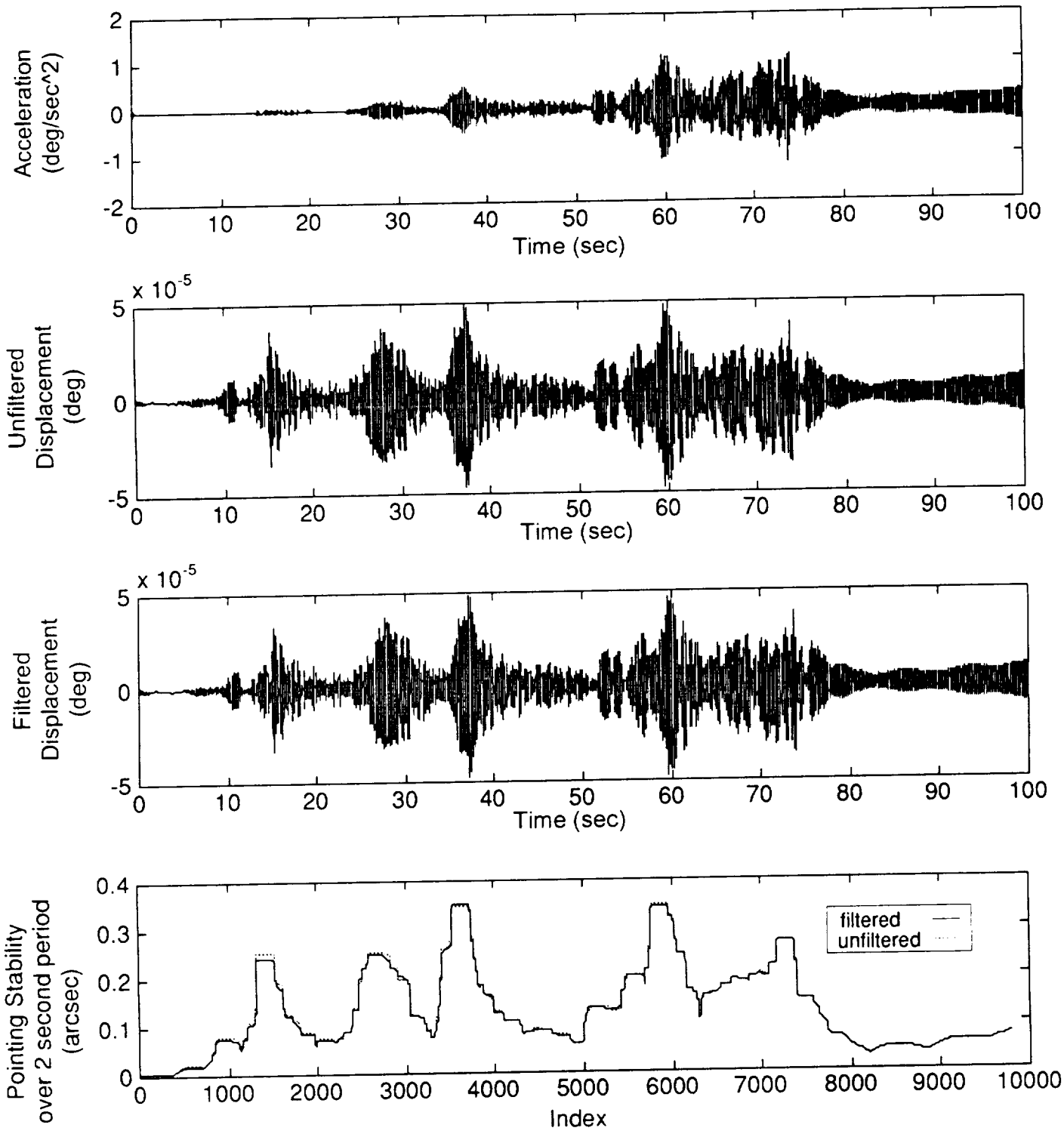

(b) Controlled response

Figure 31. - Concluded.

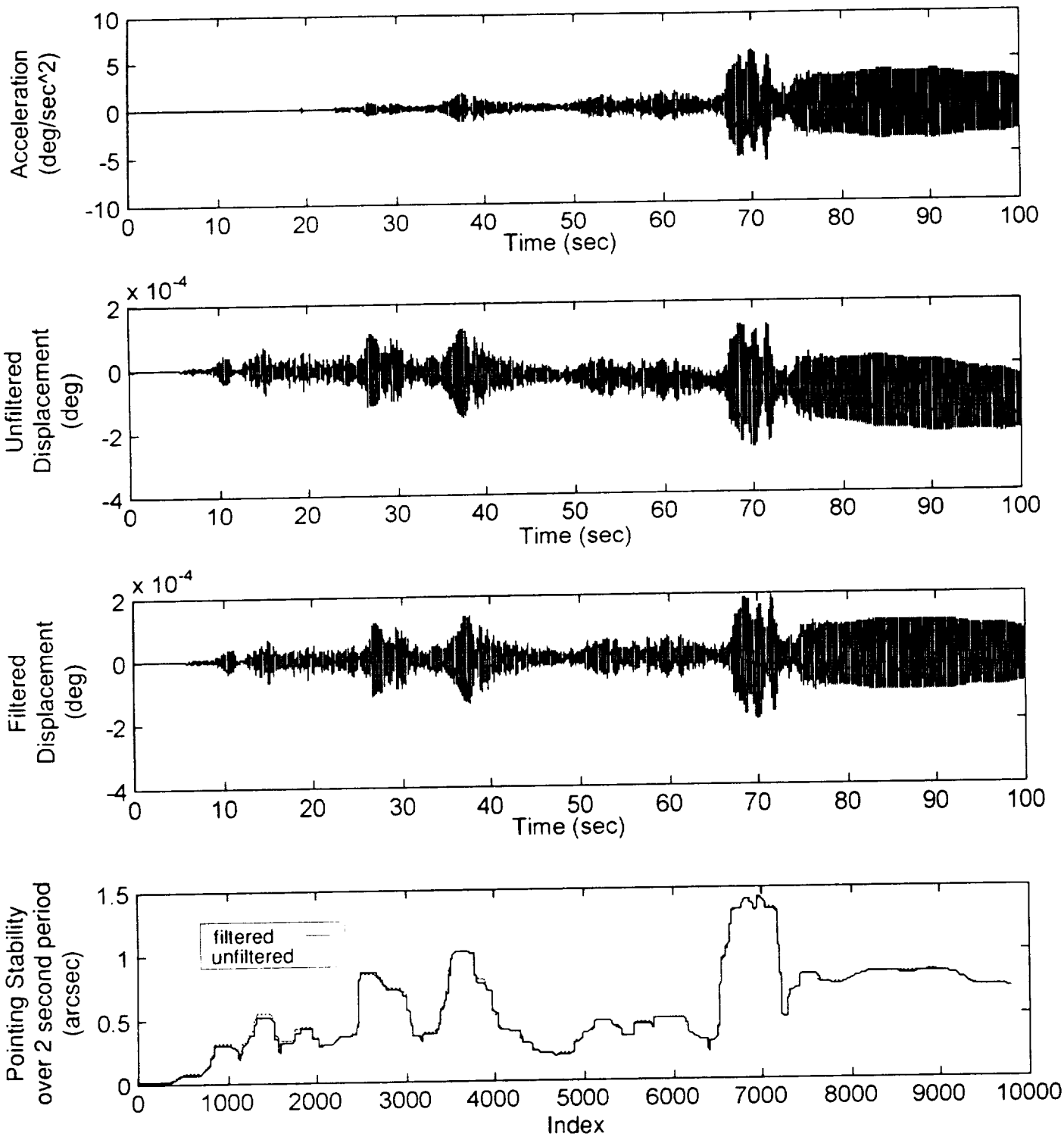

(a) Uncontrolled response

Figure 32. - Integration and pointing stability results at the SOU PAS in the Y ISS Axis for the response due to TRRJ Slew disturbance.

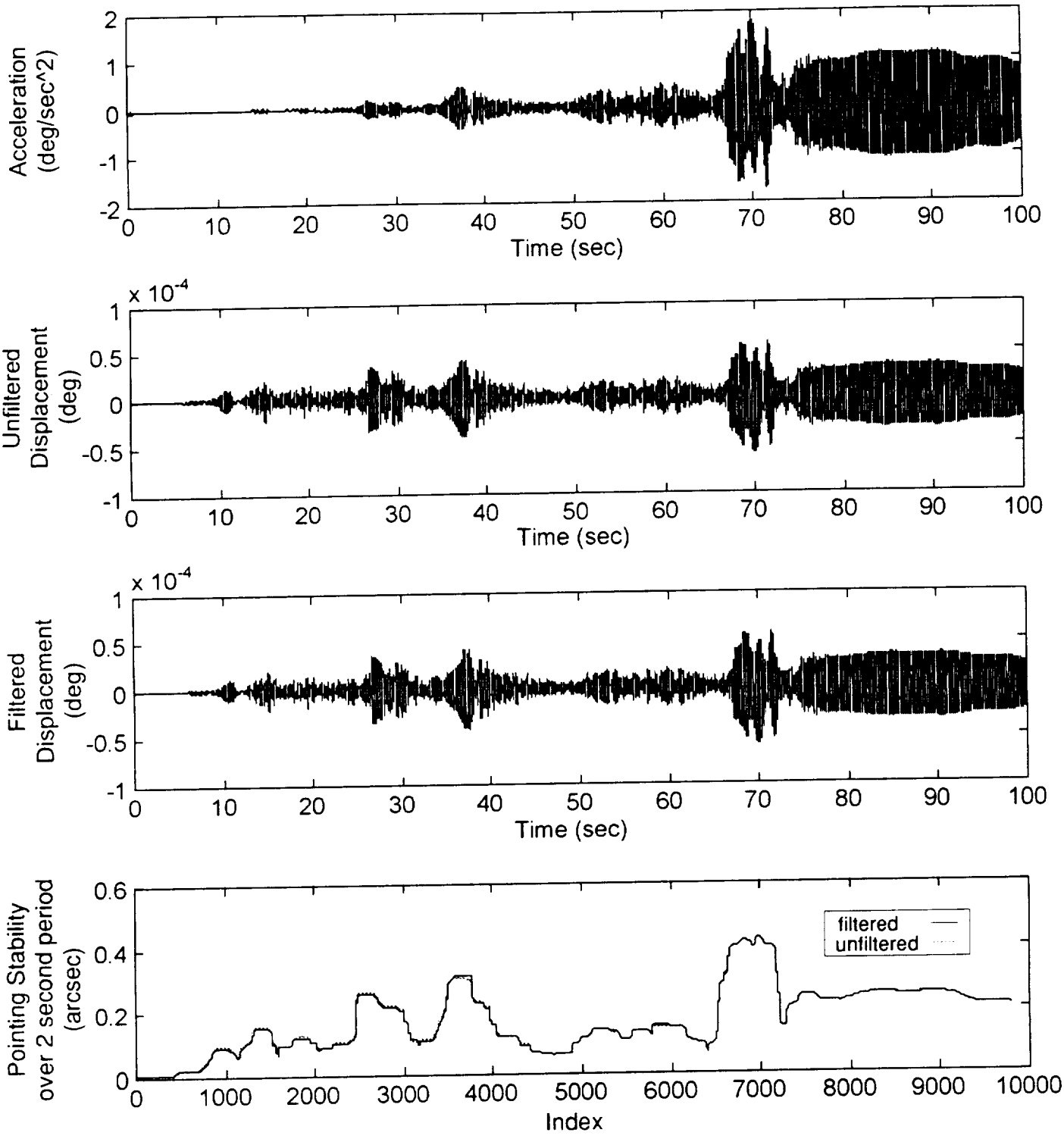

(b) Controlled response

Figure 32. - Concluded.

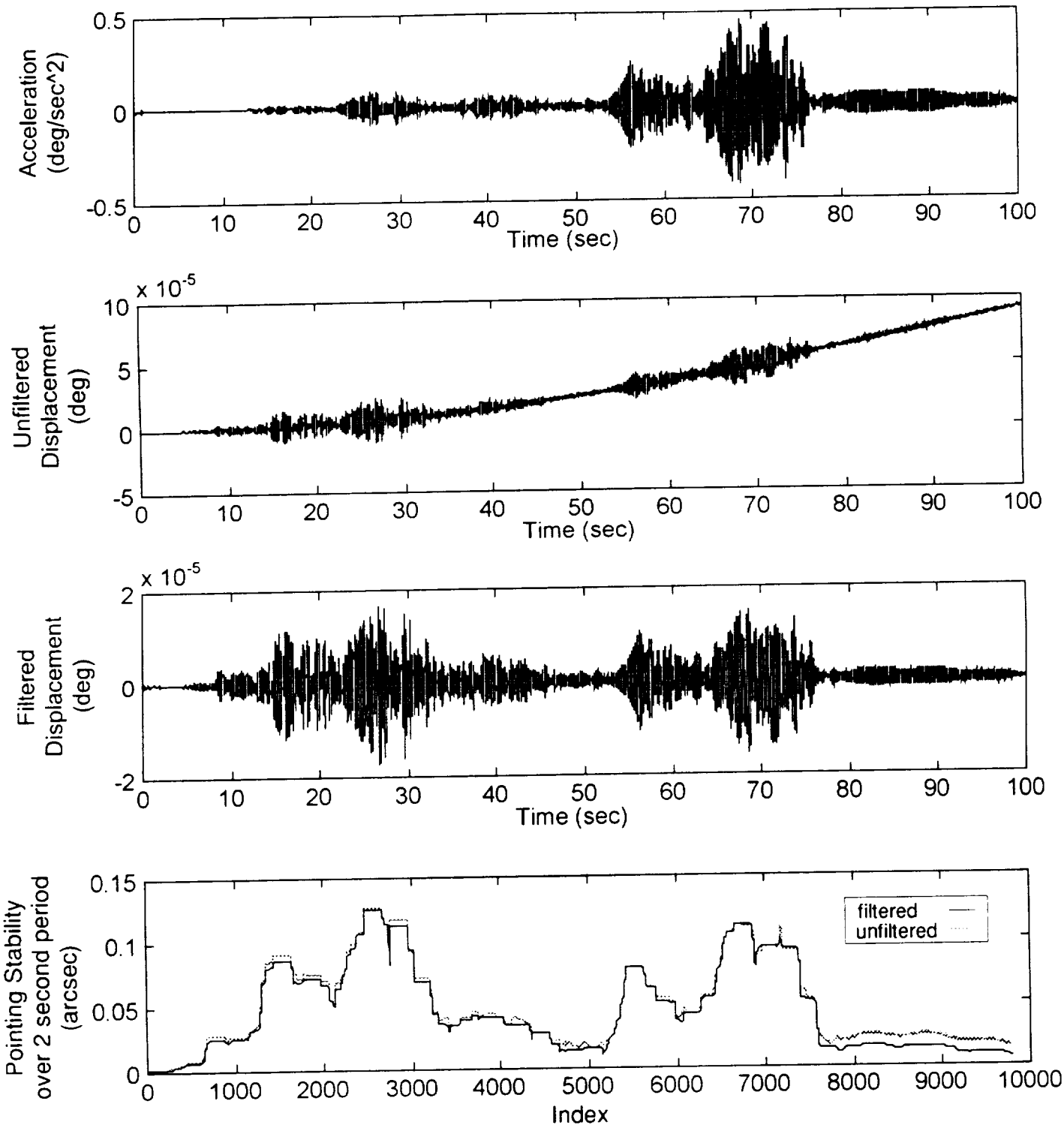

(a) Uncontrolled response

Figure 33. - Integration and pointing stability results at the SIL PAS in the -Z ISS Axis for the response due to TRRJ Slew disturbance.

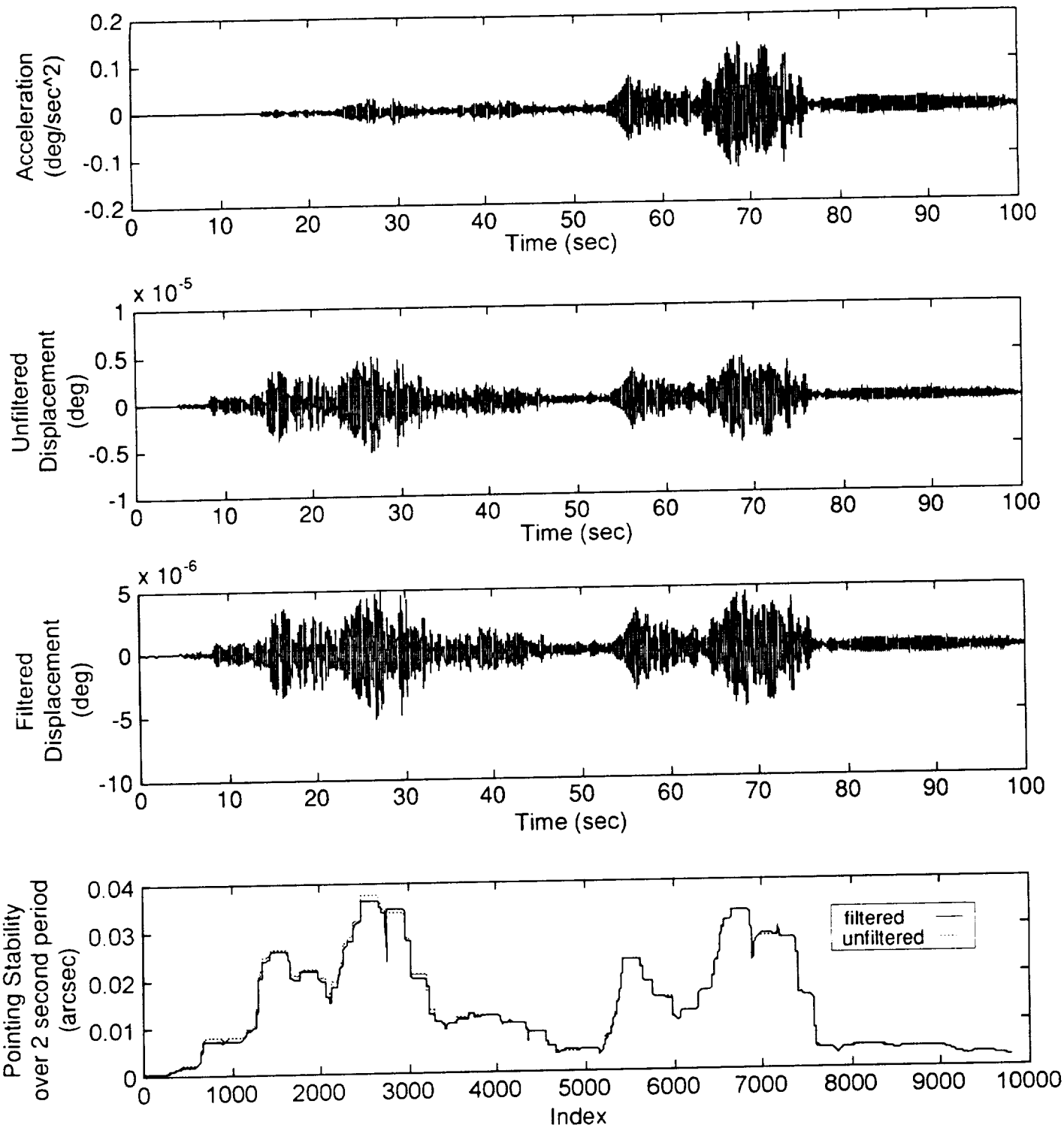

(b) Controlled response

Figure 33. - Concluded.

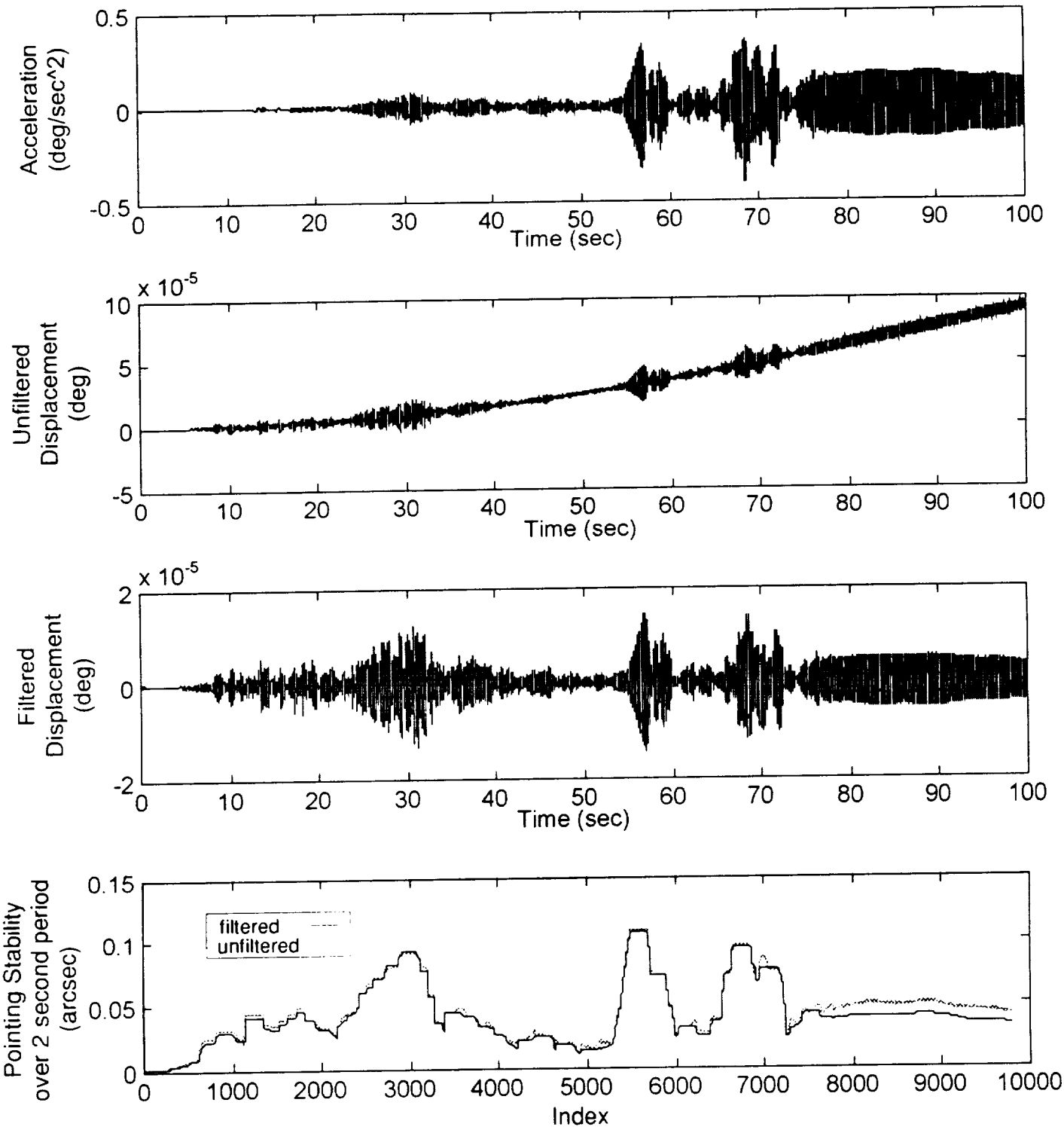

(a) Uncontrolled response

Figure 34. - Integration and pointing stability results at the SIU PAS in the -Z ISS Axis for the response due to TRRJ Slew disturbance.

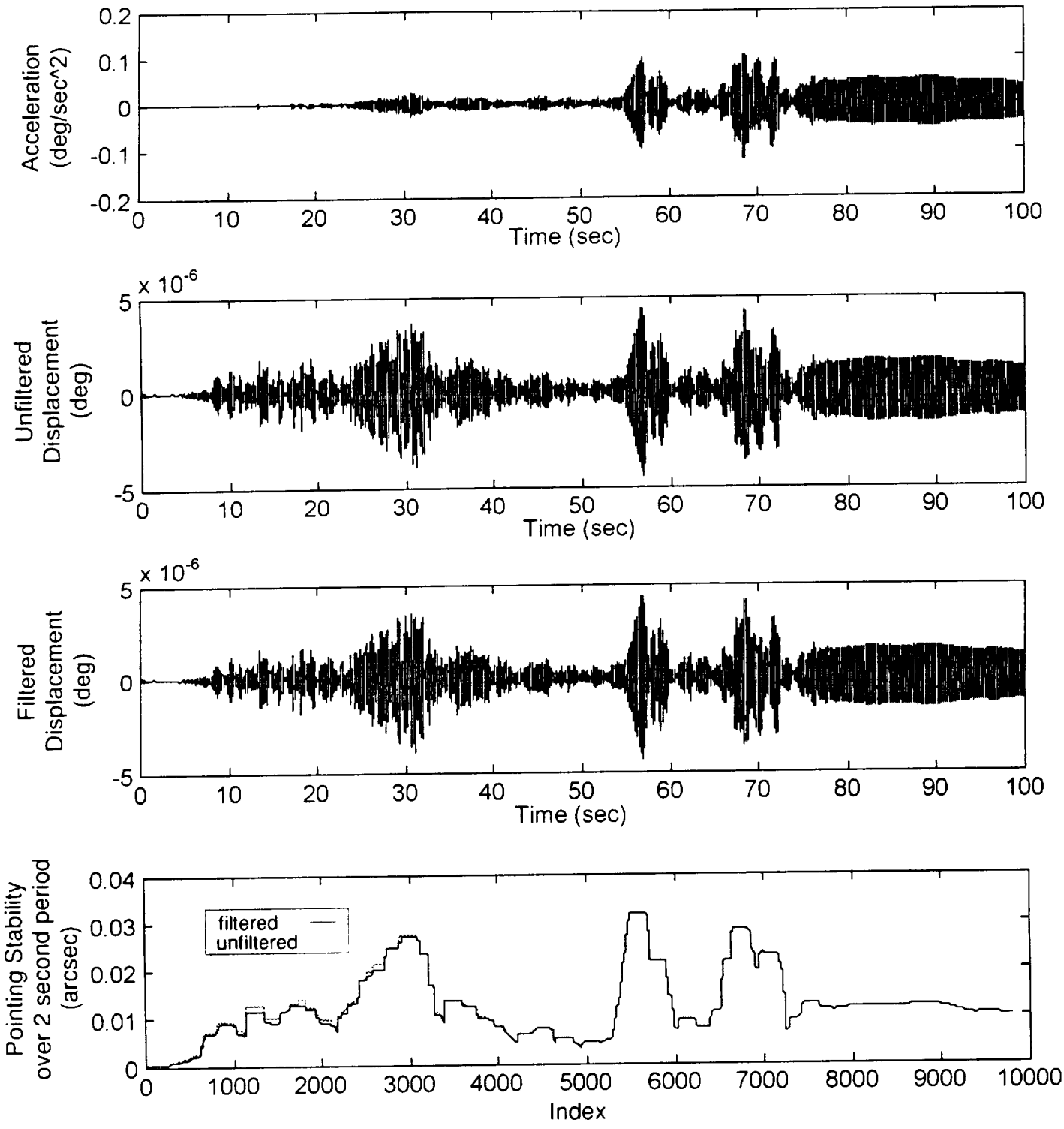

(b) Controlled response

Figure 34. - Concluded.

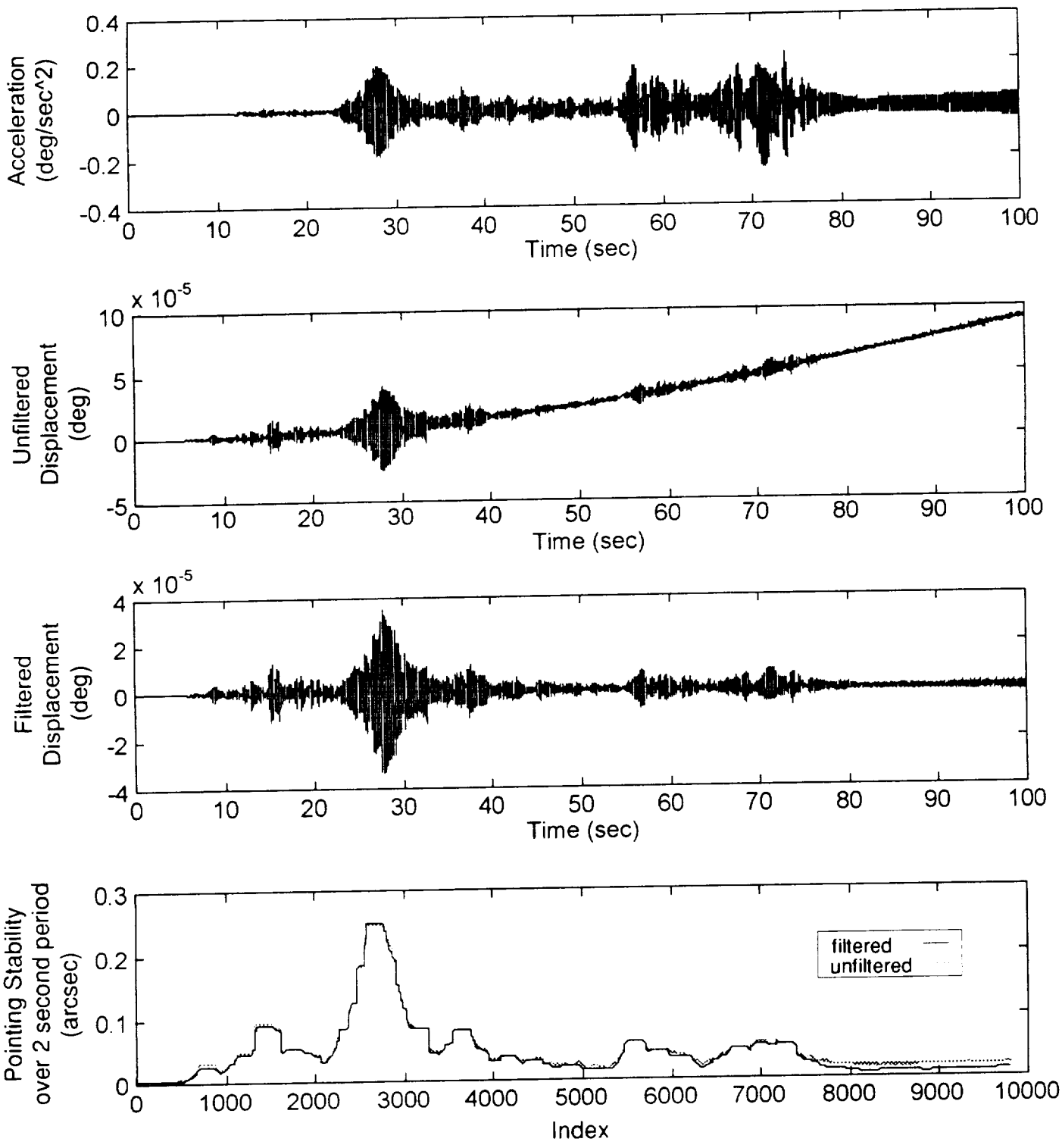

(a) Uncontrolled response

Figure 35. - Integration and pointing results results at the SOL PAS in the -Z ISS Axis for the response due to TRRJ Slew disturbance.

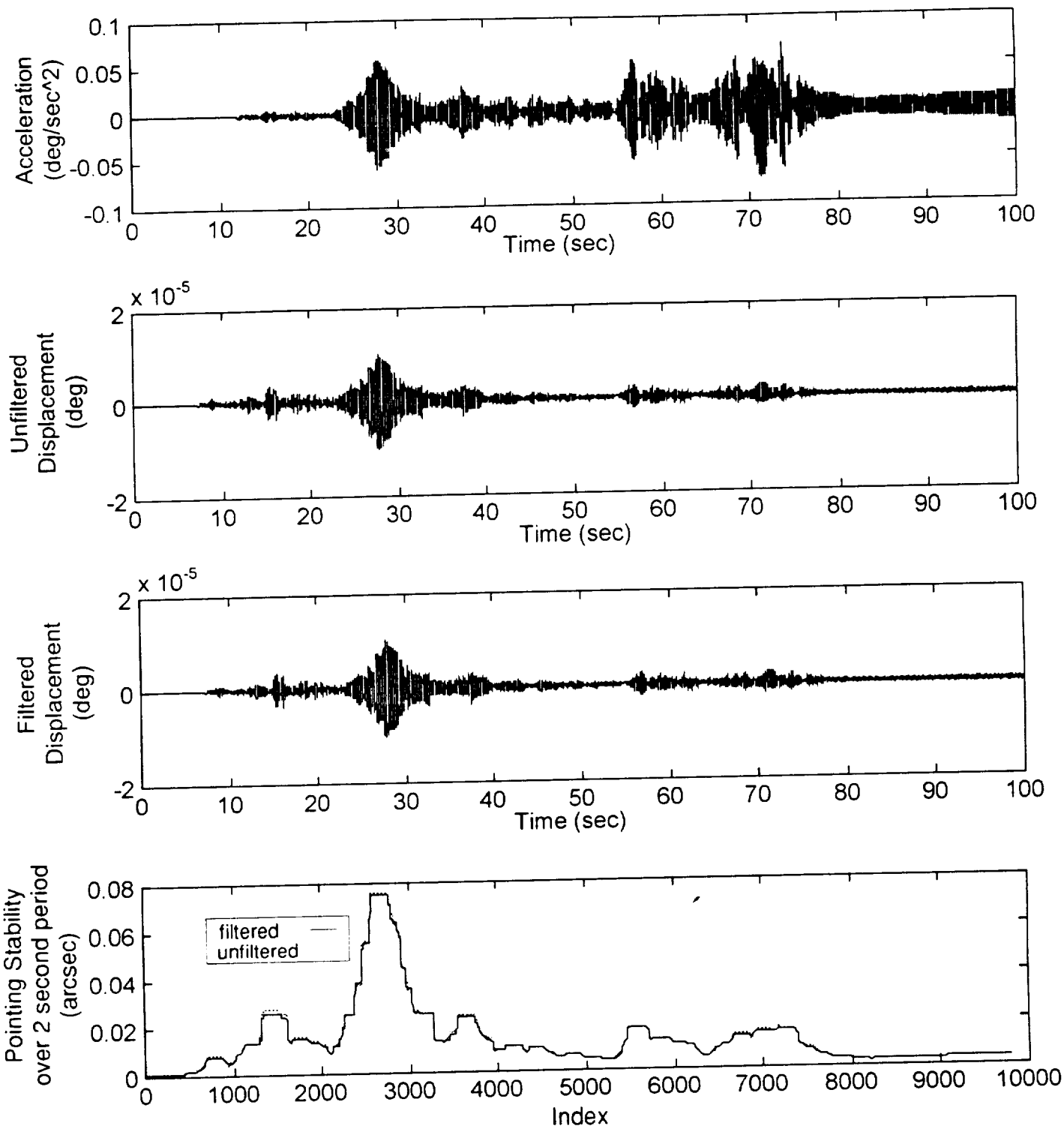

(b) Controlled response

Figure 35. - Concluded.

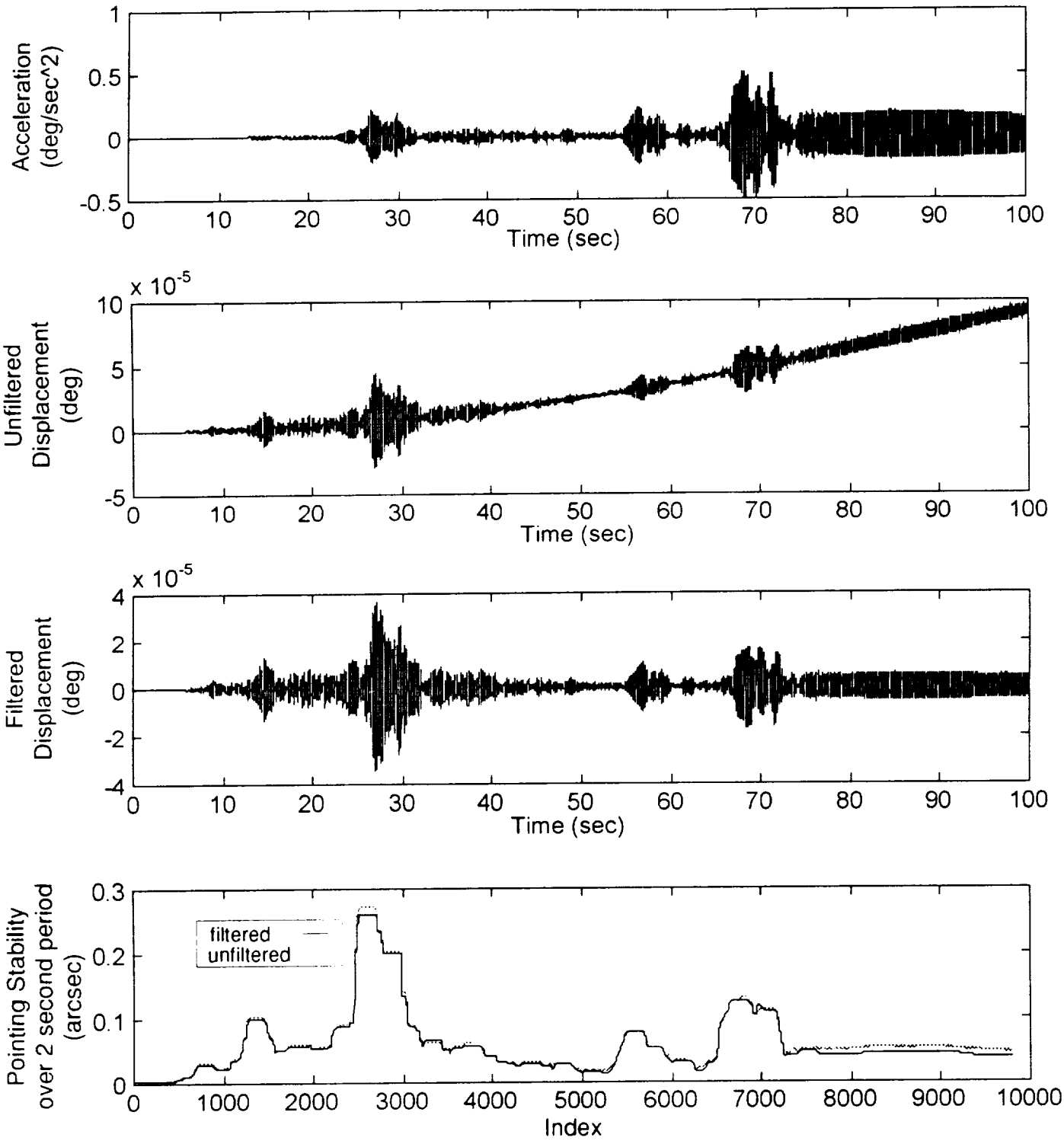

(a) Uncontrolled response

Figure 36. - Integration and pointing stability results at the SOU PAS in the -Z ISS Axis for the response due to TRRJ Slew disturbance.

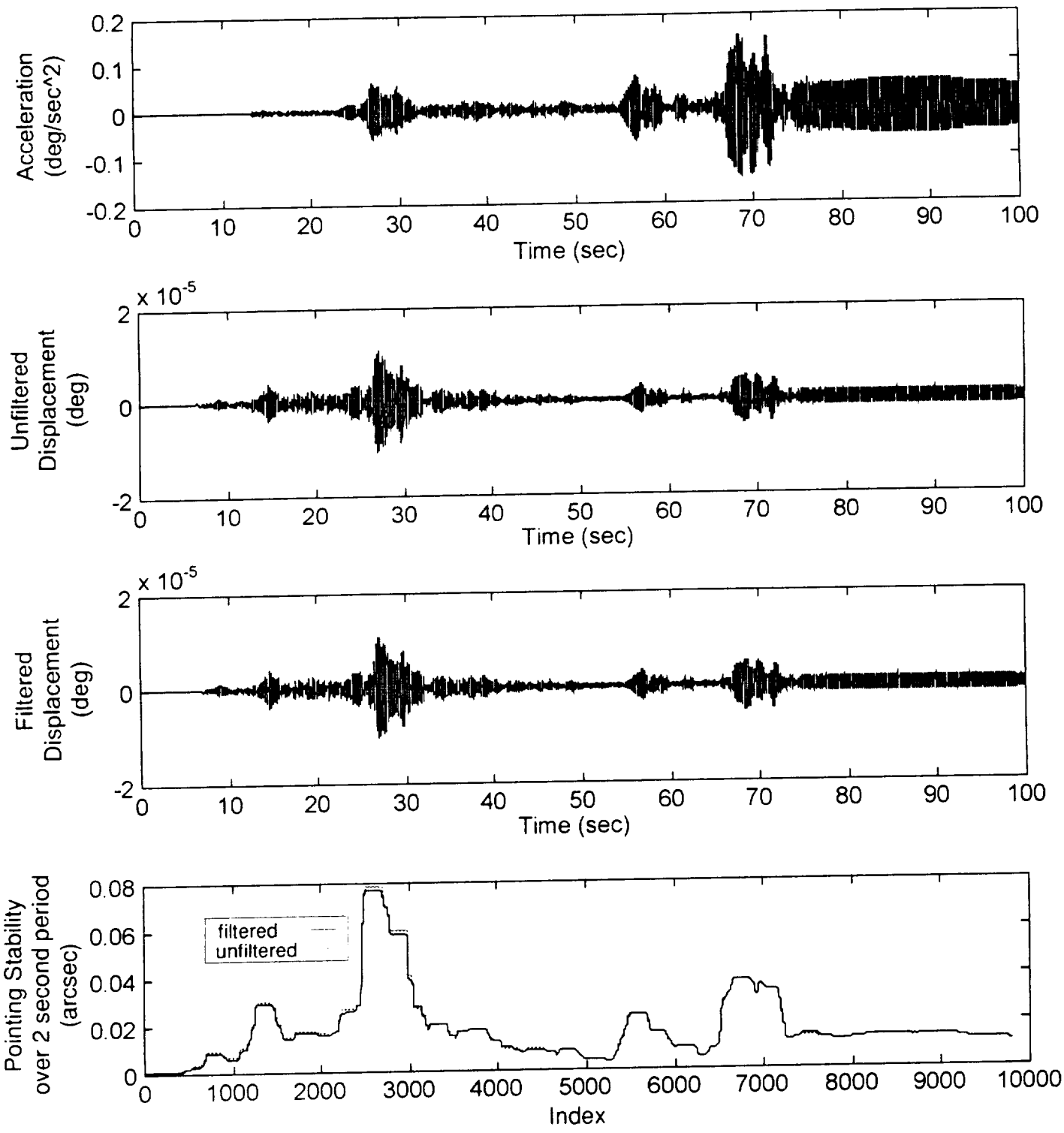

(b) Controlled response

Figure 36. - Concluded.

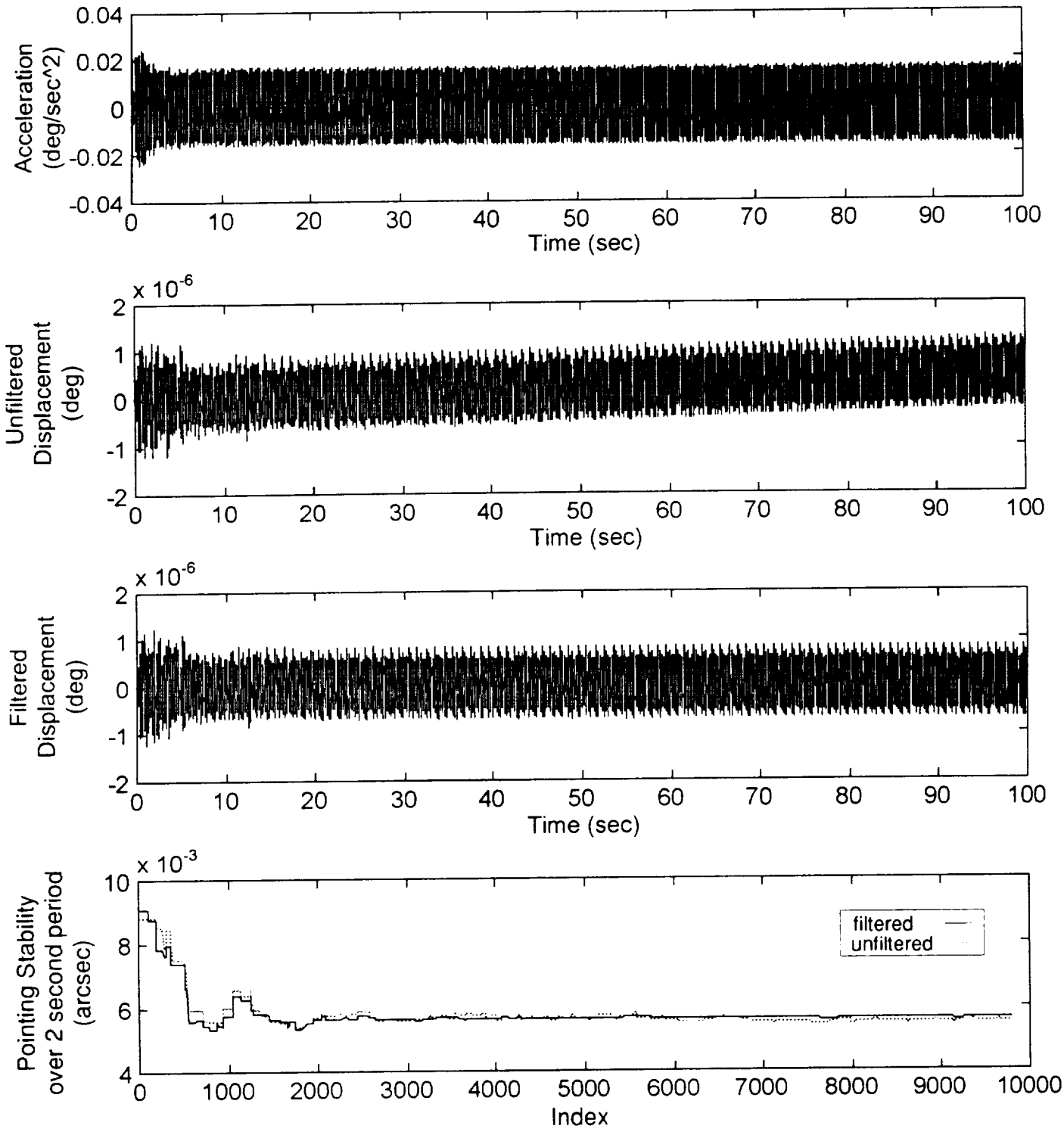

Figure 37. - Integration and pointing stability results at the SIL PAS in the -X ISS Axis for the response due to CMG Y disturbance.

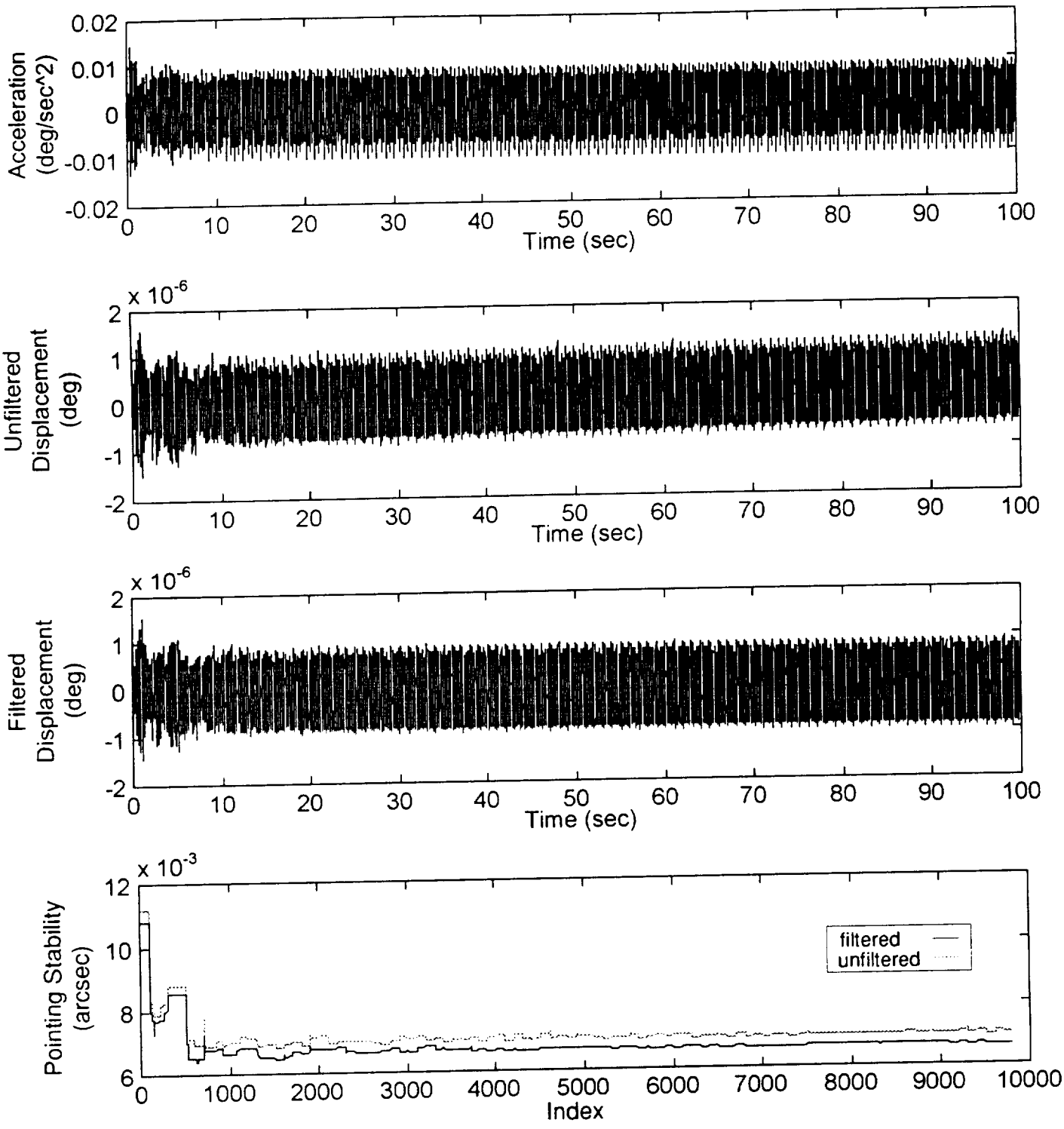

Figure 38. - Integration and pointing stability results at the SIU PAS in the -X ISS Axis for the response due to CMG Y disturbance.

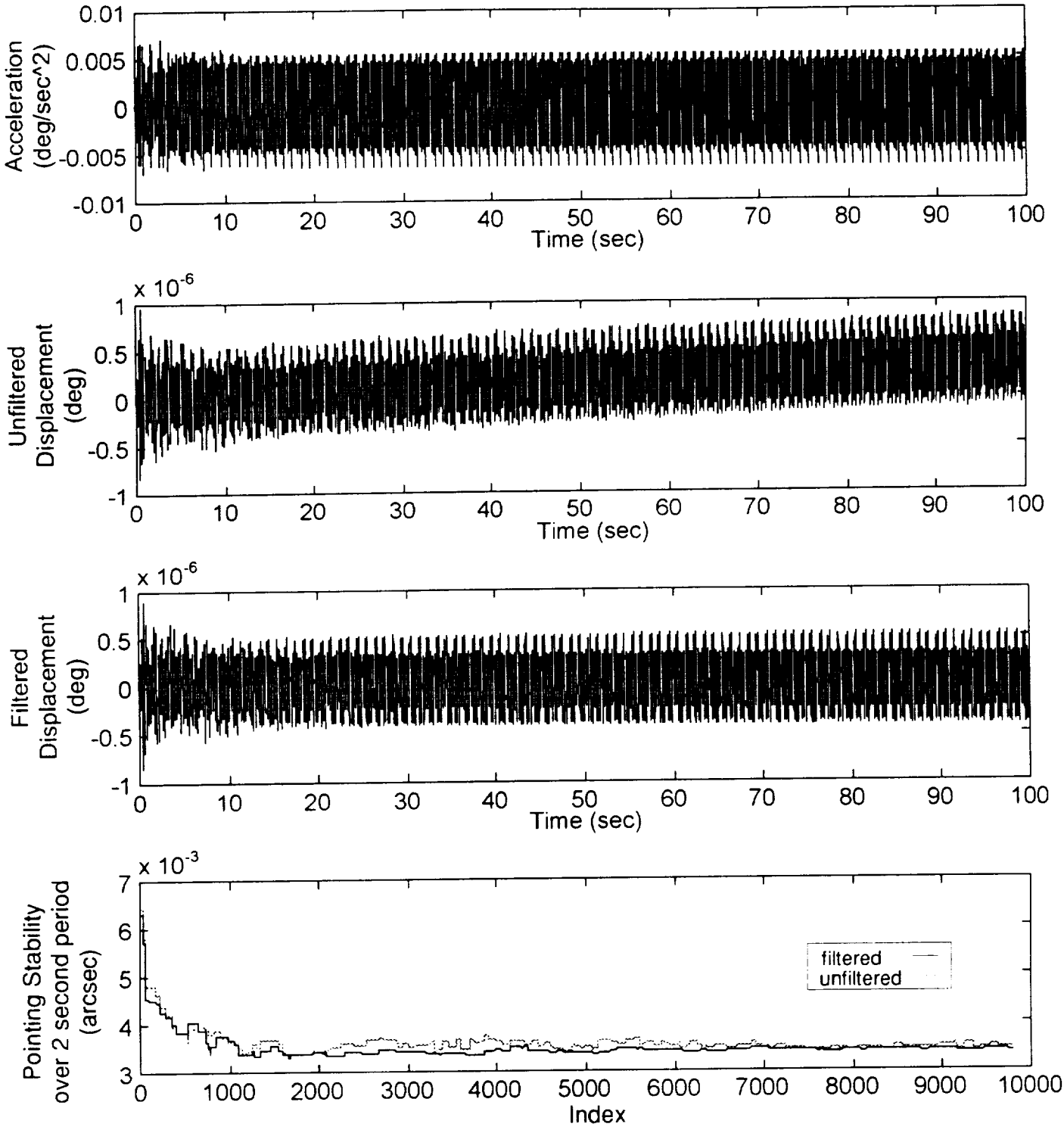

Figure 39. - Integration and pointing stability results at the SOL PAS in the -X ISS Axis for the response due to CMG Y disturbance.

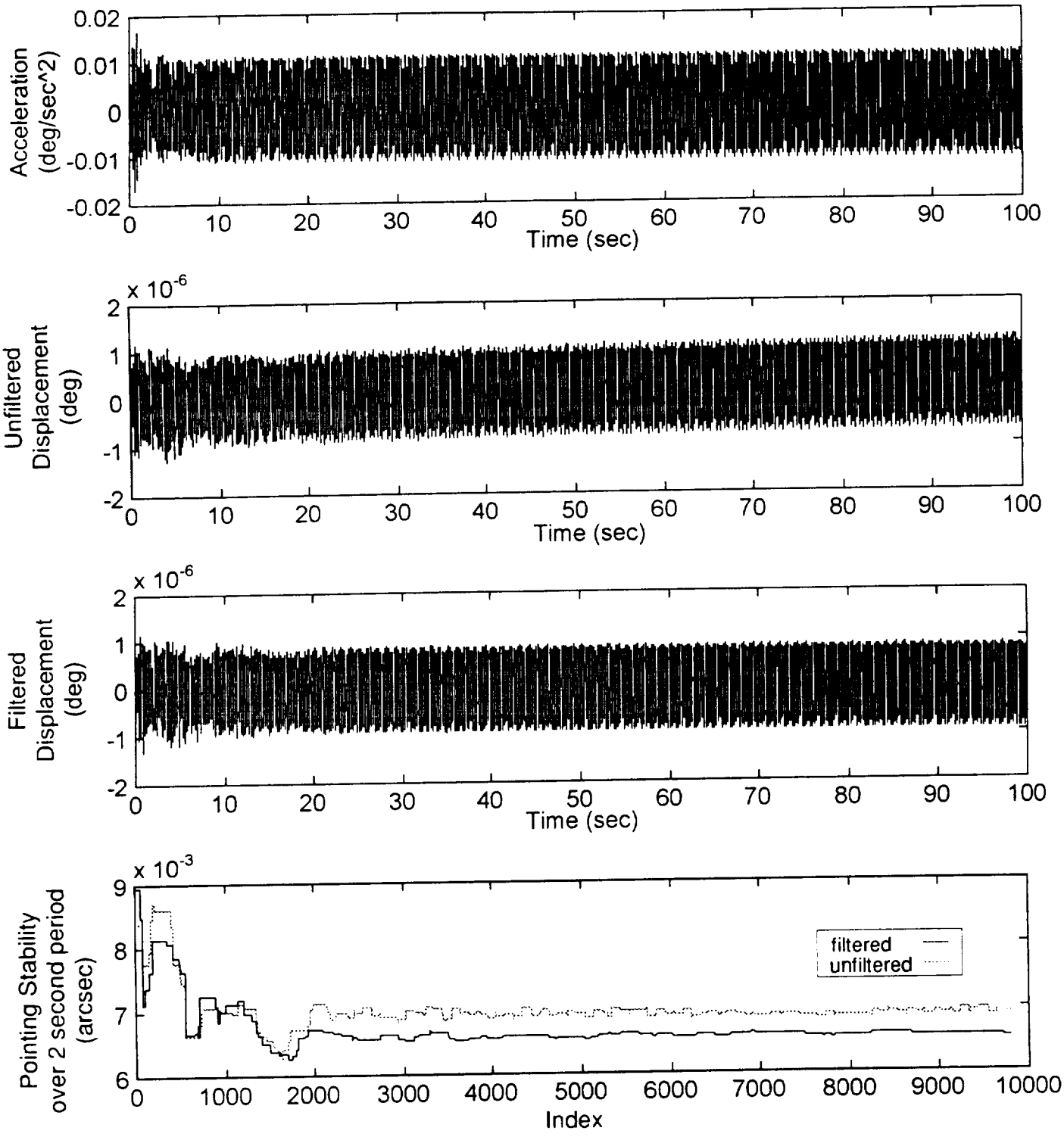

Figure 40. - Integration and pointing stability results at the SOU PAS in the -X ISS Axis for the response due to CMG Y disturbance.

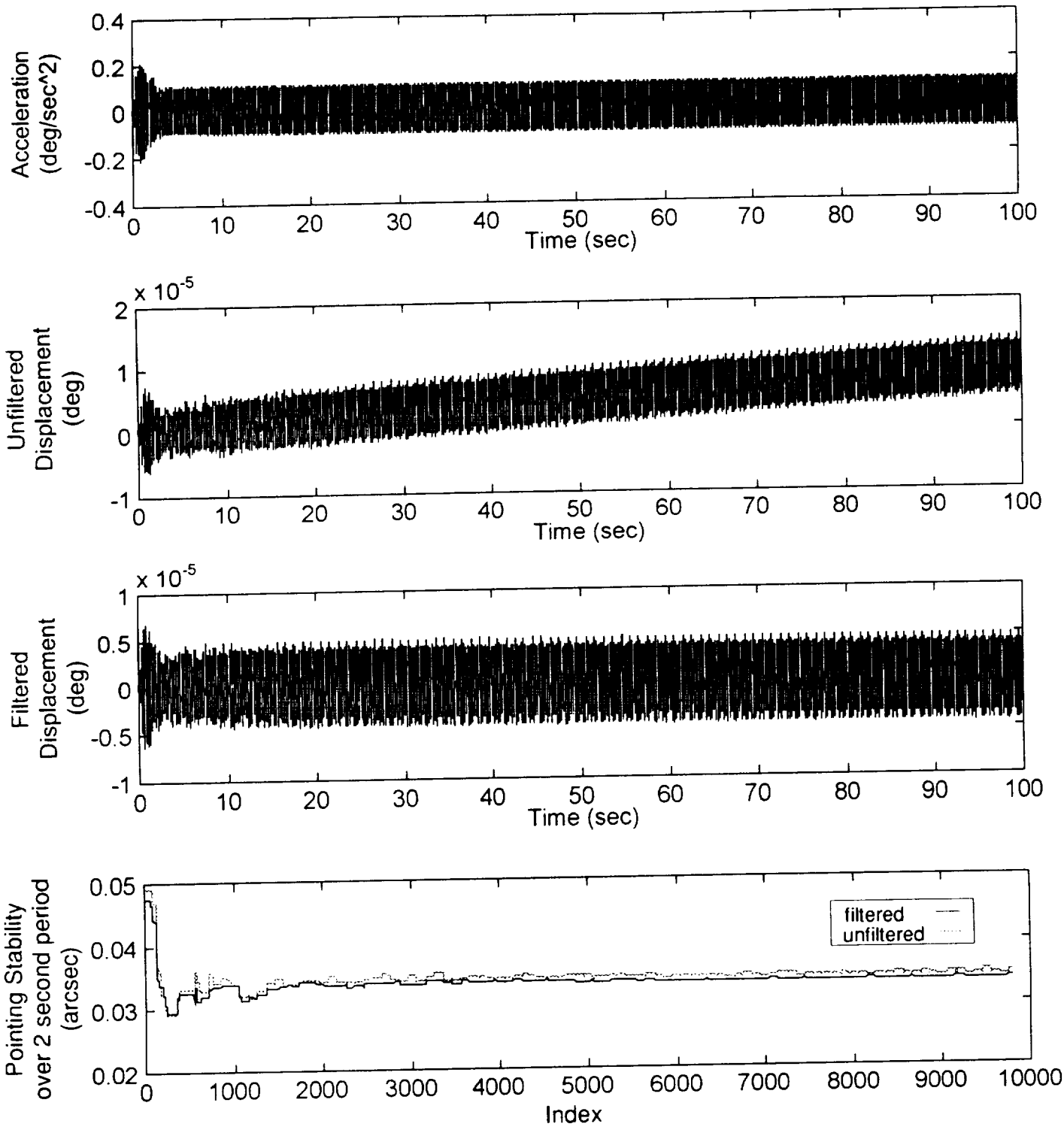

Figure 41. - Integration and pointing stability results at the SIL PAS in the Y ISS Axis for the response due to CMG Y disturbance.

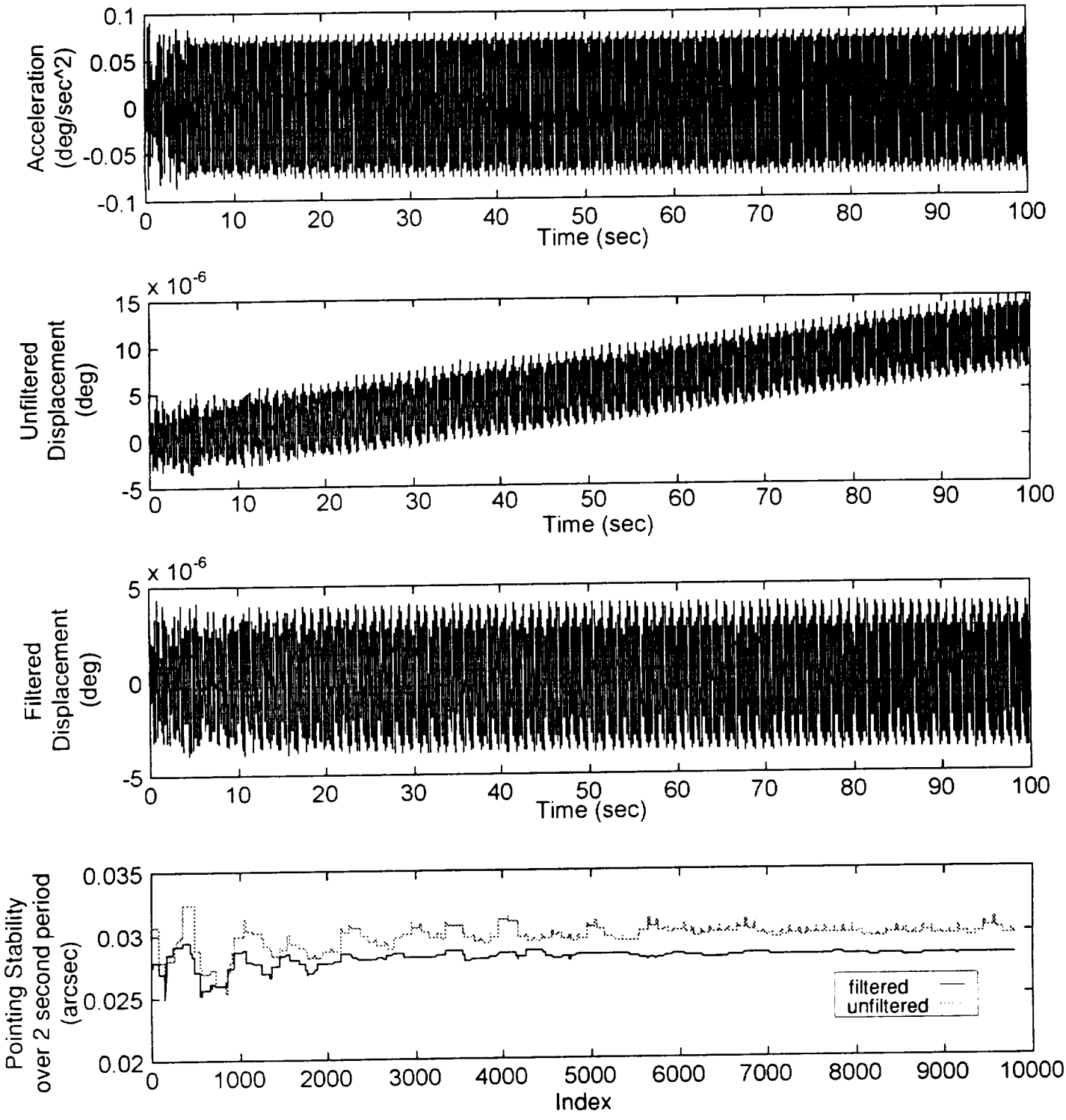

Figure 42. - Integration and pointing stability results at the SIU PAS in the Y ISS Axis for the response due to CMG Y disturbance.

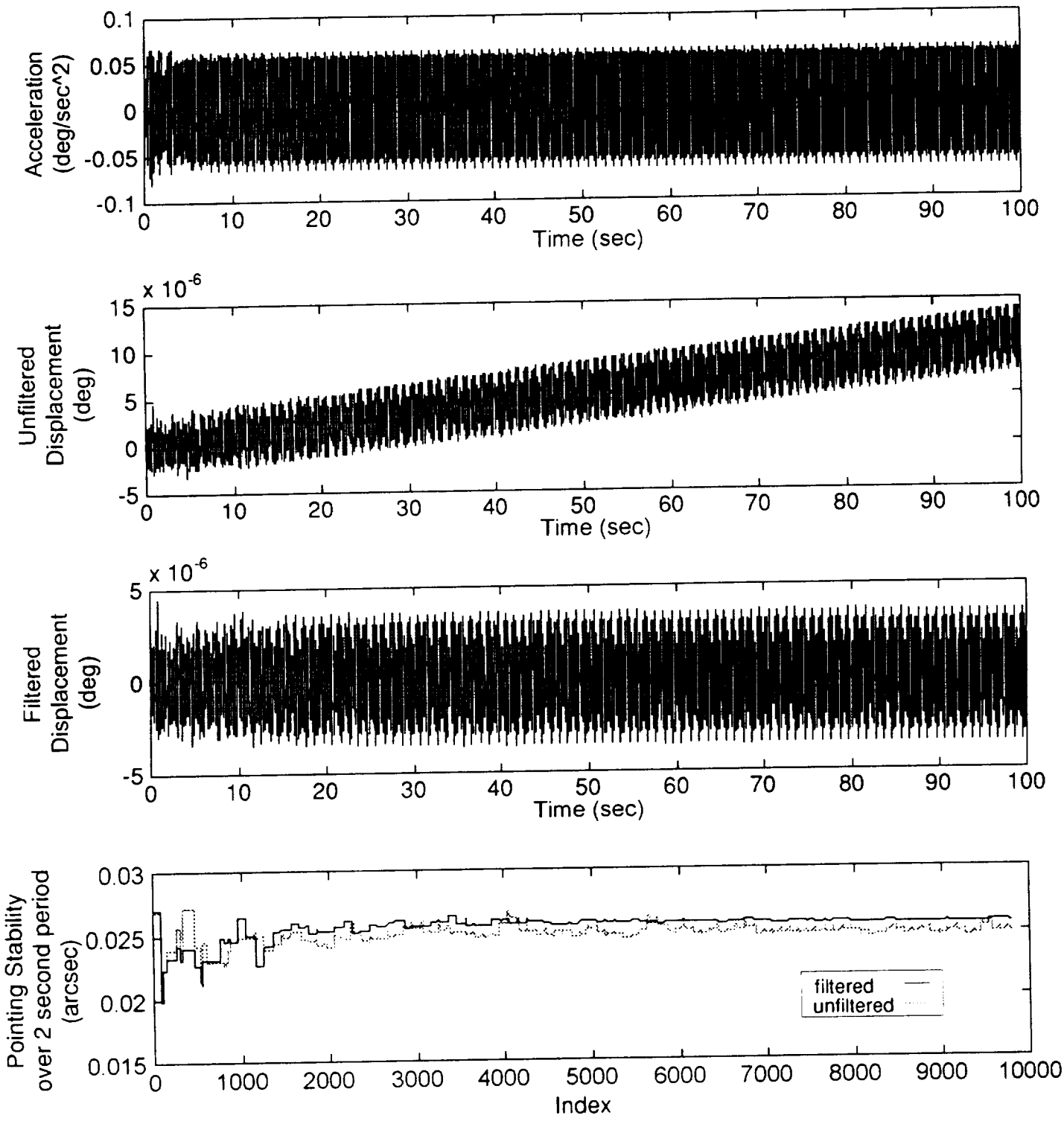

Figure 43. - Integration and pointing stability results at the SOL PAS in the Y ISS Axis for the response due to CMG Ydisturbance.

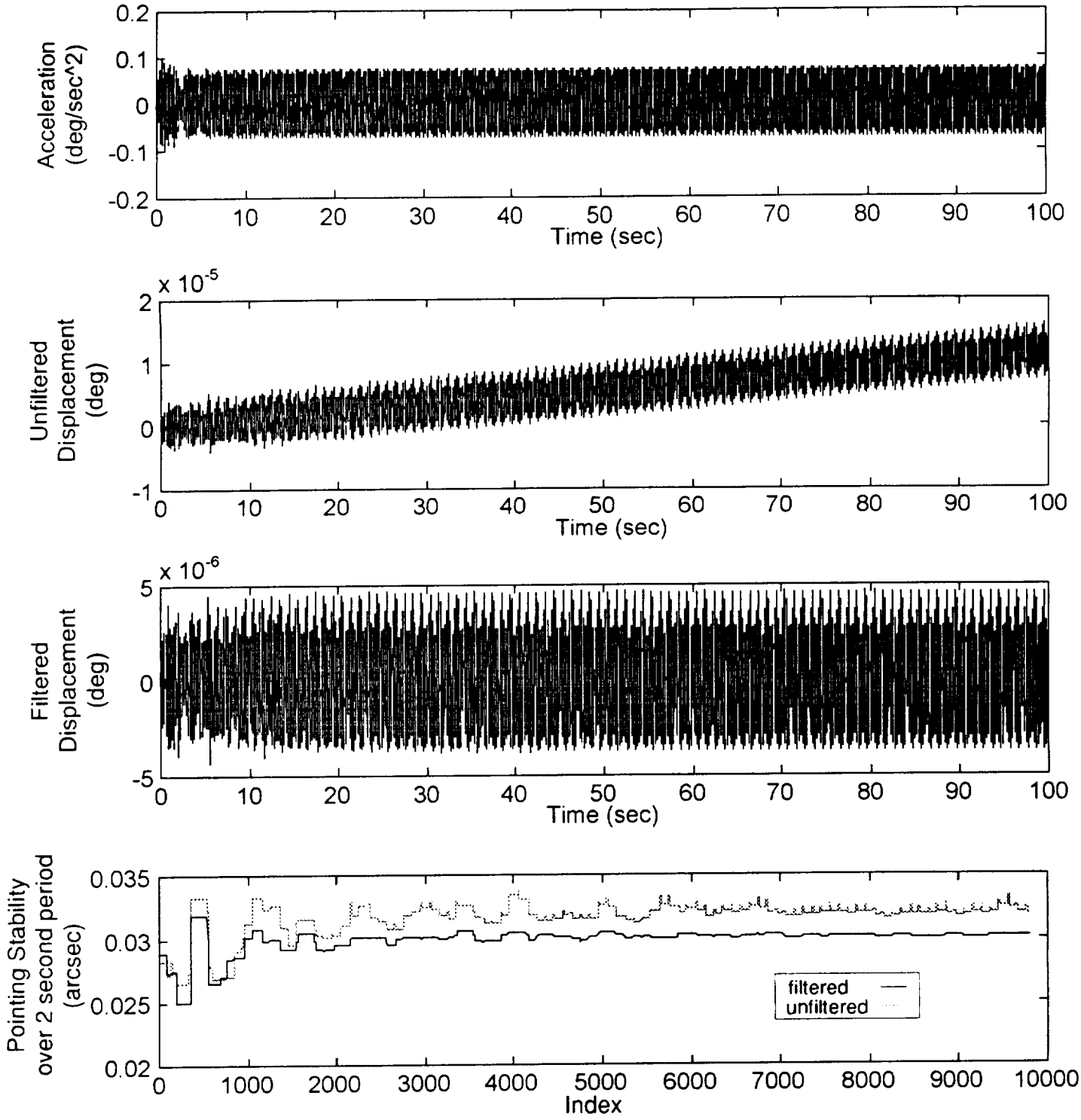

Figure 44. - Integration and pointing stability results at the SOU PAS in the Y ISS Axis for the response due to CMG Y disturbance.

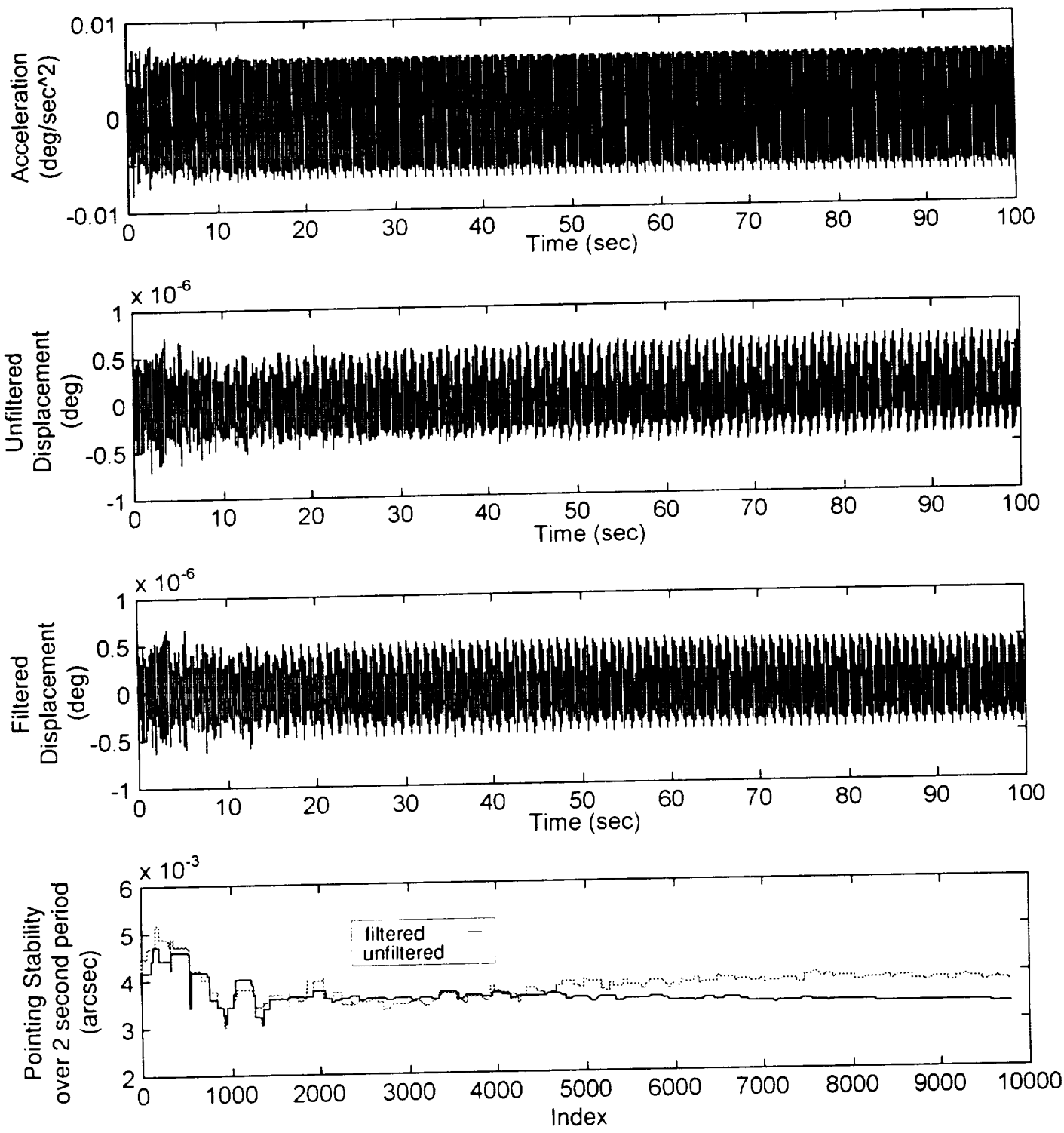

Figure 45. - Integration and pointing stability results at the SIL PAS in the -Z ISS Axis for the response due to CMG Y disturbance.

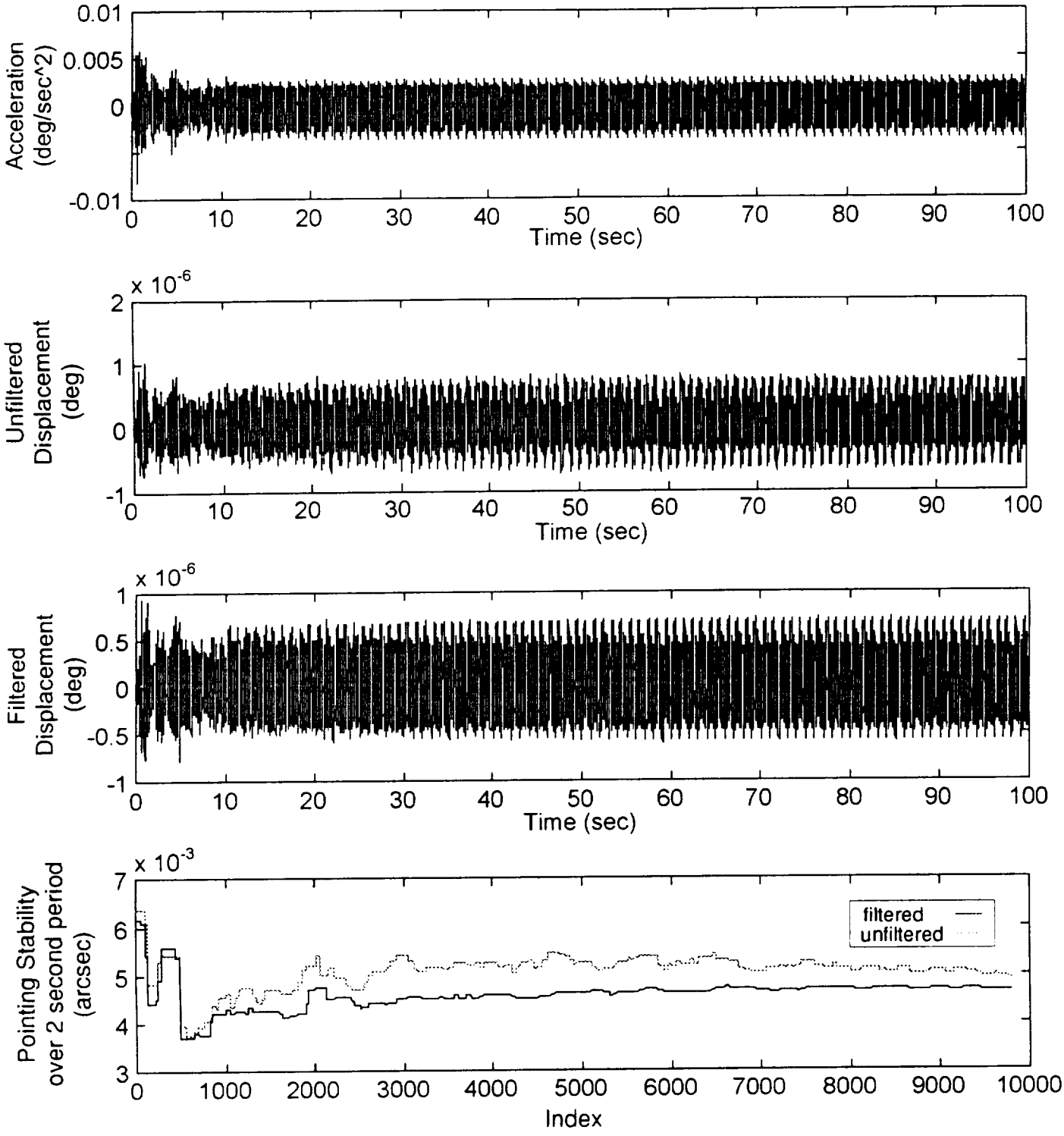

Figure 46. - Integration and pointing stability results at the SIU PAS in the -Z ISS Axis for the response due to CMG Y disturbance.

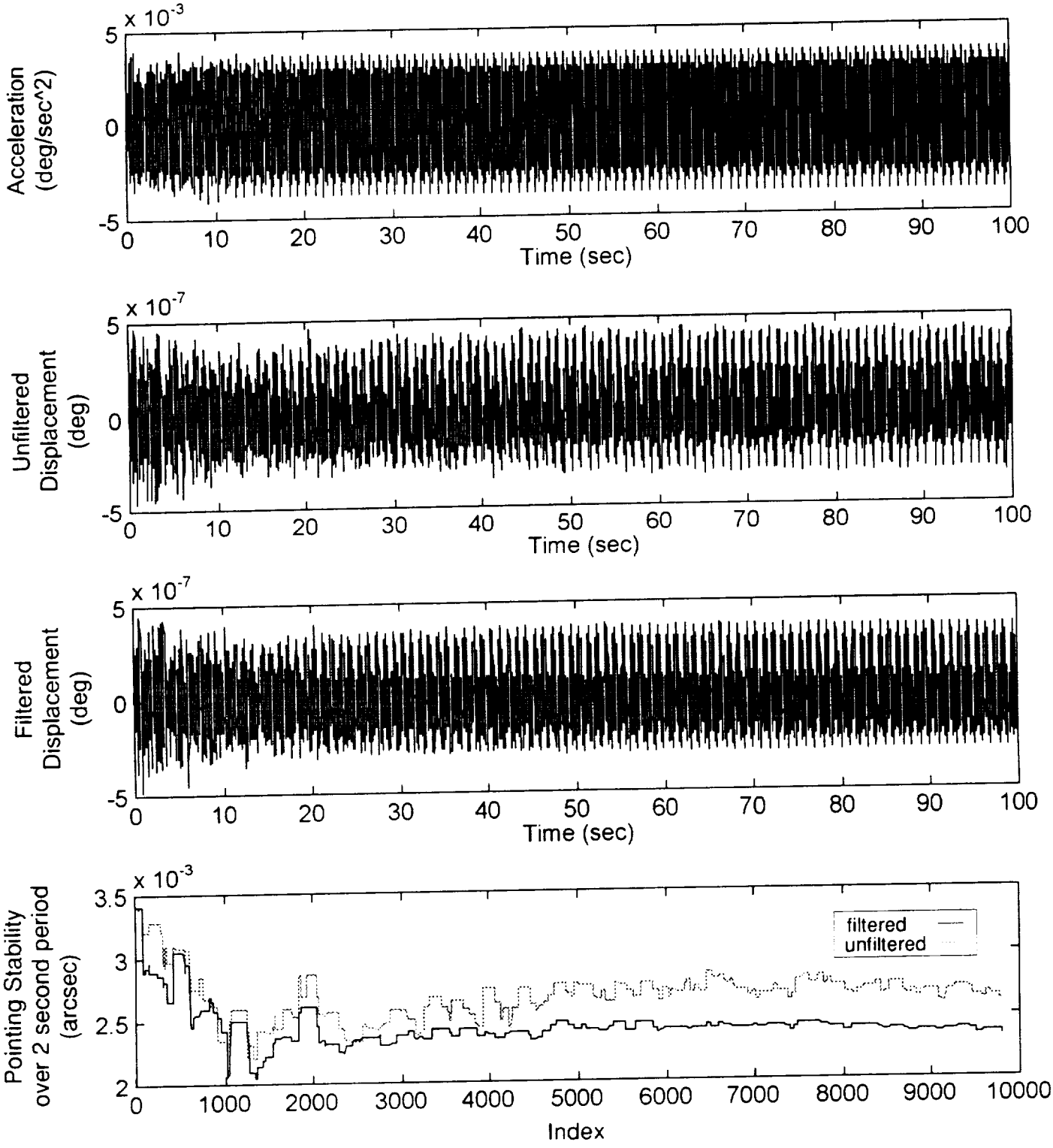

Figure 47. - Integration and pointing stability results at the SOL PAS in the -Z ISS Axis for the response due to CMG Y disturbance.

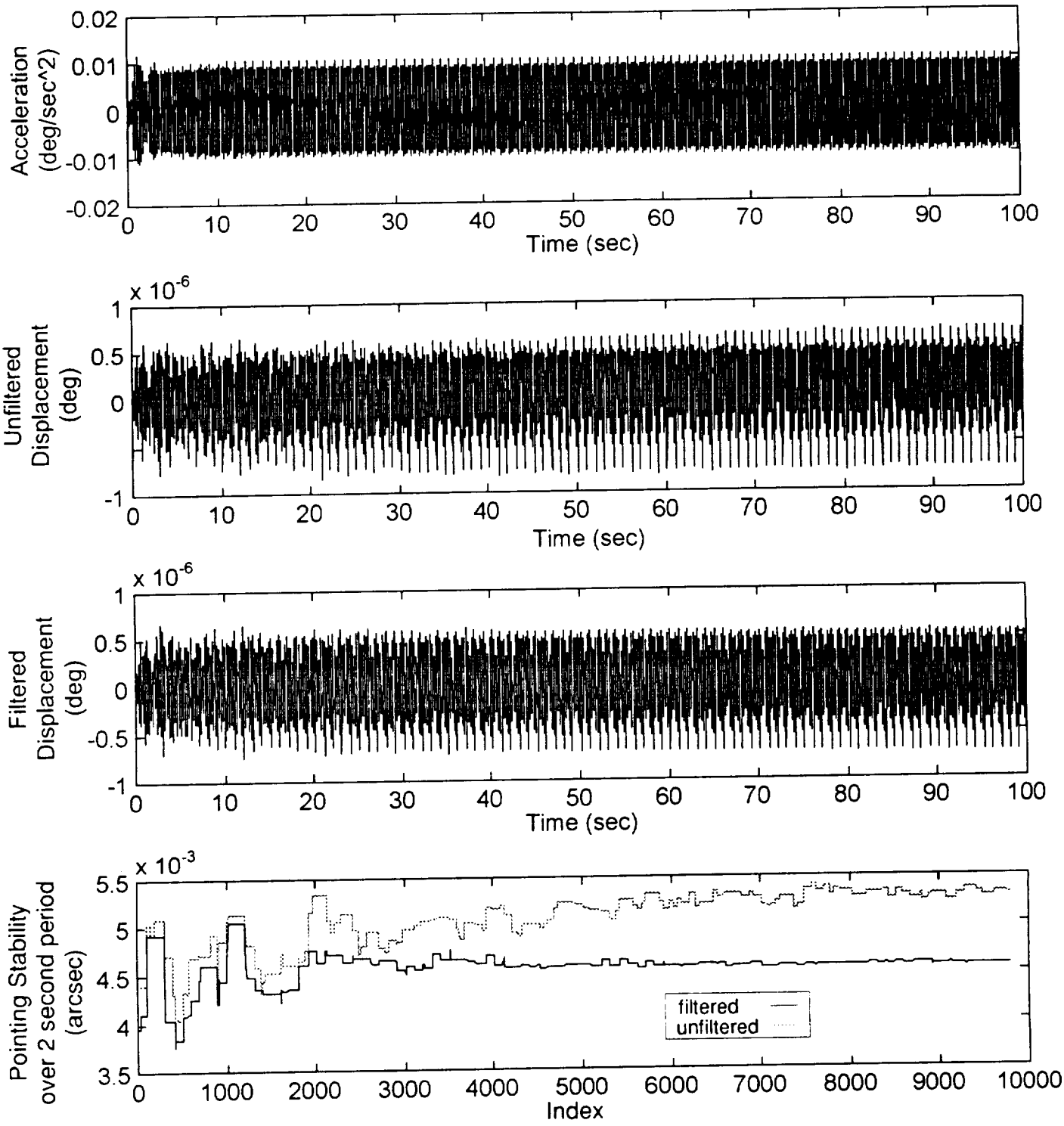

Figure 48. - Integration and pointing stability results at the SOU PAS in the -Z ISS Axis for the response dueto CMG Y disturbance.

REPORT DOCUMENTATION PAGE

Form Approved
OMB No. 0704-0188

1. AGENCY USE ONLY (Leave blank)	2. REPORT DATE	3. REPORT TYPE AND DATES COVERED
	January 1997	Technical Memorandum

4. TITLE AND SUBTITLE

DAC-3 Pointing Stability Analysis Results for SAGE III and Other Users of the International Space Station (ISS) Payload Attachment Sites (PAS)

5. FUNDING NUMBERS

WU 632-20-21-11

6. AUTHOR(S)

Jessica A. Woods-Vedeler
Gabriel Rombado

7. PERFORMING ORGANIZATION NAME(S) AND ADDRESS(ES)

NASA Langley Research Center
Hampton, VA 23681-0001

8. PERFORMING ORGANIZATION REPORT NUMBER

9. SPONSORING / MONITORING AGENCY NAME(S) AND ADDRESS(ES)

National Aeronautics and Space Administration
Washington, DC 20546-0001

10. SPONSORING / MONITORING AGENCY REPORT NUMBER

NASA TM-110318

11. SUPPLEMENTARY NOTES

Woods-Vedeler: Langley Research Center, Hampton, VA
Rombado: Grumman Aerospace Corp., Houston, TX

12a. DISTRIBUTION / AVAILABILITY STATEMENT

Unclassified - Unlimited
Subject Category 39

Availability: NASA CASI, (301) 621-0390

12b. DISTRIBUTION CODE

13. ABSTRACT (Maximum 200 words)

The purpose of this paper is to provide final results of a pointing stability analysis for external payload attachment sites (PAS) on the International Space Station (ISS). As a specific example, the pointing stability requirement of the SAGE III atmospheric science instrument was examined in this paper. The instrument requires 10 arcsec stability over 2 second periods. SAGE III will be mounted on the ISS starboard side at the lower, outboard PAS. In this engineering analysis, an open-loop DAC-3 finite element model of ISS was used by the Microgravity Group at Johnson Space Flight Center to generate transient responses at PAS to a limited number of disturbances. The model included dynamics up to 50 Hz. Disturbance models considered included operation of the solar array rotary joints, thermal radiator rotary joints, and control moment gyros. Responses were filtered to model the anticipated vibration attenuation effects of active control systems on the solar and thermal radiator rotary joints. A pointing stability analysis was conducted by double integrating acceleration transient over a 2 second period. Results of the analysis are tabulated for ISS X, Y, and Z Axis rotations. These results indicate that the largest excursions in rotation during pointing occurred due to rapid slewing of the thermal radiator. Even without attenuation at the rotary joints, the resulting pointing error was limited to less than 1.6 arcsec. With vibration control at the joints, to a maximum 0.5 arcsec over a 2 second period. Based on this current level of model definition, it was concluded that between 0 - 50 Hz, the pointing stability requirement for SAGE III will not be exceeded by the disturbances evaluated in this study.

14. SUBJECT TERMS

SAGE III, ISS, International Space Station, atmospheric science, pointing, stability, payload attachment sites, PAS, jitter, rotary joints, solar array, thermal radiator

15. NUMBER OF PAGES

101

16. PRICE CODE

A06

17. SECURITY CLASSIFICATION OF REPORT	18. SECURITY CLASSIFICATION OF THIS PAGE	19. SECURITY CLASSIFICATION OF ABSTRACT	20. LIMITATION OF ABSTRACT
Unclassified	Unclassified	Unclassified	